J Nanopart Res (2009) 11:1251–1310
DOI 10.1007/s11051-009-9632-z

PERSPECTIVES

In quest of a systematic framework for unifying and defining nanoscience

Donald A. Tomalia

Received: 2 December 2008 / Accepted: 30 March 2009 / Published online: 26 May 2009

Abstract This article proposes a systematic framework for unifying and defining nanoscience based on historic first principles and step logic that led to a "central paradigm" (i.e., unifying framework) for traditional elemental/small-molecule chemistry. As such, a *Nanomaterials classification roadmap* is proposed, which divides all nanomatter into Category I: discrete, well-defined and Category II: statistical, undefined nanoparticles. We consider only Category I, well-defined nanoparticles which are >90% monodisperse as a function of Critical Nanoscale Design Parameters (CNDPs) defined according to: (a) size, (b) shape, (c) surface chemistry, (d) flexibility, and (e) elemental composition. Classified as either hard (H) (i.e., inorganic-based) or soft (S) (i.e., organic-based) categories, these nanoparticles were found to manifest pervasive atom mimicry features that included: (1) a dominance of zero-dimensional (0D) core–shell nanoarchitectures, (2) the ability to self-assemble or chemically bond as discrete, quantized nanounits, and (3) exhibited well-defined nanoscale valencies and stoichiometries reminiscent of atom-based elements. These discrete nanoparticle categories are referred to as hard or soft particle nanoelements. Many examples describing chemical bonding/assembly of these nanoelements have been reported in the literature. We refer to these hard:hard (H-*n*:H-*n*), soft:soft (S-*n*:S-*n*), or hard:soft (H-*n*:S-*n*) nanoelement combinations as nanocompounds. Due to their quantized features, many nanoelement and nanocompound categories are reported to exhibit well-defined nanoperiodic property patterns. These periodic property patterns are dependent on their quantized nanofeatures (CNDPs) and dramatically influence intrinsic physicochemical properties (i.e., melting points, reactivity/self-assembly, sterics, and nanoencapsulation), as well as important functional/performance properties (i.e., magnetic, photonic, electronic, and toxicologic properties). We propose this perspective as a modest first step toward more clearly defining synthetic nanochemistry as well as providing a systematic framework for unifying nanoscience. With further progress, one should anticipate the evolution of future nanoperiodic table(s) suitable for predicting important risk/benefit boundaries in the field of nanoscience.

Keywords Dendrimers · Proteins · Viruses · DNA/RNA · Metal (M^o) nanoclusters · Metal chalcogenides · Metal ligand/oxides · Fullerenes · Carbon nanotubes · Nanoelements · Nanocompounds · Nanoperiodic property patterns · Soft/hard nanoparticles · Nanoperiodic table · Atom mimicry · Nanochemistry

Electronic supplementary material The online version of this article (doi:10.1007/s11051-009-9632-z) contains supplementary material, which is available to authorized users.

D. A. Tomalia (✉)
Department of Chemistry, The National Dendrimer & Nanotechnology Center, Central Michigan University, Mt. Pleasant, MI 48859, USA
e-mail: donald.tomalia@cmich.edu

Introduction

The nanotechnology movement is a truly interdisciplinary science driven by critical areas such as (a) chemistry, (b) physics, (c) biology, (d) mathematics, (e) engineering, (f) toxicology, and (g) environmental sciences. Although enriched by the convergence of all these important disciplines, the significance of traditional chemistry to the nanotechnology movement should not be underestimated. Without question, synthetic chemistry is the source of most nanomaterials as well as an important knowledge base for essentially all "bottom-up" synthesis strategies, key intermediates, and structural features leading to well-defined nanoparticles. The ability to predict physicochemical properties and risk/benefit boundaries enjoyed by traditional small molecule chemistry rests solidly on the existence of a systematic framework (i.e., *central dogma*) for the discipline. This systematic framework has not only served to unify and define traditional small molecule chemistry, but also has served as a platform of understanding for many important activities in physics, engineering, and biology. Although opinions may vary concerning the order of importance and content of such a framework, a general consensus usually includes the following major discoveries and events (Table 1).

First principles and step logic leading to central dogma for traditional chemistry

Building on A. Lavoisier's *reactive atom hypothesis* and J. Proust's proposal that *atoms possess well-defined masses relative to each other,* it was possible for J. Dalton to propose his *atom/molecular theory*, which is described in a simplified form below (Pullman 1998; Zumdahl and Zumdahl 2007). These statements are a modern paraphrase of Dalton's revolutionary publication: *A New System of Chemical Philosophy* (1808) that launched traditional chemistry as it is recognized today.

Dalton's atom/molecular theory

1. Each element consists of picoscale particles called atoms.
2. The atoms of a given element are identical; the atoms of different elements are different in some fundamental way(s).
3. Chemical compounds are formed when atoms of different elements combine with each other. A given compound always has the same relative number in types of atoms.
4. Chemical reactions involve reorganization of atoms (i.e., changes in the way they are bound

Table 1 Five key criteria (patterns) observed and analyzed by eighteenth–nineteenth century scientists to define the "atom (element)-based chemistry discipline" before the advent of quantum mechanics and electronic theory (Tomalia 1993, 1994)

	Pervasive picoscale patterns supported by experimental observations	Discovering scientist	Contributions
I	Atoms form chemical bonds	Antoine Lavoisier (1743–1794)	"Traite Elementaire de Chimie" (1789)
II	Atoms (elements) possess well-defined masses relative to each other (combining weights)	Joseph L. Proust (1754–1844)	"Law of Definite Proportions" (1797)
III	Atoms (elements) form chemical bonds with well-defined valency	John Dalton (1766–1844)	"Law of Multiple Proportions" "New System of Chemical Philosophy" (1808)
IV	Atoms (the elements) exhibit periodicity in their reactivity and emerging properties	Dmitri Mendeleev (1834–1907) J. Lothar Meyer (1830–1895)	Periodic Table of Elements (1869) (1870)
V	Atoms (elements) exhibit well-defined directionality in the formation of chemical bonds	Louis Pasteur (1822–1895) Joseph-Achille LeBel (1847–1930) Jacobus V'ant Hoff (1852–1911)	Spatial Chemistry Tetrahedral Nature of Carbon (1874) Tetrahedral Nature of Carbon (1874)

together). The atoms themselves are not changed in a chemical reaction.

From the perspective of a chemist, the emergence of the central dogma for traditional chemistry began with the seminal contributions of Lavoisier and Dalton (Fig. 1). Acceptance of the atom/molecular hypotheses set into motion significant developments leading to the Mendeleev Periodic Table (1869) and ultimately our contemporary understanding of atomic, molecular, and chemical theories. Critical parameters that allowed this important progress evolved around discrete, reproducible features exhibited by each atomic element such as well-defined (a) atomic masses, (b) reactivities, (c) valency, (d) stoichiometries, (e) mass-combining ratios, and (f) bonding directionalities. These intrinsic elemental properties, inherent in all atom-based elemental structures (Pullman 1998), have been attributed to certain Critical Atomic Design Parameters (CADPs) (Tomalia et al. 1990; Tomalia and Durst 1993). Simply stated, the function and nature of elemental atoms are largely dependent on these well-defined CADPs which include (a) size (atomic number), (b) shape (bonding directionality), (c) surface chemistry (valency), and (d) flexibility (polarizability).These parameters are unique and highly controlled within each of the atomic elements and are manifested by their intrinsic electron orbitals, electron saturation levels, valency, etc., and determined by their relative positions in the Periodic Table.

From the perspective of a physicist/quantum chemist, chemical bond formation (molecular orbitals) involves the linear combination of atomic orbitals. As such, one can now describe sub-nanoscale, molecular structures as a function of Critical Molecular Design Parameters (CDMPs), wherein CADPs (a)–(d) above are presumed to be conserved but modified in the formation of molecular structure. In general, molecular size is determined by the elemental composition (i.e., atomic number) and number of elemental modules comprising the molecular structure, as well as the bonding directionality. Molecular shape/architecture is defined by elemental valency and bonding directionality (i.e., valence shell electron pair repulsion theory (VSEPR)). Molecular level surface chemistry is of course determined by a wide range of familiar parameters, namely, molecular composition (i.e., molecular modules and functional groups), molecular architecture, and steric environment (Tomalia et al. 2003). Molecular flexibility is largely determined by elemental composition, architectural confinement of structure (i.e., inorganic vs. organic structures), bonding types (i.e., *pi* vs. *sigma* bonding), and spacial placement of functional groups (i.e., cross linking, etc.).

The main thrust of this present concept is to use appropriate first principles and step logic invoked in the historic *atom/molecular hypothesis* by Dalton (i.e., *Philosophy for a Chemical System* (1808)) and others, as a starting point for defining nanomaterials. From this historic perspective, it is proposed that one might determine the extent to which such picoscale concepts/analogies might be applied to demonstrate similar "atom-like building blocks" at the nanolevel. Simply stated—Can *atom mimicry* be used as a criterion to identify suitable structure-controlled nanoparticle categories, possessing well-defined Critical Nanoscale

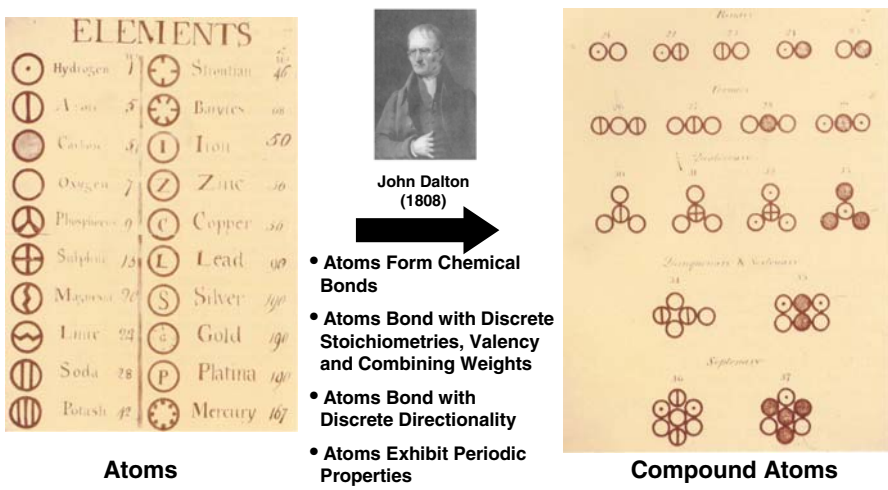

Fig. 1 Dalton's first table of elemental atoms and their conversion to compound atoms according to his atom/molecular hypotheses. Key components of traditional chemistry "central dogma" based on his hypothesis. Images reproduced with permission from (Heilbronner and Dunitz 1993). Copyright: Wiley-VCH Verlag GmbH & Co. KGaA

Design Parameters (CNDP) that might be referred to as nanoelement categories? Demonstration of well-defined chemical bonding/self-assembly patterns for such nanoelements to form more complex nanoscale molecules exhibiting reproducible stoichiometries and mass combining ratios would provide evidence for so-called nanocompound formation. Finally, many traditional periodic property patterns have been documented based on inherent structure-controlled CADPs and CMDPs inherent in all elemental atoms and small molecules, respectively. Would the conservation of CNDPs in proposed nanoelements and nanocompounds produce similar systematic nanoperiodic property patterns? Experimental documentation of such periodic patterns would be essential for ultimately defining the final objective, namely, the evolution of a nanoperiodic system or table(s). At the very least, one might hope that this exercise would lead to the development of a comprehensive classification roadmap of nanomaterial categories, a deeper understanding of the new emerging field of synthetic nanochemistry, and possibly a systematic framework for nanoscience.

Finally, based on historic precedence, it should be reasonable to believe that success at defining and experimentally demonstrating the role of such discrete, reactive/passive nanounits (i.e., nanoelements) should dramatically accelerate the development of critical insights into issues of ultimate importance, namely, *new fundamental/emerging nanoproperties, a wide range of commercial applications, as well as the definition of critical benefit/hazard boundaries of importance to society* (Roco 2008).

The importance of synthesis, characterization, and understanding the inherent periodic properties of atomic elements/compounds during the nineteenth century was critical to the emergence of a systematic central dogma for unifying traditional chemistry. Such similar activity should be considered essential for the evolution of an analogous framework for synthetic nanochemistry and nanoscience.

The present state of nanoscience

Clearly the need for a unifying framework with predictive capabilities for risk/benefit assessment remains an urgent challenge for nanotechnology (Bell 2007). Recent work by Gentleman and Chan (2009) has attempted to codify nanostructures as a function of composition, size, shape, core/ligand chemistry, etc., as an initiative toward this challenge.

To our knowledge, a unifying concept inspired by the first principles of traditional chemistry using step logic that invokes nanoscale atom mimicry, nanoelements, nanocompounds, and associated nanoperiodic property patterns has not been advanced as a framework for defining nanoscience. Today, the traditional electron-driven central dogma for chemistry remains the same; however, the hierarchical dimensions associated with *nano* versus *traditional chemistry* have increased by 10^3 fold. One must ponder a variety of issues such as: Can we extend the concepts of CADP and CMDP to structure control at the nanoscale level (i.e., CNDPs)? What new synthesis strategies must be invoked to gain such structure control of CNDPs? What new theories, rules, concepts, relationships, parameters must be considered to practice chemistry, physics, biology, medicine, engineering, etc., at the nanoscale? With a focus on nanochemistry, can one predict reactivity, stoichiometry, physical properties, toxicology, environmental impact, etc., at these new dimensions? Can nanochemistry be understood and treated as a systematic science such as traditional chemistry has evolved with a scientifically grounded central dogma based on "well-defined units" (i.e., nanoscale building blocks or nanoelements)? Will these nanobuilding blocks form valency-driven stoichiometric nanocompounds and exhibit periodic property patterns? Could such patterns be used to define and predict nanoscale physicochemical properties, nanomodule relationships, and dynamics? In answer to these questions, it is apparent that significant challenges remain.

This approach begins by introducing widely accepted "bottom-up" aufbau principles and synthetic strategies that have been developed over the past several decades to produce well-defined nanomodules such as *dendrons* and *dendrimers*. Intense activity in this area, with over 12,000 literature references, clearly demonstrates that many features of elemental atom structure and behavior have been heuristically mimicked at the nanoscale level. As such, we were encouraged to develop new thinking and approaches for capturing critical functional and periodic features manifested by atoms at the nanoscale level (Tomalia et al. 1990, 2007; Tomalia and Durst 1993; Tomalia 1994, 2005). We refer to

extensions of these picoscale features to reactive/passive nanomodules as a form of *atom mimicry*.

Dendrons and dendrimers as models for understanding other well-defined nanomaterial categories

Structure control of nanoscale objects (i.e., dendrons and dendrimers) (Tomalia and Durst 1993; Tomalia 2005), as a function of CNDPs such as (a) size, (b) shape,(c) surface chemistry, and (d) flexibility, was first reported in 1990 (Tomalia et al. 1990). Since the discovery of this important category of quantized soft nanostructures (Tomalia et al. 1985, 1990; Tomalia and Fréchet 2002; Tomalia 2005; Newkome et al. 1996), these materials have been synthesized with a wide range of compositions, while maintaining precise structural control over CNDPs (a)–(d). As such, it was compelling to view dendrimers/dendrons as fundamental nanoscale building blocks reminiscent of elemental atoms that one might refer to as nanoelements (Tomalia and Durst 1993; Tomalia 2005). This notion was strongly supported by their nanoscale core–shell structures that mimicked atoms, their ability to form well-defined stoichiometric nanocompounds and assemblies, as well as their manifestation of many interesting new nanoperiodic property patterns (Tomalia 1994, 2005, 2008). In order to better understand these issues, we examined certain pervasive core–shell architecture patterns that were noted for a variety of other well-defined nanomaterial categories.

A comparison of elemental atom, metal nanocluster, and dendrimer core–shell architectures

The concept of atom mimicry was first practiced by Dalton beginning with the naïve use of wooden spheroids to represent the known elements at that time (Pullman 1998). This is perhaps the most profound example of heuristic macroscale atom mimicry. Dalton invoked the use of wooden spheroid cores, possessing sticky surface shells (coronas), to demonstrate chemical bonding principles; thus, also suggesting that atoms might possess core–shell topologies. To our knowledge, the first comparison of nanoscale structures as heuristic atom mimics was introduced in the early 1990s (Tomalia et al. 1990; Tomalia 1994). Such atom mimicry was invoked to describe the core–shell architectural similarities of atoms and certain modular behavior also noted for dendrimers. Although atoms are driven by non-Newtonian quantum physics and nanoscale dendrimers would be expected to obey Newtonian physics, it was compelling to ponder several analogous and quantized features observed in each system.

Considering the anatomy of core–shell particle architectures, it is possible to articulate several pervasive core–shell component patterns that appear to persist at both the picoscale and nanoscale level. For example, such architectural configurations arise when a central core component is able to exercise either an energy-driven (i.e., charge neutralization) or chemical bonding influence on satellite components. In either case, principle concentric shells (n) result wherein satellite component saturation values (Z_n) for each shell are determined by either energy or space parameters. Such Z_n values are determined and driven by quantum mechanical energy principles at the picoscale level (i.e., atoms) or by spacial bonding and congestion constraints at the nanoscale level (i.e., dendrimers, metal nanoclusters, etc.). These Z_n values describe the maximum number of satellite components that may be energetically or spacially accommodated at each of these principle shell levels (n) and are attained by stepwise introduction of satellite components *via* a variety of aufbau principles and patterns. These shellfilling aufbau events are accompanied by the emergence of two discrete satellite parameter patterns, namely, (i) an arbitrarily defined series of discrete particle numbers (i.e., P_n) representing a summation of satellite saturation values up to the respective principle shell levels and (ii) discrete particle mass (M_n) values that are a summation of the core and satellite masses at each principle shell level. An illustration of these general features for elemental atoms is shown in Fig. 2a.

Using these general assumptions, it is clear that a heuristic comparison of picoscale and nanoscale core–shell architectures may be made by introducing appropriate satellite components to various cores. In the case of elemental atoms, the energy-driven self-assembly of electrons around neutron/proton cores produces the familiar principle shells, electron saturation levels, and associated reactivity/inertness based on shell saturation levels. Similarly, well-defined hard nanoparticles such as gold nanoclusters are observed

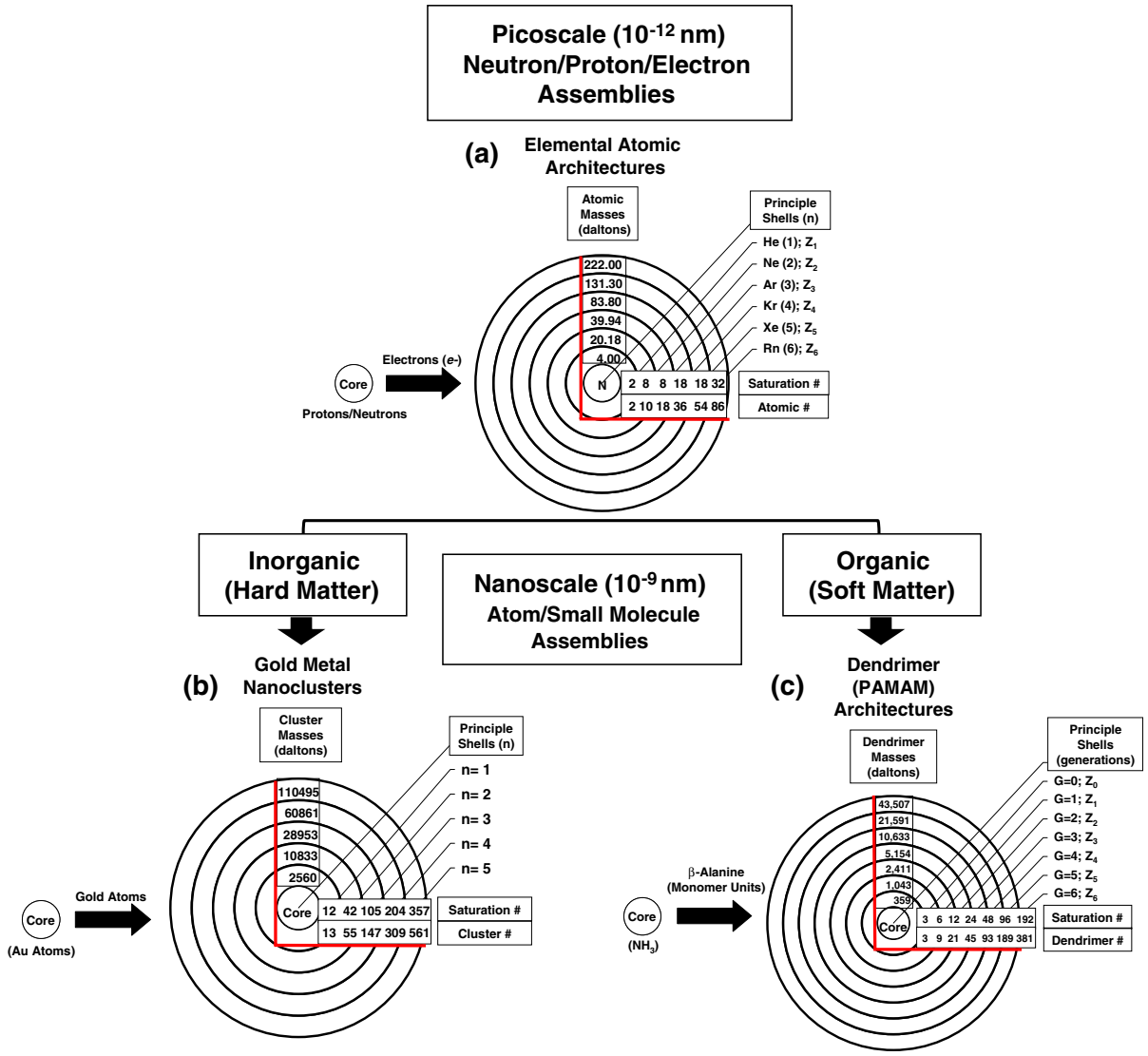

Fig. 2 **a** Illustration of elemental atomic core–shell architecture describing four critical parameters: (i) atomic masses (daltons) (i.e., at each electron shell saturation level), (ii) principle shell numbers (n), (iii) shell saturation numbers (Z_n), and (iv) atomic number (i.e., total number of electrons in atom). **b** Illustration of gold metal nanocluster core–shell architectures describing four critical parameters: (i) cluster masses (daltons) at each shell saturation level, (ii) principle cluster shell numbers (n), (iii) cluster shell saturation numbers (Z_n) (closed atom shell values) $= 10n^2 + 2$ (Schmid 1990), and (iv) cluster number (i.e., total number of gold atoms in nanocluster). **c** illustration of dendrimer core–shell architectures describing four critical parameters: (i) dendrimer masses (daltons) at each shell saturation level (generations), (ii) principle dendrimer monomer shell numbers (n), (generations), (iii) dendrimer monomer shell saturation numbers (Z_n) (closed monomer shell values) $= N_c N_b^G$, where N_c = core shell multiplicity, N_b = branch shell multiplicity, G = generation or (n) principle monomer shell number, and (iv) dendrimer number (i.e., total number of monomer units in the dendrimer or degree of polymerization)

to be formed by a gold atom core + discrete numbers (i.e., magic numbers or closed shells) of gold atoms (satellite components) associated by metal–metal bonds to form gold nanoclusters (Fig. 2b). Similarly, beta-alanine monomer units (satellite components) may be chemically bonded according to dendritic aufbau principles around an ammonia (NH_3) core to produce "closed shells" of very well-defined soft

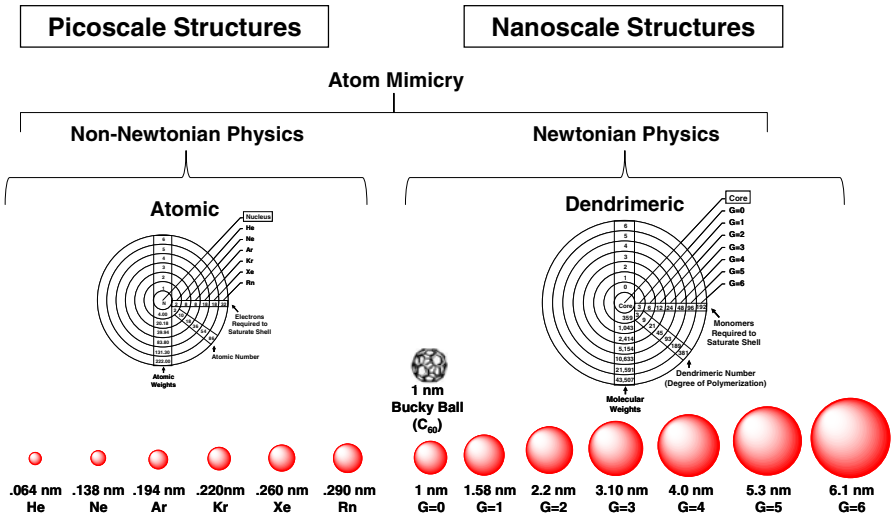

Fig. 3 An example of atom mimicry. A comparison of core–shell structures representing picoscale atoms and nanoscale dendrimers, as well as the continuum of sizes that prevails over the 2D ranges that are controlled by quantum mechanics and Newtonian physics, respectively

nanoparticles such as poly(amidoamine) (PAMAM) dendrimers as shown in Fig. 2c.

Based on the comparisons above and Fig. 3 illustrated above, the issue of nanoscale *atom mimicry* exhibited by PAMAM dendrimers should be apparent and clear. Furthermore, it is immediately obvious that a comparison of size enhancements (i.e., diameters) for both elemental atoms and dendrimers as a function of their respective shell saturation levels produces a very smooth continuum of well-defined sizes that bridge picoscale to nanoscale structures.

Each ideal saturated dendrimer generation will exhibit a surface valency that is mathematically defined by $Z = N_c N_b^G$, where N_c = core multiplicity, N_b = branch cell multiplicity, and G = generation level (Tomalia et al. 2000). The number of monomer units (Z) that are required to saturate the outer monomer shell is predicted by the above equation. Therefore, the monomer aufbau process for building each of these PAMAM dendrimer generations requires the stepwise covalent dendritic attachment of beta-alanine monomer units until the mathematically defined shell saturation limit is reached.

Extending the heuristic aufbau principles/component analogies and assumptions above allowed us to publish an abbreviated comparison of dendrimer and atom-based periodic tables, as illustrated in Fig. 4 (Tomalia 1993, 1994). This comparison clearly demonstrates the analogous core–shell architectural functions in each system. Although the principal quantum numbers (i.e., principle electron shell levels) do not numerically match the generational level (G) (i.e., principle monomer shell level), the stepwise electron- or monomer-based aufbau shell filling patterns are apparent in each case. It should be noted that the sequential boxed numbers in the dendrimer aufbau process indicates the total number of monomers that have been introduced into the dendrimer structure at each aufbau stage. The electron or monomer saturation levels may be noted in each case and corresponds to a closed or saturated principal shell level in each system. The inert, non-autoreactive behavior of such shell-saturated atoms or dendrimers, respectively, is compared later (Fig. 11). Indeed, the well-known autoreactive behavior of atomic elements possessing unsaturated principal electron shells is mimicked by dendrimers (i.e., dendrimers that possess unsaturated principal monomer shells). Although outer-shell-saturated dendrimers will not exhibit autoreactivity, they do retain traditional functional group reactivity with other dendrimers or reagents possessing complimentary functionality (i.e., nucleophilic and electrophilic groups).

Comparison of abbreviated atom and dendrimer periodic tables based on respective electron and monomer aufbau stages

One can compare the first three periods of an abbreviated Mendeleev Period Table of atomic elements with the first three periods (i.e., generations 0, 1, and 2) of an abbreviated dendrimer-based periodic table for a poly(amidoamine) dendrimer

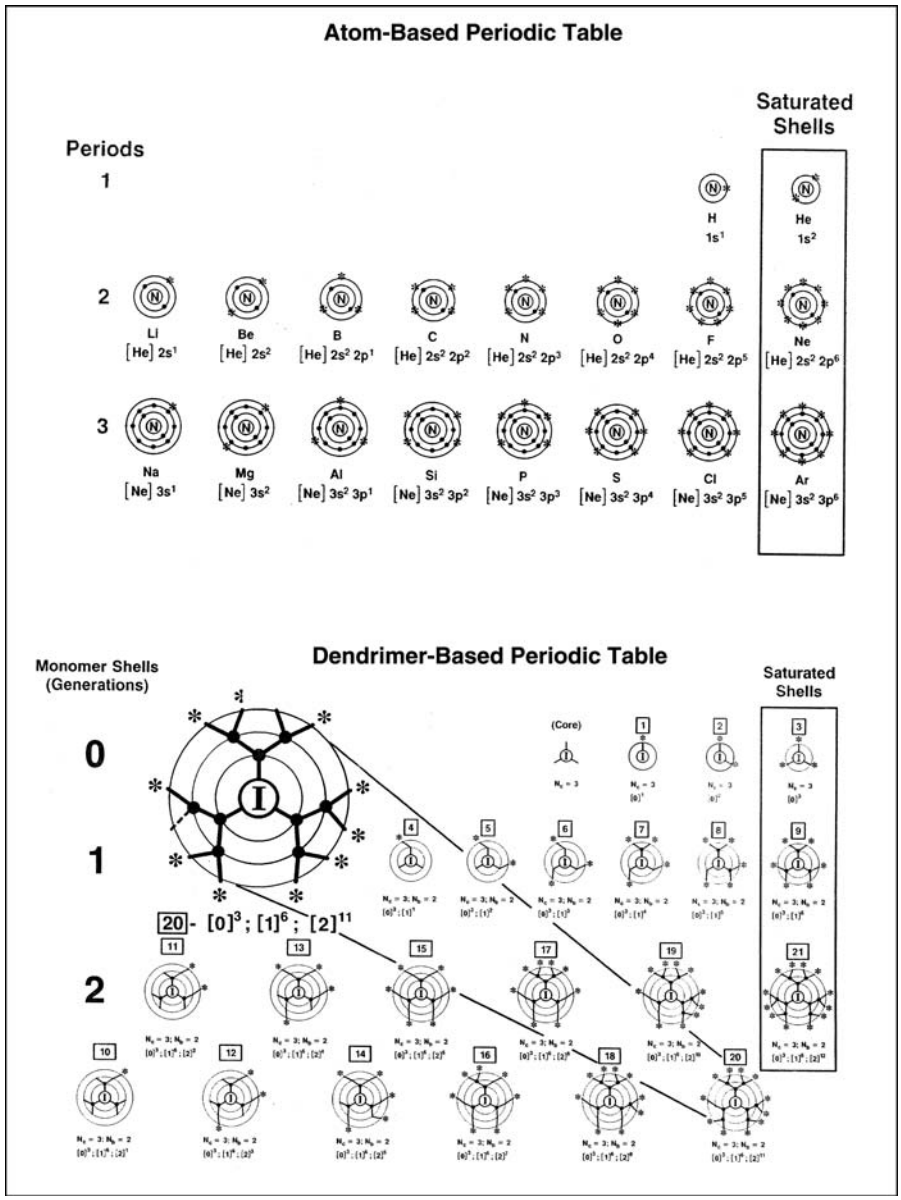

Fig. 4 A comparison of abbreviated atom-based and dendrimer-based periodic tables (Tomalia 1994) for the first three periods

family, namely, core: (NH_3) $N_c = 3$; Gen: 0, 1, 2; and *dendri*-poly(amidoamine)-$(NH_2)_{12}$ (PAMAM) dendrimers (Fig. 4). The atom-based periodic table readily illustrates the stepwise electron aufbau steps that are involved by introducing electrons to produce various elements leading to the saturated noble gas configurations for He, Ne, and Ar with atomic numbers 2, 10, and 18 in Periods 1, 2, and 3. Similarly, one can follow an analogous aufbau introduction of beta-alanine monomer units (•- - -*) to produce the respective saturation states for the first three dendrimer periods (i.e., generations). For generation = 0, the sequential introduction of three monomer units leads to the saturated state for that monomer shell with dendrimer number 3. Next, for generation = 1, the sequential introduction of six monomer units produces the unsaturated shell dendrimer number species 4, 5, 6, 7, and 8 leading to the saturated state for that monomer shell with a dendrimer number of 9 (i.e., to give a total of nine monomer units) possessing six surface amine groups all tethered to the NH_3 core. Finally, the sequential

introduction of 12 monomer units produces the unsaturated monomer shell dendrimer species with dendrimer numbers 10, 11, 12, 13, 14, 15, 16, 17, 18, 19, and 20 leading to the closed saturated monomer shell species 21. *It should be noted that the highlighted dendrimer unsaturated shell species 20 which is penultimate to the saturated shell species 21, may be thought of as heuristically analogous to the atomic element chlorine, whereas the saturated species 21 possesses a saturated monomer shell analogous to argon*. Indeed, the dendrimer species 20 has been shown to be autoreactive much as chlorine, whereas the saturated dendrimer species 21 has been shown to be non-autoreactive much as an inert gas configuration for an atomic element. This atom mimicry feature will be described in more detail later.

Aufbau components, intermediates, and strategies leading to small molecules, traditional polymers, dendrons, dendrimers, and core–shell dendrimer clusters

An overview of critical intermediates required for the successful "bottom-up synthesis" of precise yet complex nanoscale structures such as dendrons, dendrimers, and core–shell type dendrimer clusters (i.e., megamers) is illustrated in Fig. 5. It is readily apparent that many critical intermediates (i.e., beginning with atoms, monomers, branch cell monomers, dendrons, etc.) are involved as one progresses up the dimensional hierarchy to assemble these higher complexities. It is apparent that all strategies/processes must conserve these atom and molecular structure-controlled design parameters (i.e., CADPs, CMDPs, and CNDPs) at each stage to expect nanostructural control over CNDPs for a particular nanomaterial or system.

Mathematically defined intermediates, aufbau principles, and strategies to produce well-defined, soft nanoparticle dendron and dendrimer structures

Over 12,000 published references in the dendrimer field have clearly demonstrated the wide range of discrete nanoscale aufbau principles and atom-like property behavior (i.e., *atom mimicry*) that is possible. Many of these aufbau principles and

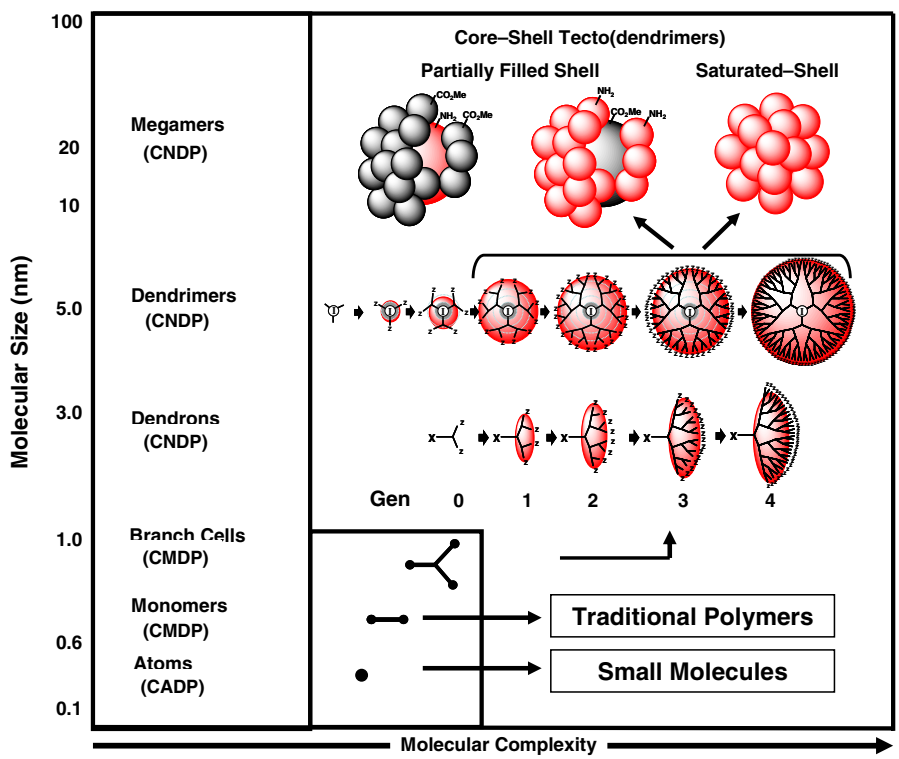

Fig. 5 Approximate nanoscale dimensions as a function of atoms, monomers, branch cells, dendrons, dendrimers, and megamers

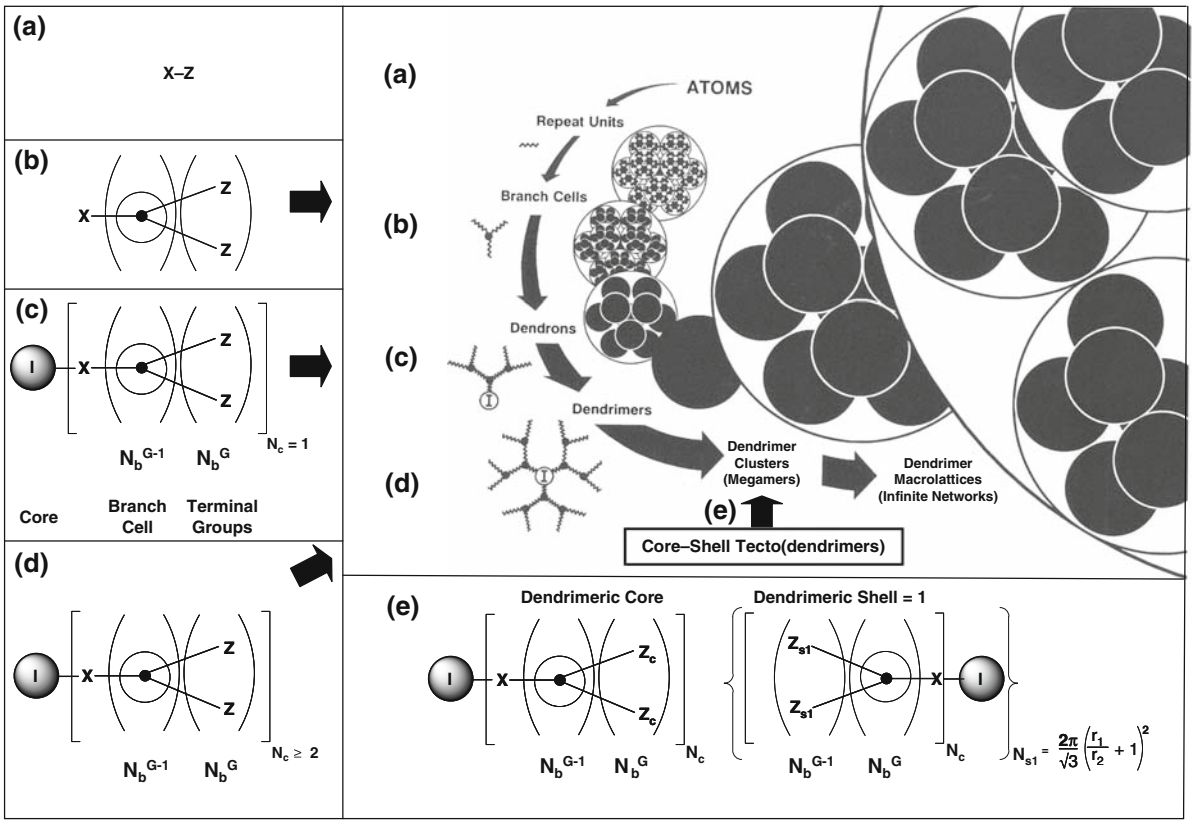

Fig. 6 Critical mathematically defined intermediates involved in bottom-up synthesis strategies leading to dendrons, dendrimers, and core–shell dendrimer clusters (megamers)

components are mathematically defined (Fig. 6) and routinely practiced in the dendrimer field as outlined in Fig. 5.

Several experimentally demonstrated analogies observed for both elemental atoms and soft nanoparticles such as dendrimers, made it compelling to propose dendrimers as fundamental models for defining and identifying other nanoscale building blocks that exhibit atom mimicry. Hence, the notion of structure-controlled CNDPs and associated atom mimicry features were invoked as important criteria for identifying other *nanoelement categories* (Tomalia et al. 1990; Tomalia and Durst 1993; Tomalia 2005). If such structure control of CNDPs and atom mimicry could be identified and confirmed for other nanoparticle compositions/architectures, then a unifying concept for classifying and identifying a wide range of nanoparticle element categories becomes possible.

A nanomaterials classification roadmap

As such, we next propose the development of a *Nanomaterials classification roadmap* from which we classify *well-defined soft and hard nanoparticle categories*. In the context of the five key criteria used to define traditional elemental atoms (i.e., Table 1, Fig. 1), these soft and hard particle categories were screened and selected according to their intrinsic CNDP and atom mimicry features. These classification/criteria selections were used to produce a proposed list of hard and soft particle nanoelement categories.

Assumptions

The proposed classification roadmap for all nanomaterials was inspired by ideas and consensus evolved from a National Science Foundation Workshop

entitled: Periodic Patterns, Relationships, and Categories of Well-Defined Nanoscale Building Blocks (Tomalia 2008). The following assumptions were made:

1. Consider all substances possessing at least one dimension in the nanoscale range of 1–100 nm as nanomaterials.
2. Based on atom-sized scaling, such nanomaterials will be macromolecular level structures, assemblies, crystals, clusters, or particles, etc., that are approximately 10^3 larger than elemental atoms. They will contain from 10^3 to 10^9 atoms and exhibit molecular weights ranging from 10^4 to 10^{10} daltons.
3. These nanomaterials are classified as:

Category (I): well-defined nanoparticles

Category I includes all homogeneous nanomaterials accessible in ≥90% monodisperse form as a function of (a) composition, (b) size, (c) mass, (d) shape, (e) surface chemistry, and (f) flexibility. This proposed criterion level of ≥90% monodispersity is based on the minimum monodispersity levels required to observe well-resolved X-ray patterns for nanoscale 3D-superlattice crystallinity, as reported by Mirkin et al. (Park et al. 2008). These well-defined materials are generally available via "bottom-up" syntheses strategies or from biologic sources.

Category (II): undefined, statistically polydispersed nanoparticles

Category II includes nanomaterials available only in polydisperse form as a function of (a) composition, (b) size, (c) shape, and (d) mass, etc., usually resulting from "top-down" engineered processes.

4. This Nanomaterials Roadmap focuses only on Category I-type nanomaterials.
5. These Category I materials were selected based on uniformity/monodispersity of CNDPs and associated atom mimicry features.
6. Materials exhibiting more rigid, lattice-like, inflexible, metallic/inorganic-type structures/assemblies are referred to as *hard nanoparticles*. This first classification was based on the traditional horizontal periodic elemental features associated with conducting or semiconducting properties usually includes metals, semi-metals, and inorganic compounds such as metal oxides, metal chalcogenides, or carbon allotropes containing extended π-systems. These elemental materials and their compounds tend to form crystalline or rigid 3D lattices. A second class consists of *soft nanoparticles* and includes those materials manifesting more flexible, non-conducting, insulator-type properties associated with covalent, organic-like structures/assemblies. Usually organic structures containing carbon, hydrogen, oxygen, nitrogen, etc., and tend to exhibit amorphous, non-crystalline behavior. Many of these materials are found in biologic systems. Of course, minor exceptions may be found in each category.
7. Based on these features, six *Hard Particle* [H:1–6] and six *Soft Particle* Nanoelement Categories [S:1–6] are proposed as described in Fig. 7.
8. Three combinatorial grids of nanocompounds, namely, hard:hard [H-*n*:H-*n*], soft:soft [S-*n*:S-*n*], and hard:soft [H-*n*:S-*n*] based on chemical bonding or assembling various hard and soft particle nanoelement categories are also illustrated in Fig. 7. Many of these nanocompounds have been reported in the literature and will be described later.
9. Based on the discrete, quantized nature of these nanoelement categories, it is significant to note that many nanoperiodic property patterns have been reported in the literature. These property patterns appear to be dependent upon well-controlled CNDPs and are reminiscent of elemental atoms. These periodic patterns may be classified into intrinsic physicochemical and functional/application-type property patterns. Literature examples of these periodic properties will be described later.

Nanoscale atom mimicry: a concept to unify and define hard and soft particle nanoelement categories

Quantized aufbau components: electrons, atoms and monomer units

The selection process for various Category-I type, hard and soft particle nanoelements (Fig. 7) was

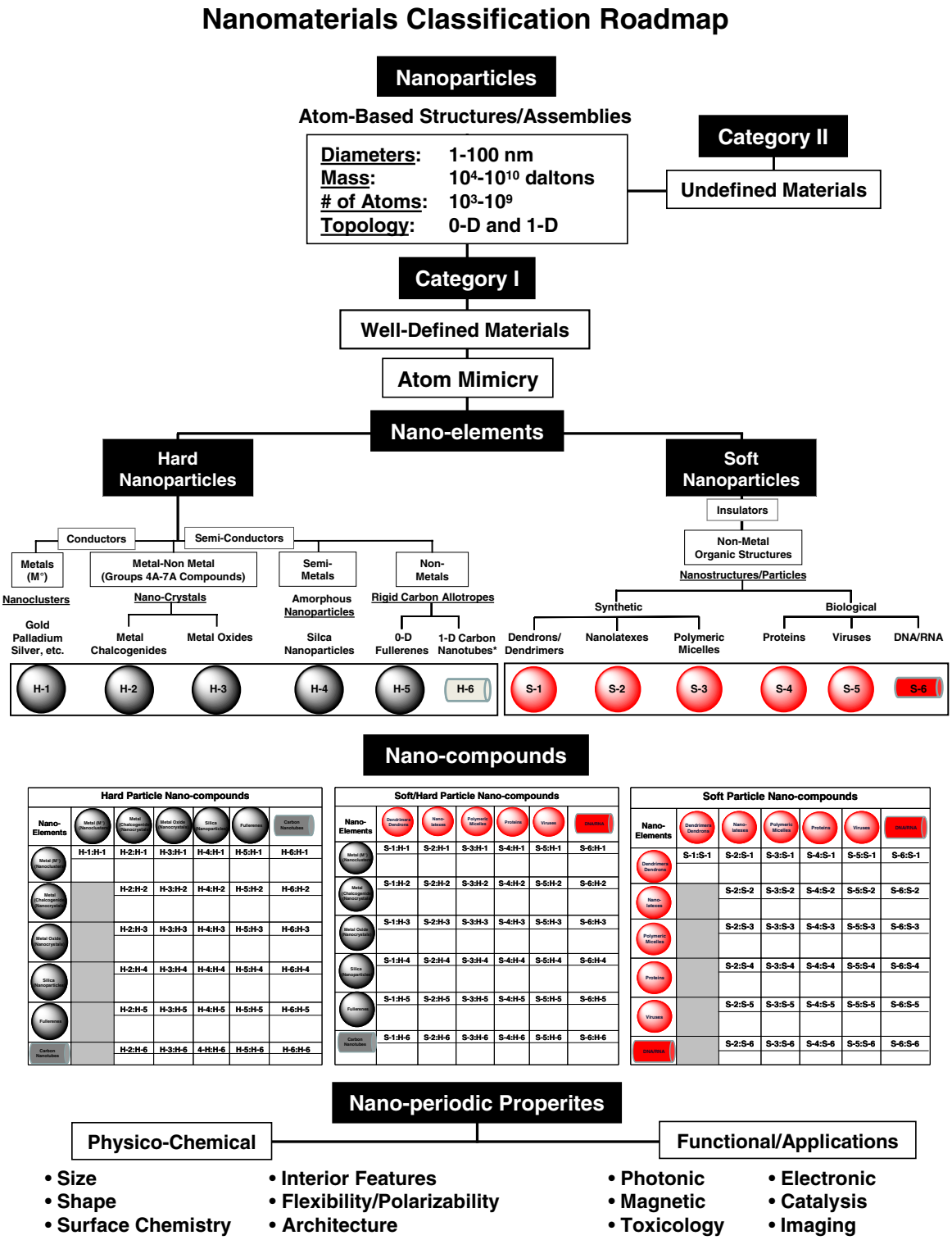

Fig. 7 Nanomaterials classification roadmap

based on certain heuristic or experimentally demonstrated *atom mimicry* features. A general atom mimicry comparison based on core–shell architecture was made in Fig. 2a–c; however, more detailed working examples are now described as shown in Fig. 8. In ascending order, analogous (i.e., heuristic) aufbau shell components (i.e., electrons, Au atoms, and beta-alanine monomer units) leading to core–shell picoscale (atoms) and nanoscale hard matter Au nanoclusters and soft matter dendrimers, respectively, are compared. This comparison illustrates aufbau component mimicry and quantized features involved to produce core–shell type structures at two diverse hierarchical dimensional levels. Well-defined sizes, atomic/molecular masses, and outer-shell saturation values (n) are inextricably connected to specific electron shell, atom shell, or monomer shell (generation) levels in each case. Such atom mimicry is clearly demonstrated for hard nanoparticle gold clusters and soft nanoparticle dendrimers. Similar architectural motif patterns may be observed to a lesser or greater degree in the pervasive core–shell taxonomy observed for all proposed hard and soft particle nanoelements as described later (Fig. 9).

Seminal work by Schmid (Schmid et al. 2000; Schmid 2004) and Rao (Thomas et al. 2001) has shown that fundamental core–shell metal nanoclusters (i.e., Au and Pd) with magic numbers of metal atoms (i.e., 13, 55, 147, 309, 561, and 1,415) corresponding to closed shells 1, 2, 3, 4, 5, and 7, respectively, do indeed exist. As noted by Schmidt, they are substantially more robust when ligand stabilized (Schmid 1990). Furthermore, they can be prepared routinely as monodisperse modules by chemical means (Vargaftik et al. 1991; Schmid et al. 1993, 2000; Rao 1994; Teranishi et al. 1997). Wilcoxon et al. (2000) have shown that these closed shell, core–shell metal nanocluster assemblies can be isolated, analyzed, and characterized using high-pressure liquid chromatography (HPLC) methodologies. It is also noteworthy that these basic hard particle nanomodules

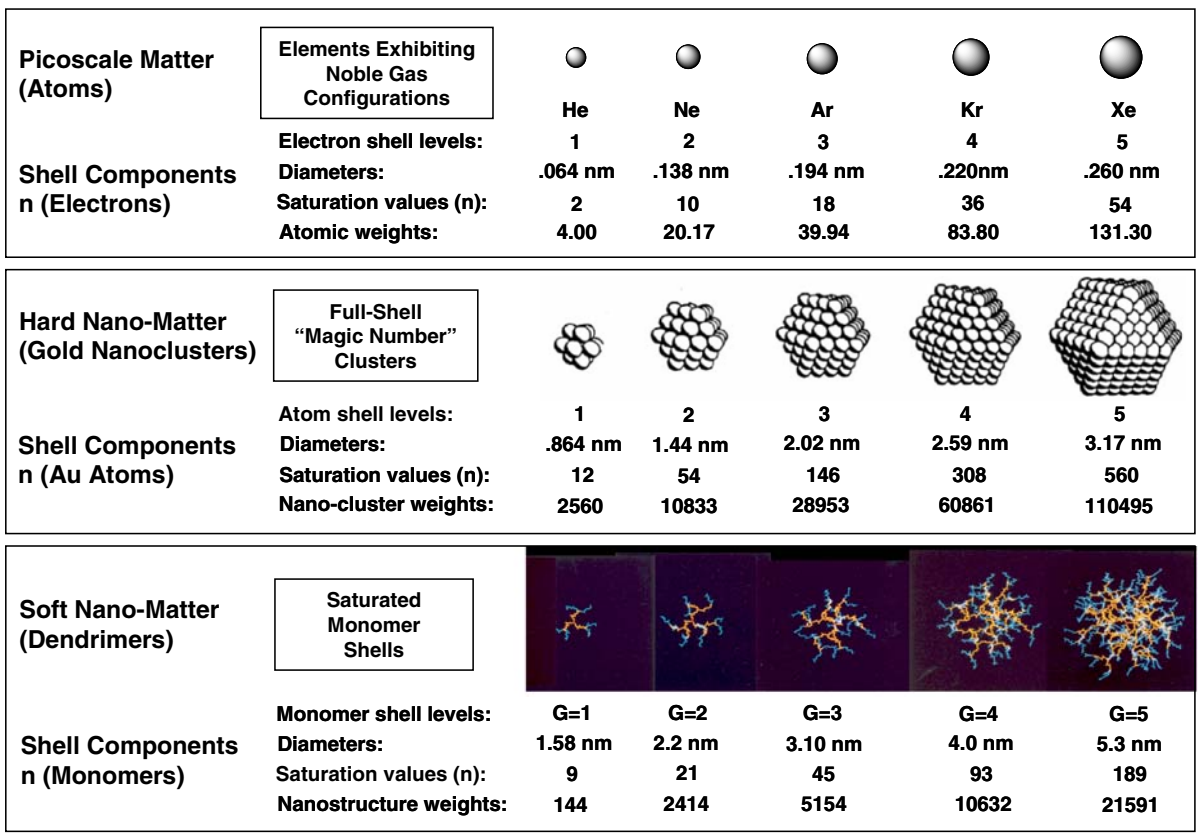

Fig. 8 Comparison of atomic picoscale particles, hard nanoparticles, and soft nanoparticles. Center image Hard-Matter. Reprinted from Schmid (1990). Copyright (1990), with permission from Elsevier

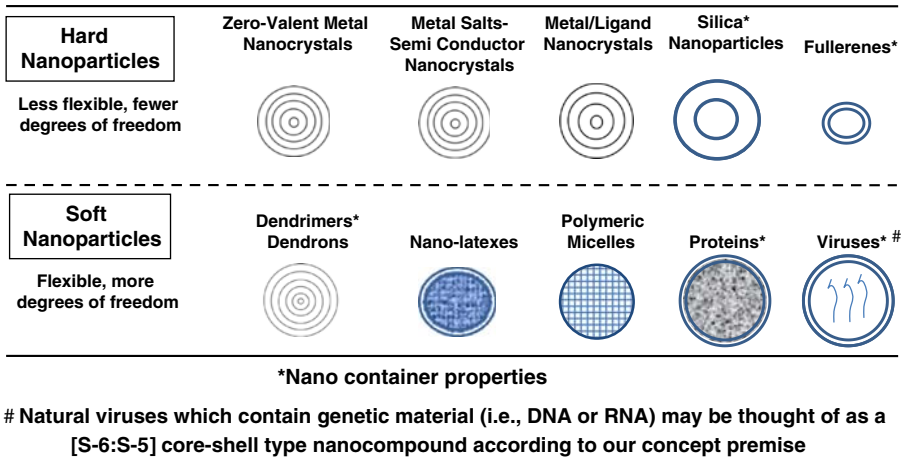

Fig. 9 Taxonomy of proposed 0D core–shell nanoelements

exhibit pervasive nanoperiodic self-assembly features by organizing into giant, self-similar core–shell nanocrystals that are invariant to scaling (Thomas et al. 2001). Similar nanoperiodic, self-assembly properties have also been noted for soft nanoparticles such as dendrimers (Tomalia et al. 1985, 1986; Jackson et al. 1998).

Core–shell architecture: a pervasive pattern observed in all well-defined nanomaterials

Core–shell architecture is a dominant pattern observed in essentially all Category-I well-defined nanomaterials. The taxonomy of all 12 nanoelement categories proposed in the nanomaterials roadmap (Fig. 7) shows some degree of core–shell architectural topology (Fig. 9). Very discrete core and shell components are observed for both hard and soft nanoparticle classifications as well as certain large diffuse core components in concert with very simple shells/surface corona components (Fig. 9). Early studies on nanoclusters exhibiting discrete "magic numbers" associated with saturated, closed shell motifs suggests that these well-defined core–shell structures are generally related to minimized surface energies (Schmid 1990; Wales 1996).

Periodic self-assembly of hard/soft core–shell nanoelements: formation of self–similar mega core–shell clusters

Extensive studies by Rao et al. (Thomas et al. 2001) and Schmid et al. (Schmid and Klein 1986; Schmid 1988, 1990; Schmid et al. 2000) have documented pervasive, non-bonding self-assembly patterns for metal nanoclusters as described in Fig. 10. Closed core–shell modules observed for both Au_n and Pd_n clusters readily self-assemble into a variety of giant self-similar nanoclusters. A Pd_{561} nanocluster with $n = 5$ atom shells (i.e., dia. = 4.1 nm) was shown to self assemble into precise self-similar core–shell structures with diameters of 27.7, 33.8, and 46.0 nm, respectively (Fig. 10). As noted by Rao et al., nanomodule monodispersity and surface features are of critical importance for these assemblies (Thomas et al. 2001). Analogous self-assembly patterns were observed for soft nanoparticles such as poly(amidoamine) (PAMAM) dendrimers possessing $n = 5$ (i.e., $G = 5$) monomer shells and sodium carboxylate surface groups, as noted in TEM studies reported by Tomalia et al. (1985, 1986) and Amis et al. (Jackson et al. 1998).

Picoscale–nanoscale module reactivity patterns: saturated/unsaturated outer-shell mimicry (i.e., atoms, dendrimers, and dendrimer clusters)

A comparison of shell-saturation states for core–shell-type atom, dendrimer, and dendrimer cluster architectures reveals a very important modular reactivity pattern that prevails at both the picoscale and nanoscale levels. Figure 11 illustrates the well-known reactivity pattern for atomic elements bearing unsaturated outer electron shells. This feature was compared to dendrimers and dendrimer clusters that possess similar unsaturated outer monomer shells

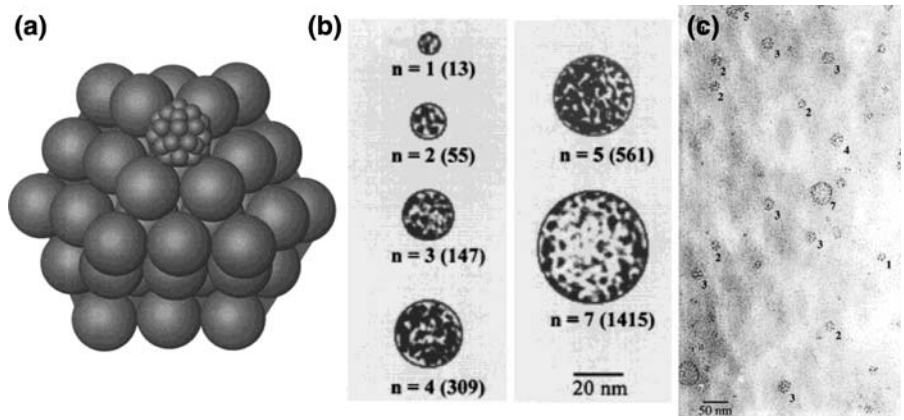

Fig. 10 **a** Schematic illustration of a $(M_{55})_{55}$ giant cluster. **b** Giant clusters of different magic nuclearities, $(Pd_{561})_n$, the circles corresponding to the diameters of the clusters calculated on the basis of the effective volume of an individual nanocrystal, and **c** TEM image of Pd_{561} nanocrystals forming giant clusters. The *numbers* correspond to the proposed number of nanocrystal shells, *n*. Reprinted with permission from Thomas et al. (2001). Copyright: 2001 American Chemical Society

	Atoms	Dendrimers	Core–Shell Tecto(dendrimers)
Dimensions	0.05–0.6 nm	1–15 nm	5.0 ≥ 100 nm
Valency (Reactivity)	Unfilled Outer Electron Shell	Unfilled Outer Branch Cell Shell	Unfilled Outside Dendrimer Shell
(Core–Shell) Architecture Induced Reactivity (Unfilled Shells)	(e.g., fluorine) Unfilled Shell (x)	Unfilled Shell (x)	Unfilled Shell (x)
Functional Components Directing Valency	Missing One Electron (y) in Outer Shell (x) Penultimate to Saturated Noble Gas Configuration	Missing One Terminal Branch Cell in Outer Shell (x) Exposing Functionality (y)	Missing One Dendrimer Shell Reagent Exposing Functionality (y)
Chemical Bond Formation Leading to Saturated Outer Shell: Atoms, Dendrimers, Core-Shell Tecto(dendrimers)			

Fig. 11 Quantized module reactivity patterns at the sub-nanoscale (atoms), lower nanoscale (dendrimers), and higher nanoscale [core–shell tecto(dendrimer)] levels involving outer unsaturated electron, monomer, or dendrimer principal valence shells

bearing surface chemical functionality. It was demonstrated experimentally that dendrimer modules (Tomalia 1994, 2005) as well as core–shell dendrimer cluster modules (Tomalia et al. 2002; Tomalia 2005) possessing unsaturated outer monomer shells exhibit high autoreactivity. This feature produces a propensity to dimerize and/or aggregate to more complex multi-modular structures. Such behavior is reminiscent of elemental atoms that autoreact to complete outer-shell saturation by electron sharing. It is apparent this reactivity pattern at the nanoscale is fulfilled by chemical bond formation involving complementary surface group reactivity. It is significant to note that this atom mimicry property is further fulfilled with dendrimers or core–shell dendrimer clusters possessing saturated outer shells. Dendrimers and core–shell dendrimer clusters possessing saturated outer shells *do not* exhibit autoreactivity properties and indeed mimic the well-known saturated outer-shell behavior of elemental noble gas configurations (Uppuluri et al. 2000; Tomalia 2005).

Picoscale–nanoscale surface features: metal nanocluster mimicry of (atom) element crystallization patterns

As observed by Ozin and Arsenault (2005) and others (Hostetler et al. 1998), both large/small diameter monodisperse silver and gold nanoclusters mimic certain nanoparticle crystallization patterns manifested by elemental atoms. It was noted that metal nanoclusters possessing short/long chain alkane thiolate surface groups (i.e., dense vs. diffuse outer corona shells) led to crystallization patterns that mimicked similar valence electron features in atoms (Fig. 12). Ozin (Ozin and Arsenault 2005) stated that these hierarchically similar crystallization patterns suggest the possibility of a new kind of *nanoperiodic table*. Such a periodic table would classify the geometry of nanoscale core–shell (corona) sphere packing much as is widely recognized for the packing behavior of the atomic elements (Hostetler et al. 1998). This pervasive pattern clearly demonstrates the importance of a key CNDP feature, namely, surface flexibility/polarizability and its influence on crystallization patterns at both the atomic and nanoscale levels.

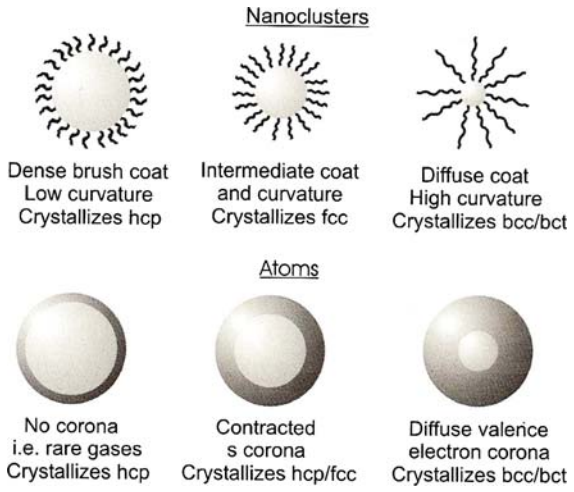

Fig. 12 Comparison of periodic polarization/crystallization properties observed for picoscale atoms and nanoscale modules (i.e., surface-modified metal nanoclusters) (Ozin and Arsenault 2005). Reproduced by permission from the Royal Society of Chemistry

Atom mimicry based on size monodispersity and uniform surface chemistry: structure control of CNDPs

Recent studies by Mirkin et al. (Park et al. 2008) and others (Nykpanchuk et al. 2008) have clearly demonstrated the importance of two key CNDP features, namely, (a) strict size monodispersity and (b) well-defined surface chemistry. It was shown that gold nanoclusters can be programmed to assemble into different 3D lattice crystallographic arrangements by simply changing the surface chemistry (i.e., the DNA linker sequencing). For example, in a single component system where gold nanoparticles are assembled using one DNA sequence, an (f.c.c.) crystal pattern is observed, whereas in a binary component system in which gold nanoclusters are assembled using two different DNA linker sequences, one observes a (b.c.c.) crystallization pattern (Fig. 13). It was shown that very monodispersed gold nanoclusters were required to obtain well-resolved (f.c.c.) or (b.c.c.) crystallization patterns, reminescent of elemental atom-based systems.

Significantly, Mirkin et al. (Park et al. 2008) determined that >90% monodispersity was a strict requirement for all metal nanoclusters used to

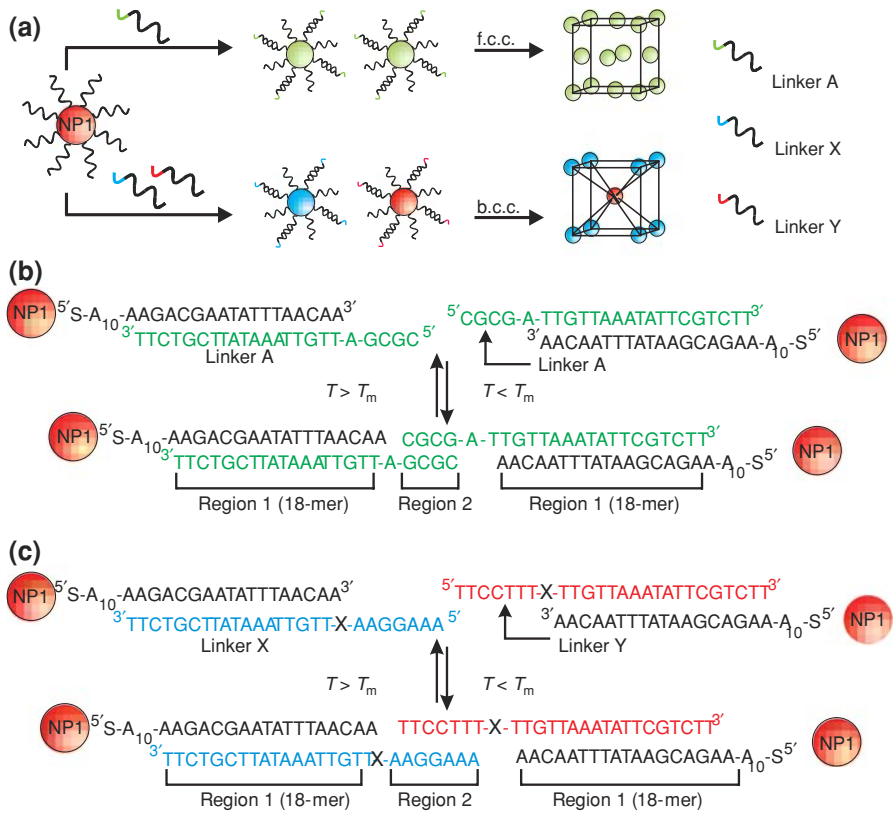

Fig. 13 Scheme of gold nanoparticle assembly methodologies. Reprinted by Macmillan Publishers Ltd.: Nature (Park et al. 2008)

produce 3D-nanocluster superlattices exhibiting well-defined X-ray patterns. As such, this requirement was deemed an important atom mimicry issue as a part of criteria for defining nanoelement categories.

Proposed nanoelement categories and criteria

Nanoelement categories

In the context of the atom mimicry concept, 12 nanoelement categories are presently proposed as abbreviated below (Fig. 14). More specifically, six hard particle and six soft particle nanoelement categories were selected based on atom mimicry criteria that included core–shell architectural motifs, well-defined monodispersity (i.e., >90% for size/mass), outer-shell reactivity features, as well as structure control of other key CNDPs such as shape, surface features, and flexibility.

The six hard particle nanoelement categories consisted of generally well-known 0D metal or semi-conducting elemental compositions and are designated as H-1 to H-5. The proposed 1D carbon nanotube category [H-6] is provisional pending the development of synthesis or sorting methods for obtaining these materials with controlled lengths/aspect ratios. A brief overview of these hard particle nanoelements with leading references to their syntheses and characterization may be found in the Supporting Information Section.

Presently, six soft particle nanoelement categories are proposed and designated as S-1 to S-6 based on the previously described selection criteria. Soft nanoelement categories S-1 through S-4 are 0D nano-objects. Although category S-4 (i.e., proteins) consists of extended 1D polypeptide chains in their primary structures, they are generally viewed as 0D objects in their folded tertiary structure states. Many important non-spheroidal protein subclasses lacking 0D shapes (e.g., IgG antibodies, etc.) must also be considered in this category. Category S-5 viruses include many well-defined 0D- and 1D (i.e., tobacco mosaic viruses)-type shapes. It is well known that both 0D and 1D viruses, in their native forms, are generally core–shell-type structures containing DNA or RNA cores around which discrete wedge-like protein sub-units assemble

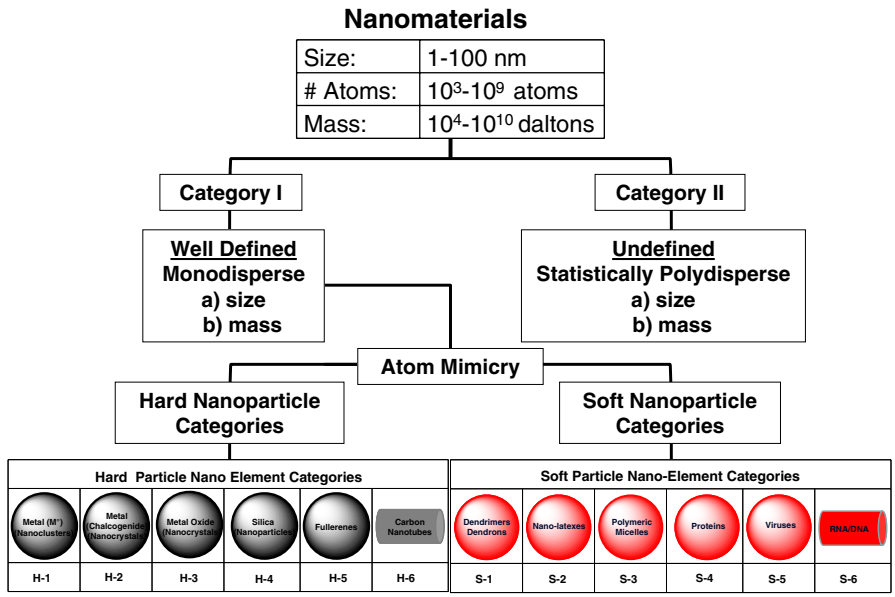

Fig. 14 Hard and soft nanoelement categories

to produce viral coats or shells. In essence, this category consists of large, robust supramolecular protein subunit assemblies (i.e., nanocontainers) containing RNA or DNA interior cores.[1] The S-6 nanoelement category includes DNA and RNA. They are proposed as 1D-type single strand or duplex-type polynucleotide primary structures. Extensive study by Seeman et al. (Seeman 1998; Seeman and Lukeman 2005), Damha et al. (Damha and Oglivie 1988; Damha and Zabarylo 1989; Damha et al. 1990), and others has shown that DNA may exist in many forms and shapes, including dendritic-type architectures (Nilsen et al. 1997; Wang et al. 1998). Although DNA and RNA both fulfill proposed nanoelement category selection criteria, DNA is more often used as a well-defined, sequence-specific, nanoscale connector rather than a 0D nanomodule. As such, more attention will be focused on their very specific Crick–Watson base-pairing assembly features for connecting a wide variety of both hard and soft nanomatter elemental modules (i.e., metal nanoparticles, dendrimers, etc.). A brief overview of these soft particle nanoelements with leading references to their syntheses and characterization may be found in the Supporting Information Section.

Just as Dalton's original list of atomic elements grew from approximately 20 to over 100, the present nanoelement category list is expected to expand substantially in the future.

A more detailed description of nanoelement selection criteria includes the following.

Nanoelement criteria

- Nanoelement categories consist of atom clusters/assemblies or structures possessing at least one dimension between 1 and 100 nm, containing 10^3–10^9 atoms with masses of 10^4–10^{10} daltons.
- Nanoelements are homogenous, uniform nanoparticles exhibiting well-defined (a) sizes, (b) shapes, (c) surface chemistries, and (d) flexibilities (i.e., polarizability).
- Typical nanoelement categories exhibit certain nanoscale atom mimicry features such as (a) core–shell architectures, (b) predominately (0D) zero dimensionality (i.e., 1D in some cases), (c) react and behave as discrete, quantized modules in their manifestation of nanoscale physicochemical properties, and (d) display discrete valencies, stoichiometries, and mass combining ratios as a consequence of active atoms or reactive/passive functional groups presented in the outer valence shells of their core–shell architectures.
- Nanoelements must be accessible by synthesis or fractionation/separation methodologies with typical monodispersities >90% (i.e., uniformity)

[1] Based on the exquisite stoichiometric relationship of DNA/RNA cores to the viral capsids in natural viruses, one might consider these entities to be core-shell type [S-6:S-5] nanocompounds.

(Park et al. 2008) as a function of mass, size, shape, and valency. Wilcoxon et al. (2000) have shown that hard nanoparticle Au nanoclusters are as monodisperse as 99.9% pure (C_{60}). Soft nanoparticle dendrimers are routinely produced as high as generation = 6–8 with polydispersities ranging from 1.011 to 1.201 (Islam et al. 2005a; b; Desai et al. 2008).

- Nanoelement categories must be robust enough to allow reproducible analytical measurements to confirm size, mass, shape, surface chemistries, and flexibility/polarizability parameters under reasonable experimental conditions.
- Chemical bonding or non-bonding assembly of 0D nanoelements may be expected to produce more complex 1D-, 2D-, and 3D nanostructures; referred to as *nanocompounds* or *nanoassemblies*. Such entities are expected to exhibit new emerging properties not observed for the 0D nanoelement precursors as well as certain nano-periodic property patterns (Fig. 7).

Chemical bonding or non-bonding assembly to form nanocompounds

Criteria for an ideal nanocompound are described with the simplicity and spirit that Dalton used in 1808 for the 20 known atomic elements to form *compound atoms* (Fig. 1). Traditional elemental/small molecule chemistry clearly demonstrated the endless varieties of molecular level shapes/topologies that were possible based on outer valence shell bonding/assembly features. Many of these same simple Dalton-type morphologies (i.e., binary, tertiary, quaternary, and core–shell-like shapes) are observed by AFM (Fig. 23) (Betley et al. 2002; Bielinska et al. 2002; Choi et al. 2004) or TEM (Jackson et al. 1998; Azamian et al. 2002) by combining nanoelements to form nanocompounds. Interestingly, even more complex Dalton-type core–shell morphologies (as depicted in Fig. 1) are observed extensively in both the hard and soft particle nanoelement categories (Figs. 10, 16, 25).

Criteria for defining nanocompounds

Adhering to first principles and criteria described for traditional compound atoms (i.e., small compound formation) (i.e., Table 1), the following criteria are proposed to describe and define the formation of *nanocompounds* and *nanoassemblies*:

- Nanocompounds/assemblies are robust, well-defined nanostructures obtained by binding two or more *nanoelements* as a result of their intrinsic outer-shell surface atoms, surface chemical functionality, or non-bonding surface assembly features. Bonding may occur by (a) supramolecular self-assembly or (b) chemical bonding (i.e., involving any of the known traditional modes). The resulting *nanocompounds* must be sufficiently robust to be analyzed by traditional methodologies to yield reproducible values/parameters: (i) gravimetric analysis (i.e., as a function of precursor masses), (ii) elemental composition ratios, (iii) spectroscopic methodologies, and/or by a variety of (iv) direct imaging methodologies (i.e., TEM, AFM, etc.). Reproducible sizes, shapes, and reactivity should be observed. Crystallography (i.e., single crystal-X-ray) may be applicable to hard particle nanocompounds; however, small angle X-ray (SAXS) analyses may be used in some cases for soft particle nanocompounds that do not exhibit amorphous behavior.
- These well-defined nanocompounds will be expected to exhibit reproducible mass-combining ratios, stoichiometries, and emerging physicochemical properties that are different than their nanoelement precursors.
- Desymmetrizing the functional surface chemistry of a nanoelement may be expected to introduce well-defined valency and bonding directionality features into all resulting nanocompounds. As such, valency and directional bonding may be designed and introduced to the outer corona of a nanoelement to produce a variety of nanocompound shapes. Such bonding modes may be manifested as 1D-, 2D-, or 3D-nanomolecular structures of reproducible sizes and shapes.
- Nanoelements possessing highly functionalized/reactive surfaces may lead to nanocompound stoichiometries and limited bonding sites that are defined by so-called *nanoscale sterically induced stoichiometry* (NSIS) rules (Tomalia et al. 1990; Tomalia 2005; Swanson et al. 2007).
- Bonding or assembling nanoelements may be expected to produce isomeric nanocompounds

exhibiting stereoproperties analogous to traditional small molecule isomerism (e.g., asymmetric centers, geometric isomers, symmetry properties, etc.).

Combinatorial nanoelement bonding/assembly to form nanocompounds

Based on traditional chemical compound categories, two broad areas of composition emerged, namely, *inorganic* and *organic* structures. Similar categories have also been observed in the nanohierarchy. We refer to these broad material classifications as (a) *hard-particle nanomaterials* and (b) *soft-particle nanomaterials*. A comparison of their elemental compositions/properties reveals that they parallel the traditional broad areas of inorganic and organic structures. Just as 0D atoms may combine to form 1D-, 2D-, and 3D-type molecular structures, ample evidence at this time supports similar expectations for 0D nanoscale elements.

We briefly examine proposed 1D hard particle nanoelement (i.e., [H-6]; SWNT; carbon nanotubes) and 1D soft matter nanoelement (i.e., [S-6]; ss-DNA) because of the large amount of interest in the literature. At present, SWNTs should be considered provisional since they do not completely fulfill the criteria for nanoelements, as the synthetic control of aspect ratios (i.e., nanotube lengths) still remains an unresolved challenge (Haddon et al. 2004; Banerjee et al. 2005; Krupke and Hennrich 2005; Hersam 2008). In the case of 1D, single strand DNA (i.e., ss-DNA), most literature examples cite their use as *well-defined*, *sequence-specific nanoconnectors*, rather than as nanomodules. However, Seeman has pioneered the design and use of branched DNA to produce various lattice and polyhedral shapes (Seeman 2007).

As such, we report literature examples of nanocompound syntheses according to the following three nanocompound classifications: (1) *hard nanoparticle compounds*, (2) *soft nanoparticle compounds*, and (3) *hard particle–soft particle nanocompounds.* We use shorthand notation for hard and soft nanoelement categories as described earlier. Six proposed hard nanoparticle types (i.e., H-1 through H-6) and six proposed soft nanoparticle types (i.e., S-1 through S-6) are used to define a combinatorial grid of expected nanocompounds in this section. Although the literature contains an abundance of examples, our intention was not to be exhaustive in our literature survey. Often our proposed nanocompound examples are referred to as "nanohybrids" (Gomez-Romero and Sanchez 2004). These nanocompounds and assemblies may be formed in a variety of morphologies and configurations much as Dalton described in his earlier concept including binary, tertiary, quaternary, core–shell, 1D-, 2D- or 3D-type, etc. Following each of the three [H:H], [S:S], and [H:S] nanocompound combinatorial grids, (Tables 2–4), several working examples are presented to illustrate the possibilities with additional examples in the Supporting Information Section.

Hard particle nanocompounds

This section focuses on [hard:hard]; [H-*n*:H-*n*]-type nanocompounds. The nanocompounds in this category are formed by chemical bonding or assembly of two or more of the six proposed hard nanoelement categories (i.e., H-1 through H-6). A combinatorial grid (Table 2) predicts at least 31 binary nanocompound possibilities. Space does not allow a comprehensive review; however, many examples of these compound categories are reported in the literature as described in the grid entries below. Shorthand nomenclature (i.e., [H-*n*:H-*n*], wherein $n = 1$–6 for the hard particle nanoelement classifications) is used to broadly identify nanocompound categories and will not necessarily define stoichiometries or assembly ratios. A random sampling of [hard:hard]; [H-*n*:H-*n*]-type nanocompound examples is presented following the Table 2 grid.

Metal nanocrystal–metal nanocrystal: [H-1:H-1]-type compounds

Recent study by Greiner et al. (Kruger et al. 2008) demonstrates an elegant strategy for designed surface functionalization of gold nanoparticles to produce mono-carboxylic acid functionalized nanocrystals (Fig. 15). These resulting monovalent metal nanocrystals were then allowed to react with an alkylene diamine to produce [hard:hard] [H-1:H-1] gold nanocrystal dimers by exhibiting 2:1 stoichiometry with alkylene diamines as illustrated in Fig. 16.

Similarly, recent study by Stellacci et al. (DeVries et al. 2007, 2008) described the desymmetrization of gold nanocrystals to produce divalent gold nanocrystals. This provided the ground work for the

Table 2 Published hard particle nanocompounds (see Chart below)

[H:1:H-1][1]	Kiely et al. (2000), Shevchenko et al. (2006a, b, 2007), Chen et al. (2007), DeVries et al. (2007), Perepichka and Rosei (2007), and Su et al. (2007)
[H-3:H-1][2]	Cozzoli et al. (2006) and Shevchenko et al. (2006a, b)
[H-4:H-1][3]	Haremza et al. (2002) and Hirsch et al. (2003)
[H-6:H-1][4]	Azamian et al. (2002)
[H-2:H-2][5]	Xie et al. (2008)
[H-3:H-2][6]	Redl et al. (2003) and Burda et al. (2005)
[H-4:H-2][7]	Koole et al. (2008)
[H-6:H-2][8]	Ravindran (2003)
[H-2:H-3][9]	El-Sayed et al. (2003)
[H-4:H-3][10]	Bridot et al. (2007)
[H-2:H-4][11]	Koole et al. (2008)
[H-2:H-6][12]	Banerjee and Wong (2002) and Haremza et al. (2002)
[H-3:H-6][13]	Banerjee and Wong (2002), Haremza et al. (2002), and Ravindran et al. (2003)

Hard Particle Nano-compounds

Nano-Elements	Metal (M°) (Nanoclusters)	Metal (Chalcogenide) (Nanocrystals)	Metal Oxide (Nanocrystals)	Silica (Nanoparticles)	Fullerenes	Carbon Nanotubes
Metal (M°) (Nanoclusters)	H-1:H-1	H-2:H-1	H-3:H-1	H-4:H-1	H-5:H-1	H-6:H-1
	1		2	3		4
Metal (Chalcogenide) (Nanocrystals)		H-2:H-2	H-3:H-2	H-4:H-2	H-5:H-2	H-6:H-2
		5	6	7		8
Metal Oxide (Nanocrystals)		H-2:H-3	H-3:H-3	H-4:H-3	H-5:H-3	H-6:H-3
		9		10		
Silica (Nanoparticles)		H-2:H-4	H-3:H-4	H-4:H-4	H-5:H-4	H-6:H-4
		11				
Fullerenes		H-2:H-5	H-3:H-5	H-4:H-5	H-5:H-5	H-6:H-5
Carbon Nanotubes		H-2:H-6	H-3:H-6	4-H:H-6	H-5:H-6	H-6:H-6
		12	13			

We derive the nanocompound nomenclature in this report by describing the combination of [Hn] elements (left to right horizontally) with [Hn] elements (vertically in descending order). A more systematic nomenclature based on these principles that describe stoichiometry, etc., should be expected to evolve from these basic principles

Superscript numbers for nanocompounds [H-n:H-n][1–13] above are keyed to literature references and correspond to the bold numbers noted in the nanocompound grid (Table 2)

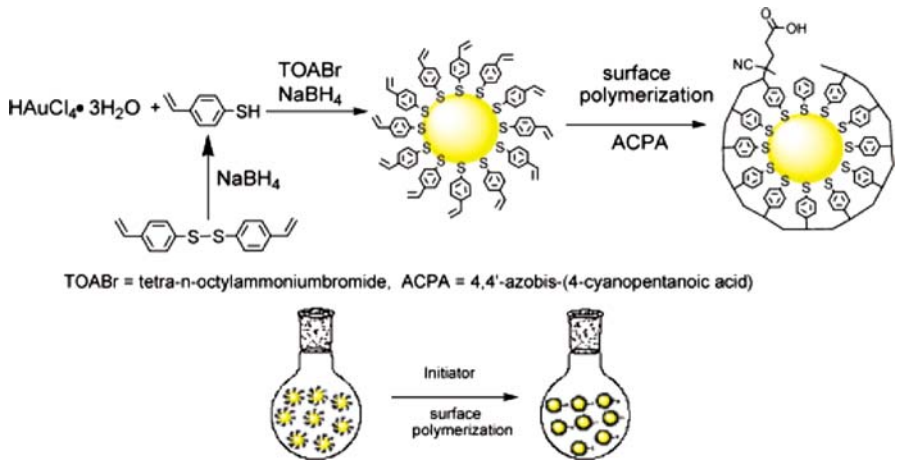

Fig. 15 Strategy for surface functionalization to produce monovalent gold nanoparticles. Reprinted with permission from Kruger et al. (2008). Copyright: 2008 American Chemical Society

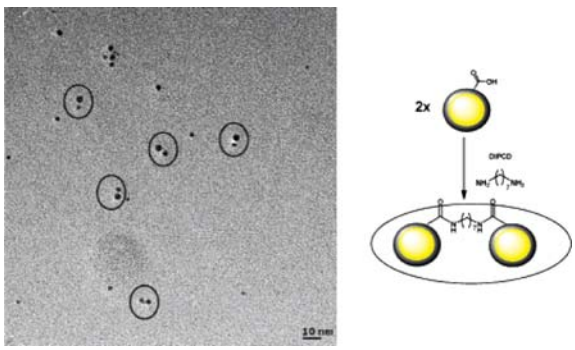

Fig. 16 Dimerization after coupling with 1,7-heptandiamine. Reprinted with permission from Kruger et al. (2008). Copyright: 2008 American Chemical Society

construction of extended, 1D $[H\text{-}1]_n$-type nanocompound examples in this category. Synthesis of these 1D extended arrays was reported in the subsequent study by Perepichka et al. (Perepichka and Rosei 2007). In an article appropriately entitled "From Artificial Atoms to Artificial Molecules" they utilized intrinsic polar defects present on these nanoparticles (Fig. 17) to selectively introduce dicarboxylic acid surface chemistry on these clusters. This modification then allowed them to react the divalent gold nanocrystals with an alkylene diamine reagent to yield extended—$[H\text{-}1:H\text{-}1]_n$—linear array-type (1D) nanocompounds (e.g., nanopolymers) as shown in Fig. 17c.

Many other examples of this [H-1:H-1] nanocompound-type category have also been reported (Kiely et al. 2000; Shevchenko et al. 2006a, b; DeVries et al. 2007; Perepichka and Rosei 2007; Shevchenko et al. 2007).

Metal chalcogenide–metal chalcogenide: [H-2:H-2]-type compounds (Shevchenko et al. 2006a, b)

Some of the first examples of [H-2]-type nanoelement self-assembly were reported by Springholz et al. (1998) to produce [H-2:H-2]-type nanocompounds This group demonstrated that semiconducting PbSe/Te nanocrystals (QDs) self-assembled into 3D superlattices with fcc-like stacking and tunable lattice constants. A variety of other heterodimeric metal and metal/metal salt nanocompound categories have been reported and characterized by TEM as illustrated in Fig. 18.

Many examples of these nanocompound categories involving self-assembly of [H-2]-type nanoelements into 3D nanometal alloy lattices have been reported as shown below (Fig. 19). Size and shape can dramatically influence the assembly of these nanoelements. Assembly of these 0D nanobuilding blocks generally obeys predictions that one might make for traditional picoscale-derived crystal models. For example, nanoperiodic assembly patterns are quite predictable based on the ratio of nanocrystal sizes. These patterns parallel crystallographic alloy structures that are adopted by mixtures of two different metal elements. These patterns are influenced by Hume–Rotheny rules and governed by physical dimensions and properties of the constituent atoms (Kiely et al. 2000). Thus, it appears that certain geometric rules strongly influence pervasive assembly patterns which are observed at all hierarchical dimension levels (Sander and Murray 1978).

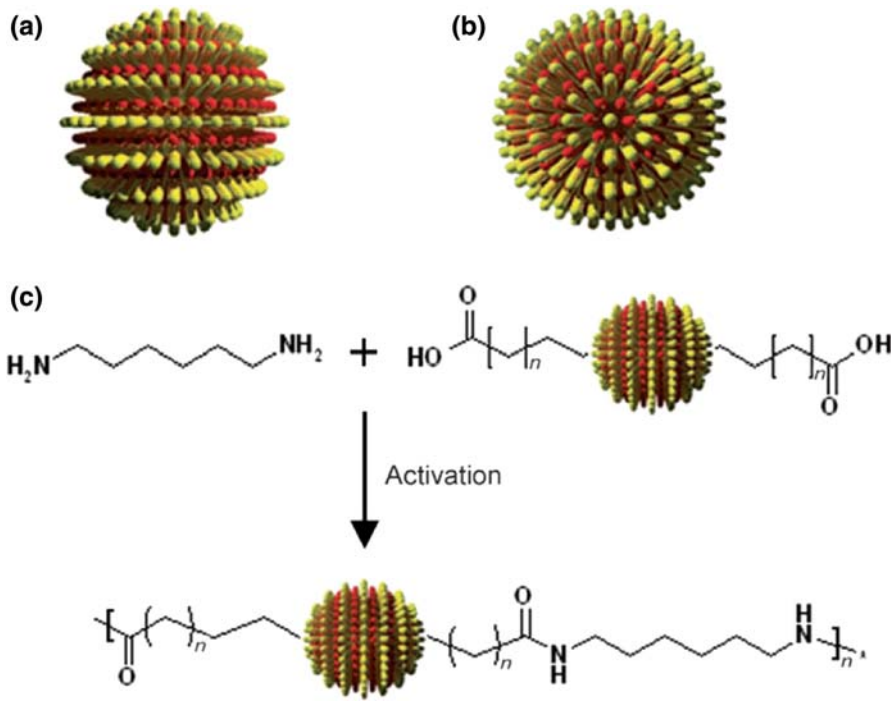

Fig. 17 **a** Side view and **b** top view of a rippled gold nanoparticle. Two polar defects allow the alternation of parallel rings of the two thiol ligands OT (*yellow*) and MPA (*red*). **c** Polymerization of the carboxy-functionalized nanoparticles with 1,7 diaminohexane (DAH). Reprinted from DeVries et al. (2007). Copyright (2007), with permission from AAAS

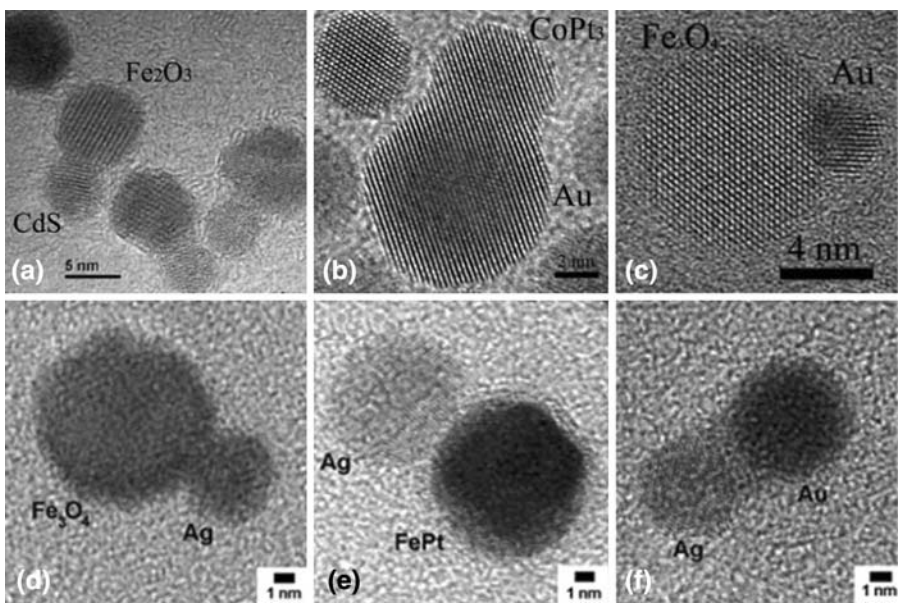

Fig. 18 High-resolution TEM images of different types of heterodimers: (**a**) γ-Fe_2O_3–CdS. Reprinted with permission from Kwon and Shim (2005). Copyright: 2005 American Chemical Society (**b**) $CoPt_3$–Au; (**c**) Fe_3O_4–Au. Reprinted with permission from Shi et al. (2006). Copyright: 2006 American Chemical Society (**d**) Fe_3O_4–Ag (**e**) FePt–Ag; (**f**) Au–Ag. Reprinted with permission from Gu et al. (2005). Copyright: 2005 American Chemical Society

Extensive study by O'Brien et al. (Redl et al. 2003; Shevchenko et al. 2006a, b) has shown that [H-2:H-3]-type nanocompounds can be obtained as 3D superlattices with very specific stoichiometries, namely, AB_2, AB_5, and AB_{13}, as shown below in Fig. 20.

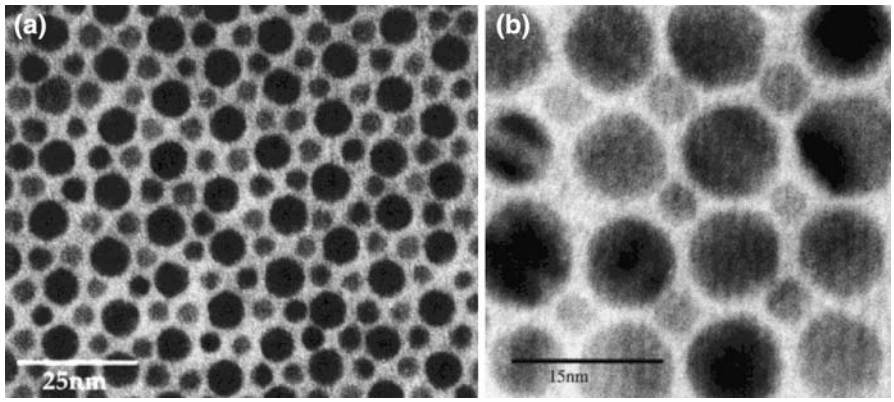

Fig. 19 Rafts of bimodal nanoparticles forming **a** ordered AB_2 and **b** ordered AB superlattice arrays (Kiely et al. 2000). Copyright: Wiley-VCH Verlag GmbH & Co. KGaA

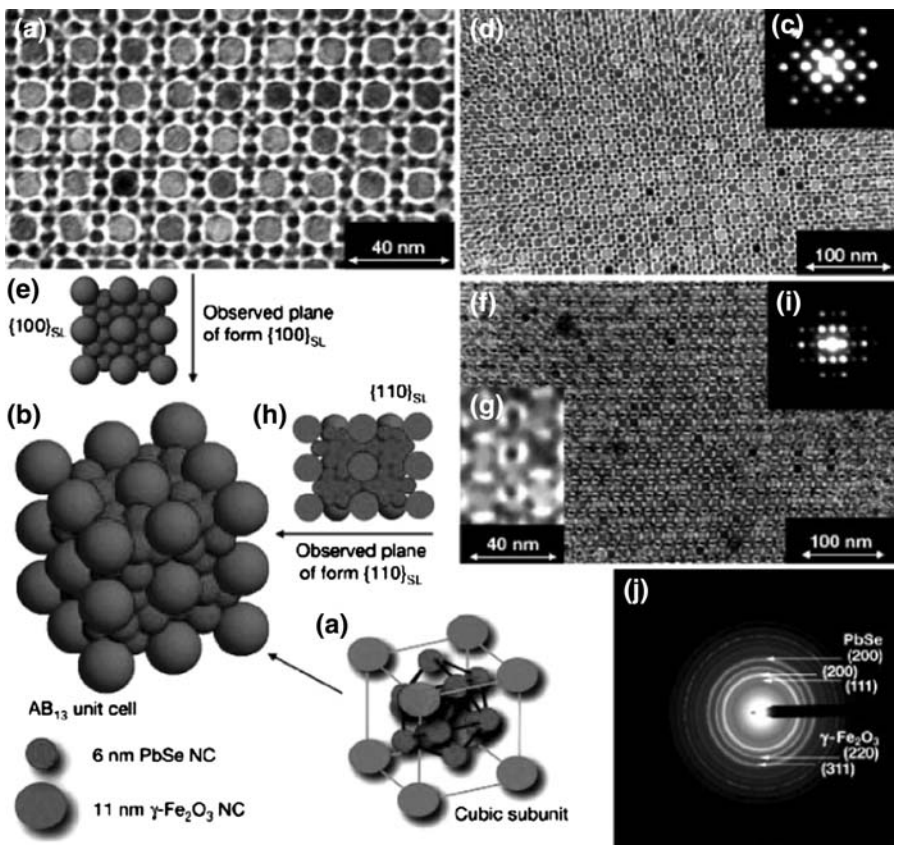

Fig. 20 TEM micrographs and sketches of AB_{13} superlattices of 11-nm γ-Fe_2O_3 and 6-nm PbSe NCs: **a** cubic subunit of the AB_{13} unit cell; **b** AB_{13} unit cell built up of eight cubic subunits; **c** projection of a $[100]_{SL}$ plane at high magnification; **d** same as **c** but at low magnification [(inset) small-angle electron diffraction pattern from a corresponding 6-μm^2 area]; **e** depiction of a [100] plane; **f** projection of a $[110]_{SL}$ plane; **g** same as **f** but at high magnification; **h** depiction of the projection of the [110] plane; **i** small-angle electron diffraction pattern from a 6-μm^2 $[110]_{SL}$ area; and **j** wide-angle electron diffraction pattern of an AB_{13}-superlattice (SAED of a 6-μm^2 area) with indexing of the main diffraction rings for PbSe and γ-Fe_2O_3. Reprinted by permission from Macmillan Publishers Ltd.: Nature (Redl et al. 2003)

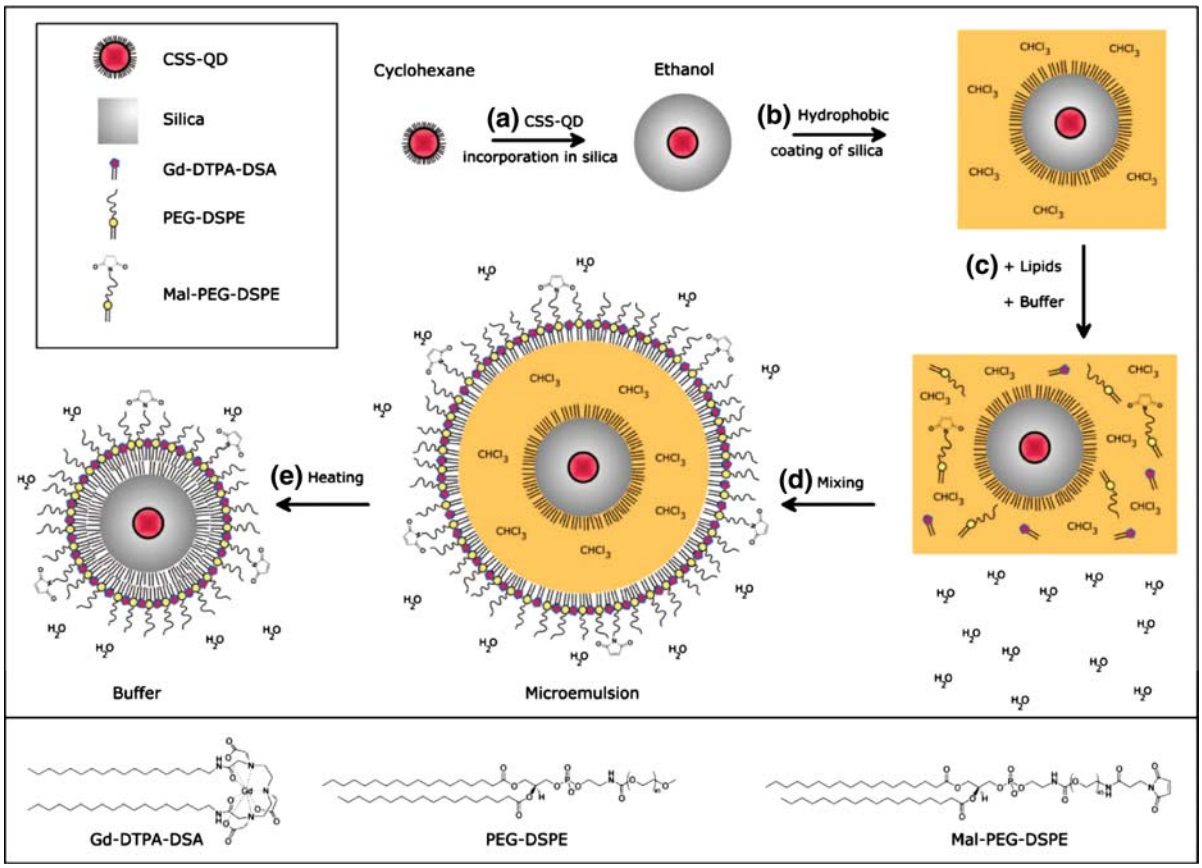

Fig. 21 **a** Incorporation of core–shell–shell (CSS)-quantum dots (QDs) into silica nanoparticles by the reverse micelle method. **b** and **c** Surface modification of the (CSS-QD) produces a water soluble form possessing PEG or gadolinium moieties suitable for MRI. Reprinted with permission from Koole et al. (2008). Copyright: 2008 American Chemical Society

Metal chalcogenide–silica nanoparticle: [H-2:H-4] core–shell-type compounds

Unique 0D core–shell, [hard:hard] nanocompounds have been recently reported by Mulder et al. (Koole et al. 2008) Beginning with a monodispersed cadmium chalcogenide core (7.7 nm), a concentric silica shell is grown around this hard particle [H-2]-type nanoelement to produce a monodisperse [H-2:H-4] core–shell-type nanocompound structure with diameter 31 nm (Fig. 21). The surface of this nanocompound is then functionalized with PEGs and a lipid coating possessing chelated gadolinium. This modification produces a multi-modal imaging agent which exhibits both fluorescence imaging and MRI contrast properties (Fig. 22).

Soft particle nanocompounds

This section focuses on [soft:soft]:[S-n:S-n]-type nanocompounds formed by chemical bonding/assembly of two or more of the six proposed soft particle nanoelement categories (i.e., S-1 through S-6). These soft particle nanoelements present a combinatorial grid that predicts at least 31 binary nanocompound possibilities (Table 3). Many examples of these nanocompounds have been reported in the literature; however, space allows description of only a few examples. Shorthand nomenclature (i.e., [S-*n*:S-*n*], wherein n = the categories 1–6 of the soft nanoelement classification) will be used to identify nanocompound categories, but will not necessarily define stoichiometries.

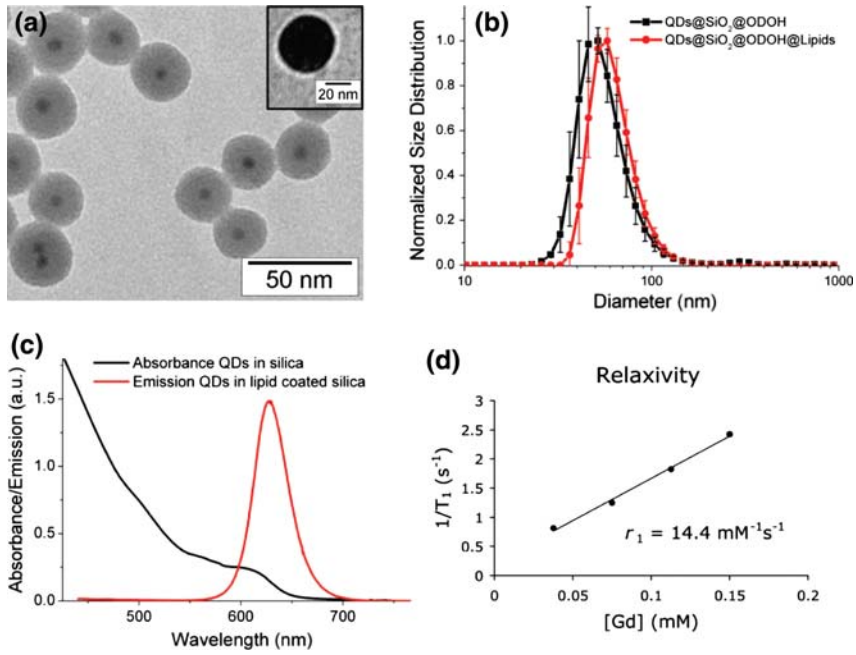

Fig. 22 **a** TEM image of monodisperse particles (31 nm) with a single QD (7.7 nm) incorporated in the center. **b–d** Normalized size distributions, absorption/emission spectra, and relaxivities of the (CSS-QDs). Reprinted with permission from Koole et al. (2008). Copyright: 2008 American Chemical Society

Dendrimer–dendrimer: [S-1:S-1]-type nanocompounds

As early as 1993–1994 (Tomalia 1993, 1994), we proposed the concept of using dendrimers as nanoscale atom mimics (i.e., nanoelements) for the construction of nanoscale molecules (i.e., nanocompounds, nanoassemblies) or propagation to a variety of nanoscale mega-molecules. These multiple dendrimer structures were referred to as *megamers* (Tomalia et al. 2000; Tomalia 2005). They consist of a broad nanostructure category that includes nanomolecules, nano-oligomers, and nanopolymers (Tomalia et al. 1985) possessing a variety of dimensions/topologies as illustrated in Fig. 23a–c. It should be noted that in addition to the basic 0D ($G = 9$; diameter; 11.4 nm.) dendrimer-based nanoelement, one can observe both 1D- and 2D-type megamer self-assemblies, exhibiting a wide range of asymmetric and symmetrical shapes. For example, Fig. 23a shows the basic 0D; [S-1]-type nanoelement, a 1D-type dimer of the nanoelement, and a triangular-shaped trimeric assembly of the [S-1] nanoelement, Fig. 23a displays a variety of asymmetric megamer assemblies (1 and 2), whereas (c) shows several more symmetrical $[S\text{-}1]_n$, trapezoidal-type assemblies as well as an extended 1D linear $[S\text{-}1]_5$-type pentamer designated as (3) in Fig. 23c. Note Banaszak–Holl (Betley et al. 2002) reported and characterized the well-defined $[G = 9]_7$ assembly by AFM as illustrated in Fig. 25b. It should be readily apparent that appropriate introduction of designed valency and directionality on the surface of these [S-1] type nanoelements would allow the syntheses of an endless variety of covalent nanocompounds. Many of these nanoassemblies possess familiar shapes and topologies normally found in traditional carbon-based sub-nanoscale organic structures.

Saturated shell, [S-1:S-1] core–shell-type nanocompounds (Fig. 24) were prepared by a two-step approach which involved (a) self-assembly of carboxylic acid terminated dendrimers (i.e., shell monomers) around a limited amount of amine-terminated dendrimer (i.e., core) in the presence of LiCl and (b) covalent amide bond formation between the core and excess dendrimer shell reagent was accomplished by the use of a carbodiimide reagent. These nanocompounds [i.e., saturated core–shell tecto(dendrimers)], referred to as *megamers,* (Tomalia et al. 2000) are prime examples of precise polydendrimer structures. These nanocompound stoichiometries may be mathematically predicted by the Mansfield–Tomalia–Rakesh equation (Fig. 46) (Tomalia 2005) and are unequivocally verified by experimental mass spectrometry, gel electrophoresis, and atomic force field microscopy (AFM) (Uppuluri et al. 1999; Tomalia 2005). Figure 25 compares (a) a

Table 3 Published soft–soft particle nanocompounds (see chart below)

[S-1:S-1][1]	Miller et al. (1997), Uppuluri et al. (1999), Li et al. (2000), Tomalia et al. (2000, 2002), Tomalia (2004, 2005) and Choi et al. (2005)
[S-2:S-1][2]	Larpent et al. (2004)
[S-3:S-1][3]	Nishiyama and Kataoka (2006)
[S-4:S-1][4]	Roberts et al. (1990), Rao and Tam (1994), Singh (2001), Patri et al. (2004), Thomas et al. (2004), Crespo et al. (2005), Kostiainen et al. (2007), Myc et al. (2007) and Wang et al. (2007)
[S-5:S-1][5]	Reuter et al. (1999) and Landers et al. (2002)
[S-6:S-1][6]	Ottaviani et al. (1999), Choi et al. (2004, 2005), DeMattei et al. (2004), Braun et al. (2005), Frankamp et al. (2005) and Patil et al. (2009)
[S-6:S-3][7]	Nishiyama and Kataoka (2006)
[S-3:S-4][8]	Zhang et al. (2008)
[S-4:S-4][9]	Chidley et al. (2008)
[S-6:S-5][10]	Levine (1992)
[S-5:S-6][11]	Strable et al. (2004)

Soft Particle Nano-compounds

Nano-Elements	Dendrimers Dendrons	Nano-latexes	Polymeric Micelles	Proteins	Viruses	DNA/RNA
Dendrimers Dendrons	S-1:S-1 1	S-2:S-1 2	S-3:S-1 3	S-4:S-1 4	S-5:S-1 5	S-6:S-1 6
Nano-latexes		S-2:S-2	S-3:S-2	S-4:S-2	S-5:S-2	S-6:S-2
Polymeric Micelles		S-2:S-3	S-3:S-3	S-4:S-3	S-5:S-3	S-6:S-3 7
Proteins		S-2:S-4	S-3:S-4 8	S-4:S-4 9	S-5:S-4	S-6:S-4
Viruses		S-2:S-5	S-3:S-5	S-4:S-5	S-5:S-5	S-6:S-5 10
DNA/RNA		S-2:S-6	S-3:S-6	S-4:S-6	S-5:S-6 11	S-6:S-6

Superscript numbers for nanocompounds [S-n:S-n][1–11] above are keyed to literature references and correspond to the bold numbers noted in the nanocompound grid (Table 3)

single $G = 9$, dendrimer, (b) a supramolecular $G = 9$, nanocluster; $[G = 9]_7$ and (c) a core–shell tecto(dendrimer); $[G = 7]$:$[G = 5]_{12}$ covalently bonded nanocluster compound. This clearly illustrates the rigidity (i.e., non-compressibility) of (d) $G = 9$ alone, and (e) in its supramolecular cluster form $[G = 9]_7$ versus (f) the $[G = 7]$:$[G = 5]_{12}$ nanocompound when imaged on a mica substrate. Careful AFM volume analyses of these

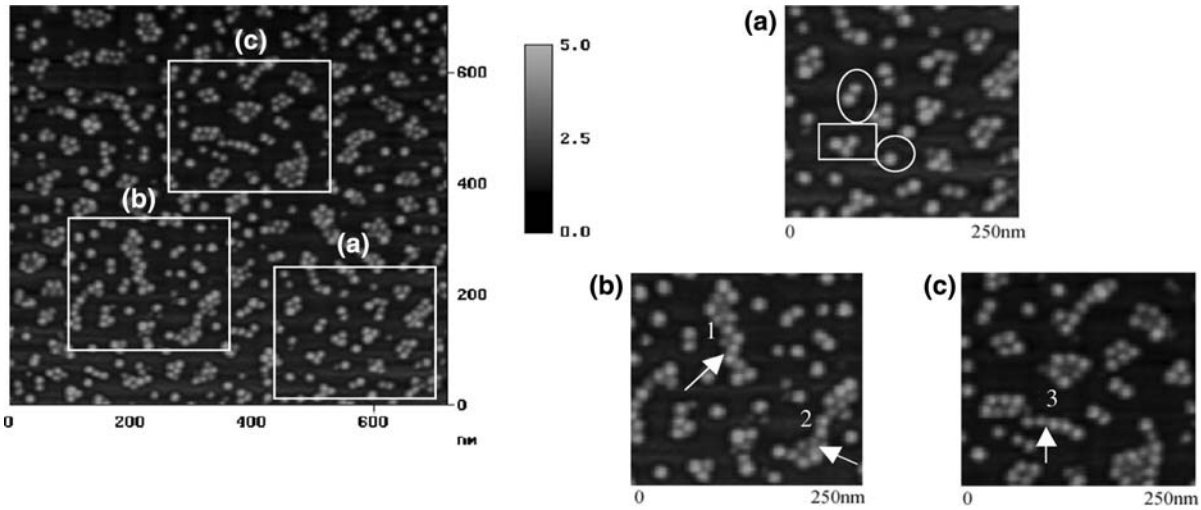

Fig. 23 Tapping mode AFM images of $G = 9$; PAMAM dendrimer molecules on a mica surface (Fréchet and Tomalia 2001)

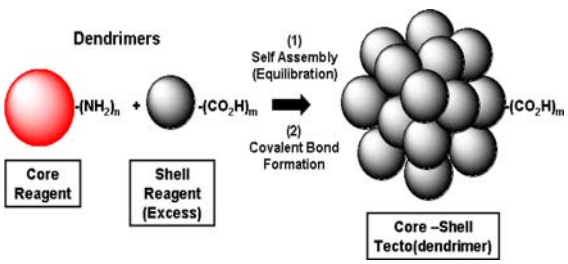

Fig. 24 The saturated-shell-architecture approach to megamer synthesis. All surface dendrimers are carboxylic acid terminated (Uppuluri et al. 2000)

nanocompounds experimentally confirm (Betley et al. 2002) that these nanocompounds are indeed the covalent shell-saturated dendrimer clusters $[G = 7]$:$[G = 5]_{12}$ and possess the correct stoichiometry predicted by the Mansfield–Tomalia–Rakesh equation (Fig. 46) (Mansfield et al. 1996; Tomalia et al. 2002).

Unsaturated shell nanocompounds are prepared by a direct covalent-bond-formation method (Fig. 26). This strategy involves the reaction of a limited amount of a nucleophilic dendrimer core reagent (e.g., amine terminated) with an excess of electrophilic (e.g., carbomethoxy ester terminated)-dendrimer shell reagent (Step A) (Tomalia et al. 2002). This route involved the random parking of the reactive shell reagent on the core substrate surface. As a consequence, partially filled shell products are obtained (Fig. 26), which possess relatively narrow, but not as precise, molecular weight distributions as noted for saturated-shell structures above. These distributions (i.e., unsaturated outer-shell surrounding core) are determined by the inefficient core–shell parking prior to covalent bond formation. As shown, these unsaturated outer-shell nanostructures will *autoreact* to form aggregates unless they are appropriately pacified as indicated in step B.

Nanolatex–dendron: [S-2:S-1] core–shell-type nanocompounds

Dendronized nanolatex structures were readily synthesized in aqueous solutions by allowing a nanolatex surface functionalized with cyclam to react with dendrons possessing activated vinyl groups (i.e., Michael addition reaction) at their focal points (Fig. 27) (Larpent et al. 2004). The lower-generation dendrons (e.g., Gen. = 0) bonded to the [S-2]; nanolatex surface to give a nanocompound with a mass ratio of 1 dendron:cyclam unit. The larger dendrons (e.g., Gen. = 1 and 2) are bonded to the nanolatex surface with mass ratios of 0.7 and 0.4 dendrons per cyclam, respectively. This may be evidence for NSIS as we have described earlier (Tomalia 2005; Swanson et al. 2007).

Dendron–protein: [S-1:S-4]-type nanocompounds

The synthesis and thorough characterization of a 1:1 dendron–bovine serum albumin (BSA) nanocompound was recently reported by Kostiainen and Smith et al. (Kostiainen et al. 2007) (Fig. 28). Synthesis of these precise [S-1:S-4]-binary type nanocompounds was achieved by allowing a dendron

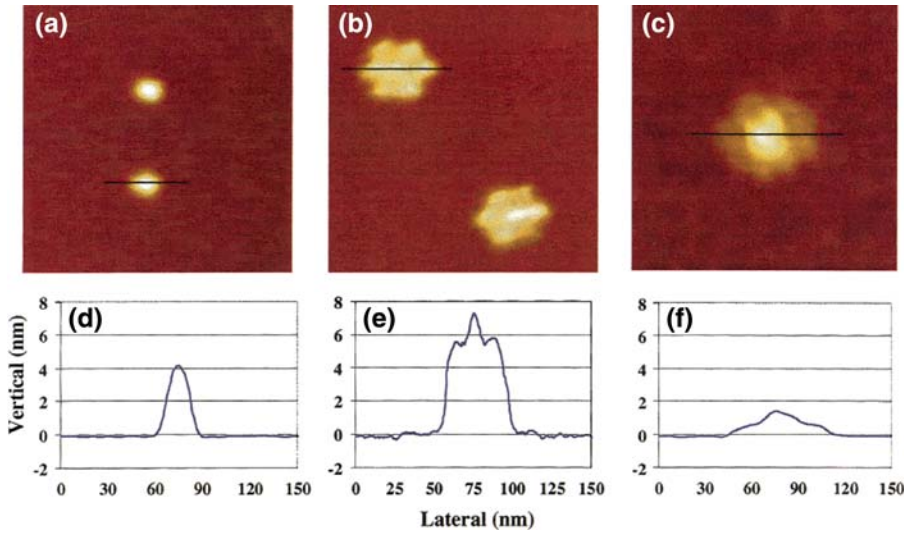

Fig. 25 Comparison of **a** a single $G = 9$, dendrimer; **b** a supramolecular $G = 9$, nanocluster $[G = 9]_7$; **c** a core–shell tecto(dendrimer) $[G = 7]$:$[G = 5]_{12}$ covalently bonded nanocluster compound; and **d** the $G = 9$ alone and in its **e** cluster form versus **f** the $[G = 7]$:$[G = 5]_{12}$ nanocompound when imaged on a mica substrate. Reprinted with permission from Betley et al. (2002). Copyright: 2002 American Chemical Society

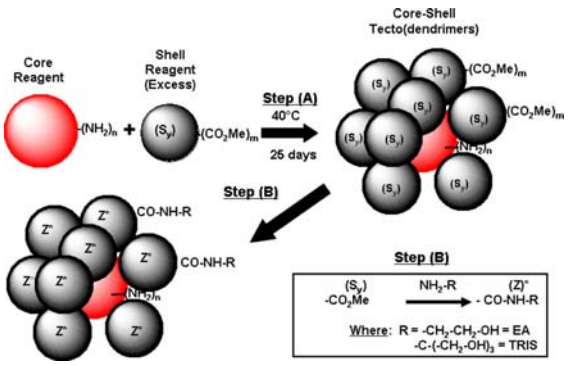

Fig. 26 *Step A* The unsaturated-shell-architecture approach to megamer synthesis. *Step B* describes surface-capping reactions (Tomalia et al. 2002)

containing a focal point N-maleimido group to react via a 1,4-conjugate addition with a single free thiol group presented on the protein surface.

Soft–hard particle nanocompounds

This section focuses on [hard:soft] [H-*n*:S-*n*]-type nanocompounds that are formed by chemical bonding or assembly of one or more of the soft particle nanoelements [S-1] through [S-6] with one or more of the six hard particle nanoelements [H-1] through [H-6]. These soft and hard element combinations present a grid (Table 4) that predicts at least 36 binary nanocompound possibilities. Space does not allow a comprehensive review; however, many examples of these categories have been reported in the literature and a few will be described below:

Metal nanocluster–dendron: [H-1:S-1] core–shell-type nanocompounds

Substantial work has been reported recently by Peng et al. (Aldana et al. 2001; Guo et al. 2003), Fox et al. (Gopidas et al. 2003a, b), and Tomalia et al. (Aldana et al. 2001; Huang and Tomalia 2005, 2006), which describes the dendronization of [H-1] metal nanocrystals or [H-2] cadmium chalcogenide quantum dots (QDs). Metal nanocluster: dendron; [S-1:H-1] core–shell-type nanocompounds are formed (Gopidas et al. 2003a, b). They exhibit well-defined stoichiometries and combining ratios and possess a wide range of surface functionality. Analogous [S-1:H-2] core–shell-type nanocompounds were reported by Peng (Aldana et al. 2001; Guo et al. 2003) and Tomalia (Huang and Tomalia 2006). Initial dendronizations involved the self-assembly of focal point, thiol-functionalized dendrons at the metal interface by ligand exchange. Although earlier thiol-functionalized dendrons were found to reduce QD fluorescence, it was subsequently found that phosphine-functionalized dendrons

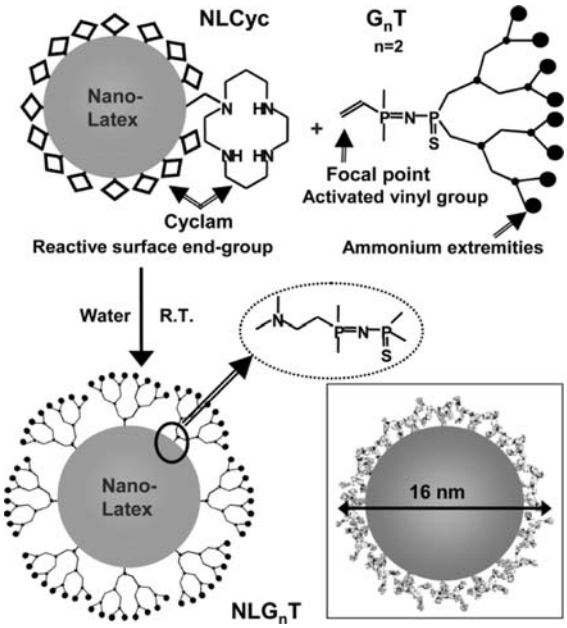

Fig. 27 Synthesis of dendronized nanolatexes; generation *n*, $\mathbf{NLG_nT}$. Inset: scaled cross section of a dendronized nanoparticle $\mathbf{NLG_1T}$ showing the thin $\mathbf{G_1T}$ shell as CPK space-filling molecular model (Larpent et al. 2004). Reproduced by permission of the Royal Society of Chemistry (Larpent et al. 2004)

(Fig. 29) substantially enhanced the fluorescence properties (Huang and Tomalia 2006).

Dendrimer–fullerene: [S-1:H-5] core–shell-type nanocompounds

Stoichiometric dendrimer (core)–fullerene (shell) nanocompounds were readily formed by allowing a generation 4, amine-terminated ($Z = 64$) poly (amidoamine) (PAMAM) dendrimer to react with an excess of buckminsterfullerene (C_{60}) (Jensen et al. 2005). Approximately, 30 (C_{60}) moieties were bonded to the dendrimer surface by Michael addition to produce the dendrimer:fullerene; core–shell-type nanocompounds (Fig. 30). These structures were exhaustively characterized by MALDI–TOF, TGA, UV–vis, and FTIR. The core–shell nanocompounds exhibited new emerging fullerene-type features that were absent for the dendrimer cores by readily generating singlet ($^1O_2$) in either aqueous or organic solvents. Adequate space was present on the dendrimer core surface to accommodate many more fullerenes than were observed to react with the core (i.e., ~ 100 according to the Manfield–Tomalia–Rakesh equation). In this case, it was determined that the combining ratio was limited by the dendrimer surface amine–fullerene reaction stoichiometry (i.e., $2x$–NH_2 groups/fullerene unit). Thus, a core–shell nanocompound possessing one-half the number of dendrimer surface primary amines (i.e., 30–32 fullerenes/$G = 4$; dendrimer core) was obtained. Similarly, Frechet et al. (Wooley et al. 1993) reported the synthesis of a fullerene (core)–dendron (shell) [S-1:H-5] core–shell nanocompound with a fullerene:dendron stoichiometry of (1:2). The new emerging property of this compound was the observation that the fullerene component was made more water soluble by the dendron moieties.

Nanolatex–metal oxides: [S-2:H-3] core–shell-type nanocompounds

Core–shell-type nanolatex: polyoxometalates (POM) compounds have been readily synthesized in aqueous solvents by the covalent attachment of thiol-

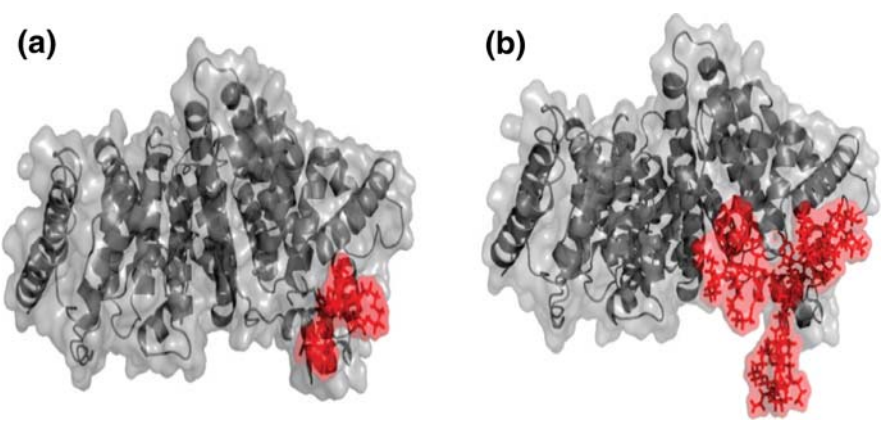

Fig. 28 Protein–dendron nanocompounds. **a** BSA–dendron (Gen. = 1) and **b** BSA–Dendron (Gen. = 2); Cys-34 and the attached dendron are shown in *red*. Reprinted with permission from Kostiainen et al. (2007). Copyright: 2007 American Chemical Society

Table 4 Published soft–hard particle nanocompounds (see chart below)

[S-1:H-1][1]	Schmid et al. (2000), Huang and Tomalia (2005), Srivastava et al. (2005), Shi et al. (2006, 2007), Wilcoxon and Abrams (2006), and Knecht and Crooks (2007)
[S-4:H-1][2]	Ueno et al. (2004), Chen et al. (2006), Jiang et al. (2008), and Bardhan et al. (2009)
[S-5:H-1][3]	Chen et al. (2006)
[S-6:H-1][4]	Mucic et al. (1998), Nykpanchuk et al. (2008), and Park et al. (2008)
[S-1:H-2][5]	Wang et al. (2002), Zhang et al. (2002), and Huang and Tomalia (2005)
[S-3:H-2][6]	Duxin et al. (2005)
[S-4:H-2][7]	Mamedova et al. (2001), Cai et al. (2006), and Medintz et al. (2008)
[S-5:H-2][8]	Joo et al. (2008)
[S-1:H-3][9]	Frankamp et al. (2005), Juttukonda et al. (2006), and Martin et al. (2009)
[S-2:H-3][10]	Cannizzo et al. (2005)
[S-4:H-3][11]	Vriezema et al. (2005), Hultman et al. (2008), and von Maltzahn et al. (2008)
[S-1:H-4][12]	Cho et al. (2007)
[S-1:H-5][13]	Wooley et al. (1993), Hawker et al. (1994), Catalano and Parodi (1997), Rio et al. (2003), Jensen et al. (2005), and Deschenaux et al. (2007)
[S-4:H-5][14]	Qu et al. (2008)
[S-4:H-6][15]	McDevitt et al. (2007)

Soft/Hard Particle Nano-compounds

Nano-Elements	Dendrimers Dendrons	Nano-latexes	Polymeric Micelles	Proteins	Viruses	DNA/RNA
Metal (M°) (Nanoclusters)	S-1:H-1	S-2:H-1	S-3:H-1	S-4:H-1	S-5:H-1	S-6:H-1
	1			2	3	4
Metal (Chalcogenide) (Nanocrystals)	S-1:H-2	S-2:H-2	S-3:H-2	S-4:H-2	S-5:H-2	S-6:H-2
	5		6	7	8	
Metal Oxide (Nanocrystals)	S-1:H-3	S-2:H-3	S-3:H-3	S-4:H-3	S-5:H-3	S-6:H-3
	9	10		11		
Silica (Nanoparticles)	S-1:H-4	S-2:H-4	S-3:H-4	S-4:H-4	S-5:H-4	S-6:H-4
	12					
Fullerenes	S-1:H-5	S-2:H-5	S-3:H-5	S-4:H-5	S-5:H-5	S-6:H-5
	13			14		
Carbon Nanotubes	S-1:H-6	S-2:H-6	S-3:H-6	S-4:H-6	S-5:H-6	S-6:H-6
				15		

Superscript numbers for nanocompounds [S-n:H-n][1–15] above are keyed to literature references and correspond to the bold numbers noted in the nanocompound grid (Table 4)

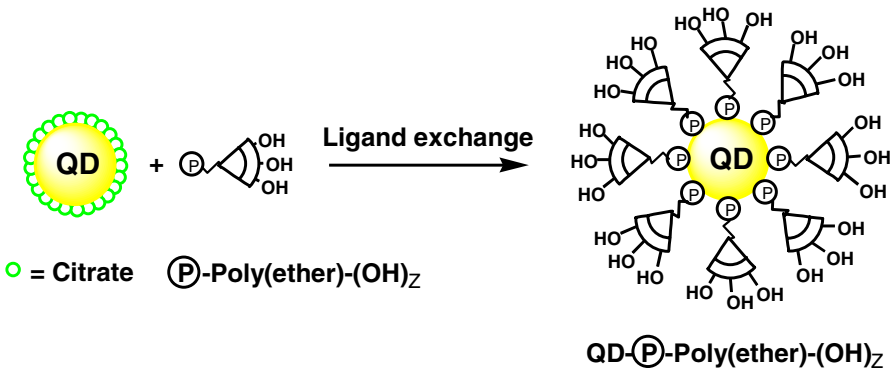

Fig. 29 Ligand exchange of citrate-protected QDs with phosphine focal point-functionalized poly(ether) dendrons (Huang and Tomalia 2006). Reprinted from Huang and Tomalia (2006). Copyright (2006), with permission from Elsevier

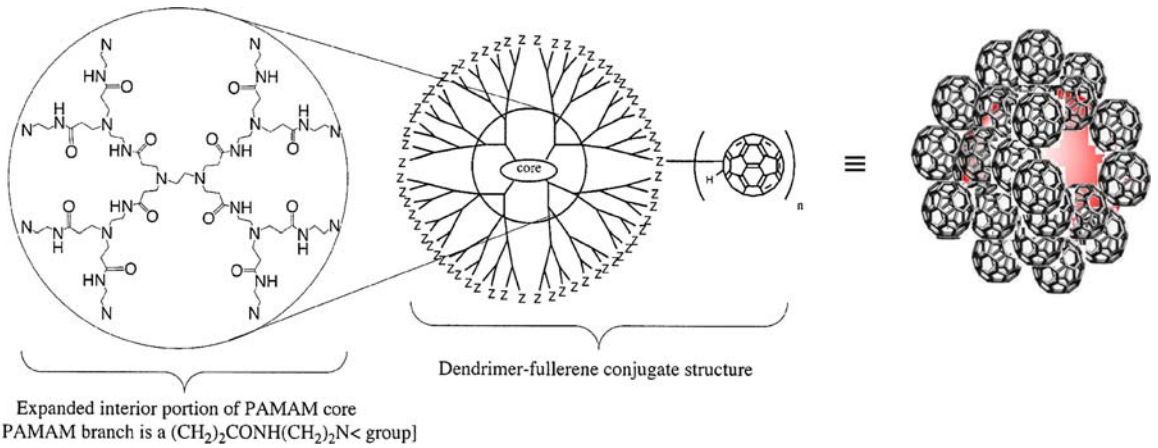

Fig. 30 Dendrimer core–fullerene-shell nanocompounds, where Z = peripheral $-NH_2$ or –NH (PAMAM) dendrimer core surface groups and n = 30–32 fullerene shell components in the core–shell nanocompounds. Reprinted with permission from Jensen et al. (2005). Copyright: 2005 American Chemical Society

functionalized POMs to chlorobenzyl-functionalized [S-2]-type nanolatex element surfaces (Cannizzo et al. 2005). Solutions of these nanocompounds did not exhibit significant aggregation even after several months. These nanocompounds, (Fig. 31), were characterized by TEM, FTIR, EDX, and TGA. The inorganic Dawson-type POM shells were found to act as electron-scattering domains and allowed their direct visualization by TEM that confirmed average nanoparticle diameters of 25 nm. Furthermore, new emerging photochromic properties normally associated with unbound POM compositions were now observed for these [nanolatex:POM] core–shell-type nanocompounds.

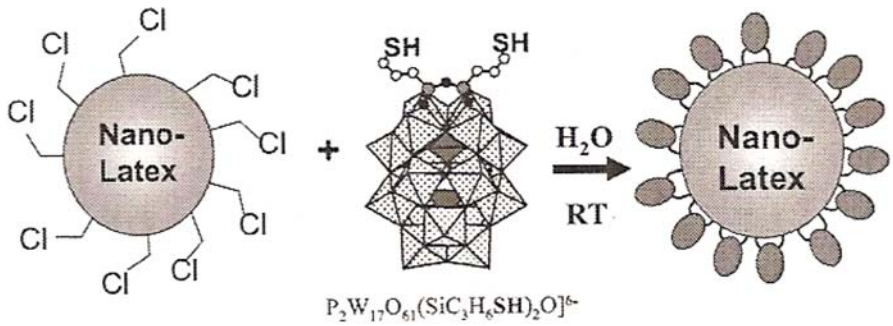

Fig. 31 Room temperature synthesis of [nanolatex(core): POM (shell)]-type nanocompounds. Reproduced with permission from Cannizzo et al. (2005). Copyright: Wiley-VCH Verlag GmbH & Co. KGaA.

Nanoperiodic property patterns

It is generally recognized that quantized and systematic CADPs such as uniform sizes, shapes (i.e., electron orbitals), surface chemistry (i.e., valency), and polarizability (flexibility) associated with atomic structure are discrete for each element. These features largely determine several periodic property patterns observed for all atomic elements (Pullman 1998). Furthermore, these parameters in concert with their inherent core–shell architectures further enrich the unique compositional features that define numerous observed elemental physicochemical and functional property patterns. It was the accumulation and analysis of these periodic patterns that eventually led to the emergence of Mendeleev's Periodic Table in 1869.

The present challenge is to determine to what extent these first principles may be applied in concert with atom mimicry to describe and understand the more complex Category I-type nanoparticles and structures. The step logic and rationale used in this a priori analysis was as follows: first, all CADP and CMDP features present in aufbau components involved in the "bottom-up" synthesis of Category I-type nanoparticles are assumed to be conserved. Secondly, a >90% CNDP monodispersity criteria is imposed as a critical selection requirement for all proposed hard and soft particle nanoelement categories. Thirdly, based on the predictions by physicist, Nobel Laureate, Anderson (1972), there should be totally different expectations for anticipated nanoelement and nanocompound behaviors at this new level of complexity. Simply stated, as one breaks hierarchical symmetry by advancement to higher complexity, the whole becomes not only more than, but very different from the sum of its parts. One should expect to observe totally new emerging nanomaterial properties/patterns unprecedented and uncharacteristic for the less complex precursors. Finally, at the picoscale level, elemental CADPs are relatively fixed and untunable by normal means thus allowing only a limited number of elemental periodic property patterns. In contrast, the CNDPs of both hard/soft nanoelement categories are highly tunable and as such should be expected to yield an almost endless number of nanoperiodic property patterns by design. It is from this perspective, that a survey of the literature produced a surprisingly large number of nanoperiodic property pattern examples for both the hard/soft nanoelement categories and their compounds. The intention of this section is to present only a small sampling from this list. These examples appear to emerge largely from the discrete core–shell nanoarchitecture/compositions and systematic features of the CNDPs associated with the proposed hard/soft nanoelement categories and their compounds.

To our knowledge, no attempt has been made to organize these nanoperiodic property patterns as a function of nanoelement categories and nanocompounds; or more importantly in the larger context of a systematic nanomaterials framework.

With this important objective in mind, we now focus on compelling literature examples that connect an abundance of immutable nanoperiodic properties intrinsic to these proposed nanoelements and their nanocompounds. These critical connections clearly provide an initial platform for periodic property prediction and validation. Further identification and elaboration of these fundamental periodic patterns should be expected to evolve a "big picture perspective" and demonstrate the usefulness of this proposed framework for unifying nanoscience. Since there are so many CNDP-dependent properties (i.e., size, shape, surface chemistry, etc.) related to this proposed "nanoperiodic system" in the literature, we are compelled to present only a limited sampling. These periodic property patterns are presented in Tables 5–8 with leading references to (a) intrinsic physicochemical and (b) functional/application-type property patterns for specific nanoelements and in their compounds. These tables are followed by a sampling of illustrated examples and are organized as follows beginning with (Table 5):

Additional illustrated literature examples of these nanoperiodic property patterns are included in the Supporting Information Section.

Size-dependent nanoperiodicity: *melting points* (metal nanoclusters [H-1]-type nanoelements)

As a metal nanocluster becomes smaller, the percentage of surface atoms becomes greater. Therefore, as the coordination number of the surface atoms becomes smaller than 9, these atoms are more easily rearranged than those in the center. Thus, the melting process begins earlier. This accounts for the periodic and systematic decrease in melting points as a

Table 5 Hard particle nanoelement periodic property patterns

	Hard particle nanoelement categories					
						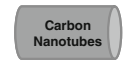
	Hard particle nanoelement nanoperiodicity					
	Metal (M°) nanoclusters	Metal chalcogenides nanocrystals	Metal oxide nanocrystals	Silica nanoparticles	Fullerenes	Carbon nanotubes
	[H-1]	[H-2]	[H-3]	[H-4]	[H-5]	[H-6]
Nanoelement (intrinsic physicochemical) periodic properties						
Encapsulation						
Melting points/glass transition temperatures	Castro et al. (1990) and Klabunde (2001)					
Reactivity/sterics						
Refractive indices						
Self-similar aggregation	Schmid et al. (2000) and Thomas et al. (2001)					
Valency/directionality	DeVries et al. (2007) and Kruger et al. (2008)					
Conductivity						Charlier (2002)
Nanoelement (functional/application) periodic properties						
Catalysis						
Electronic						Charlier (2002)
Imaging			Hultman et al. (2008)			Lacerda et al. (2008)
Magnetic			Yavuz et al. (2006)			
Nanotoxicity	(2007)				Sayes et al. (2004) and Lewinski et al. (2008)	Carrero-Sanchez (2006), Sayes et al. (2006), and Lacerda et al. (2008)
Photonics	Kelly et al. (2003), Mirkin (2005), and Ramakrishna et al. (2008)	Alivisatos (1996) and Yu et al. (2003)				
Nanomedicine	Loo et al. (2004)	Gao et al. (2008)				Lacerda et al. (2008)

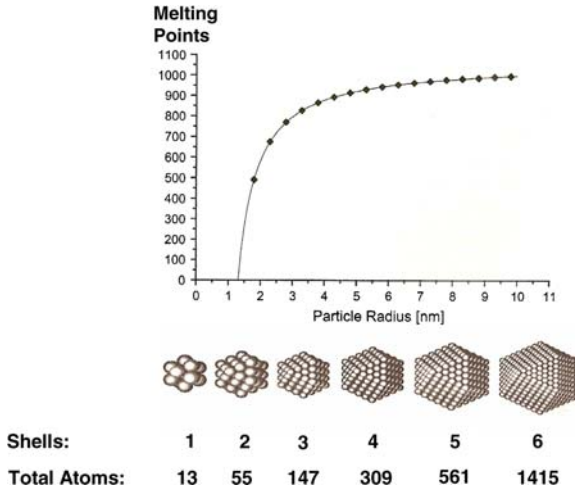

Fig. 32 The relationship between gold-nanocluster size, the total number of atoms in full (saturated) shell, metal clusters and their melting points. Reproduced with permission from Klabunde (2001). Copyright: Wiley-VCH Verlag GmbH & Co. KGaA.

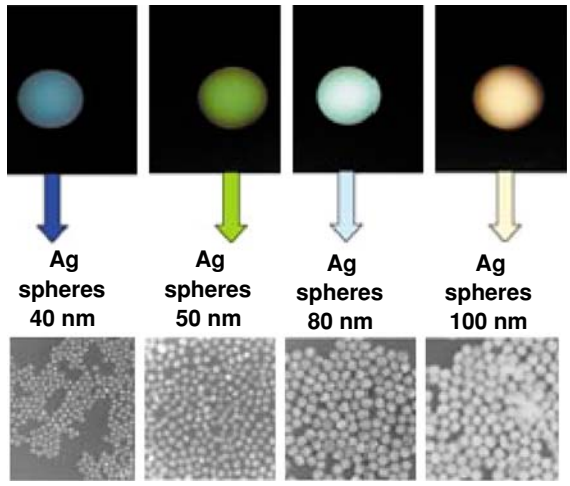

Fig. 33 Nanoperiodic Raleigh light scattering (LSPR) properties of silver nanoclusters as a function of size with associated TEM images illustrating monodispersities. Reproduced with permission from Mirkin (2005). Copyright: Wiley-VCH Verlag GmbH & Co. KGaA.

function of nanoscale size (Fig. 32). Such a periodic property does not exist in bulk materials of the same elemental composition. The "magic numbers" associated with the closed shell saturation levels and associated melting point behavior (Klabunde 2001) have been well documented by mass spectrometry (Brack 1993) and also represent a very important nanoperiodic property pattern (Fig. 32) (Castro et al. 1990).

Size/composition-dependent nanoperiodicity: *photonics* (*fluorescence*) (metal nanoclusters [H-1]-type nanoelements)

Nanoperiodic, size-dependent Rayleigh light scattering properties are widely recognized for [H-1]-type hard particle nanoelement categories such as gold or silver nanoclusters (Mirkin 2005) (Fig. 33). This phenomenon is referred to as *localized surface plasmon resonance* (*LSPR*) and involves scattering interactions between impinging light and the nanostructure. Specifically, the oscillating electric field of the incoming light causes coherent oscillation of the conduction electrons, resulting in a concomitant oscillation of the electron cloud surrounding the metal nuclei. An extensive review of LSPR has been published (Kelly et al. 2003).

Size/band-gap-dependent nanoperiodicity: *photonics* (*fluorescence*) (metal chalcogenides [H-2]-type nanoelements)

Dimensional constraints in a 0D nanoentity that are smaller than a De Broglie wavelength produce quantum confinement behavior. Such systems are referred to as *quantum dots* (Weller 1993; Schmid 2004). Accordingly, it is well known that hard nanoparticles (i.e., semiconducting cadmium chalcogenides etc.) exhibit nanoperiodic, size-dependent photonic behavior and produce size-dependent fluorescence emission colors in the visible region (Fig. 34). These emission patterns may be tuned as a function of nanoscale size, as well as band gap properties that are determined by the composition of the nanoparticle. These effects are illustrated in Fig. 34. This area has been extensively reviewed elsewhere (Weller 1993; Alivisatos 1996; Burda et al. 2005).

Size/composition-dependent nanoperiodicity: *Magnetism* (metal oxides [H-3]-type nanoelements)

An interesting nanoperiodic property pattern relating size-dependent retention of monodisperse Fe_3O_4 nanoparticles (i.e., 4–20 nm) in the presence of low magnetic fields was demonstrated by Colvin et al. (Yavuz et al. 2006). It was shown that Fe_3O_4

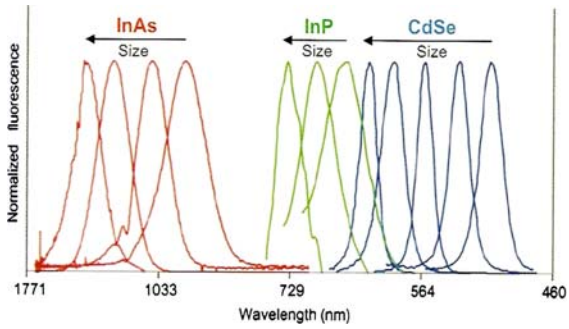

Fig. 34 Nanoperiodic fluorescence emission properties for semiconducting QD as a function of composition, band-gap mismatch, and size (Alivisatos 1996). Reprinted from Alivisatos (1996). Copyright (1996), with permission from AAAS

nanoparticles do not act independently in this differentiation process, but rather aggregate reversibly due to high field gradients present at their surfaces. This periodic behavior pattern allowed the effective separation of 4 nm from 12 nm Fe_3O_4 nanoparticle mixtures by applying different magnetic fields as illustrated in Fig. 35.

Surface chemistry-dependent nanoperiodicity: *nanotoxicology* (fullerenes [H-5]-type nanoelements)

Important periodic nanotoxicological patterns have been noted by Colvin et al. (Sayes et al. 2004) for 0D fullerenes. These cytotoxicity properties are related to

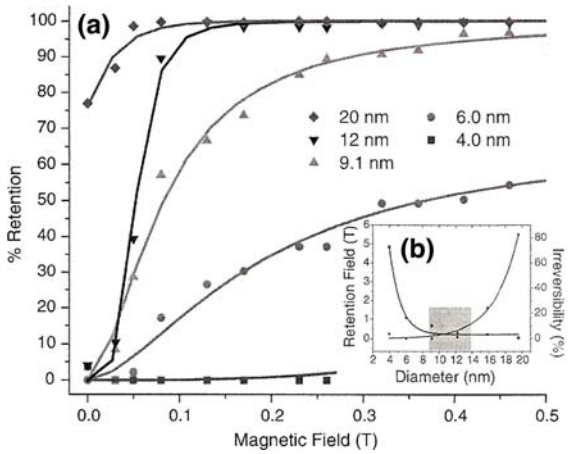

Fig. 35 Nanoperiodic magnetic-field induced retention properties as a function of metal oxide [H-3]-type nanoelement size (Yavuz et al. 2006). Reprinted from Yavuz et al. (2006). Copyright (2006), with permission from AAAS

the type and amount of nanoparticle surface functionality. Generally, higher levels of water-solubilizing functionality on a fullerene surface tend to reduce toxicity (Fig. 36). An extensive review covering periodic cytotoxicity property patterns for a large variety of hard particle nanoelements (i.e., 0D and 1D) has recently been published by Lewinski et al. (2008).

Rigid architecture-dependent nanoperiodicity: *electronic* (semiconductive/conductive) (carbon nanotubes [H-6]-type nanoelements)

As synthesized, SWNTs usually consist of a mixture of semiconducting (SC) and metallic-like conducting (C) architectures. It has been determined that the armchair (5,5) configuration exhibits metallic behavior, whereas the zigzag (7,0) architecture manifests semiconducting properties (Charlier 2002). Plots of energy versus density states, Fig. 37, clearly demonstrate this property difference due to this subtle architectural change. The value of this nanoelement category as mixtures of (C) and (SC) types is severely limited for thin-film transistors where high mobility and on/off ratios are essential. It has been found recently (Kanungo et al. 2009), that the deleterious (C) configuration may be selectively reacted out by [2 + 2] cycloaddition reactions involving fluorinated vinylethers to yield a residual (SC)-type SWNT architecture with good mobility and on/off features suitable for electronic device applications (Table 5).

Size/flexibility/architecture-dependent nanoperiodicity: *viscosities, densities, and refractive indices* (dendrimers [S-1]-type nanoelements)

Soft particle dendrimer core–shell-based nanoelements are macromolecules (polymers) that exhibit completely different physicochemical properties compared to traditional polymers. This is largely due to congestion properties that emerge as a function of generational growth. Growth of tethered branched chains from a common core produces amplification of terminal groups (Z) as a function of the core multiplicity (N_c) and branch multiplicity (N_b) according to $Z = N_c N_b^G$. Congestion increases dramatically as a function of generation (Fig. 38). Plots of intrinsic viscosity [η], density(d),

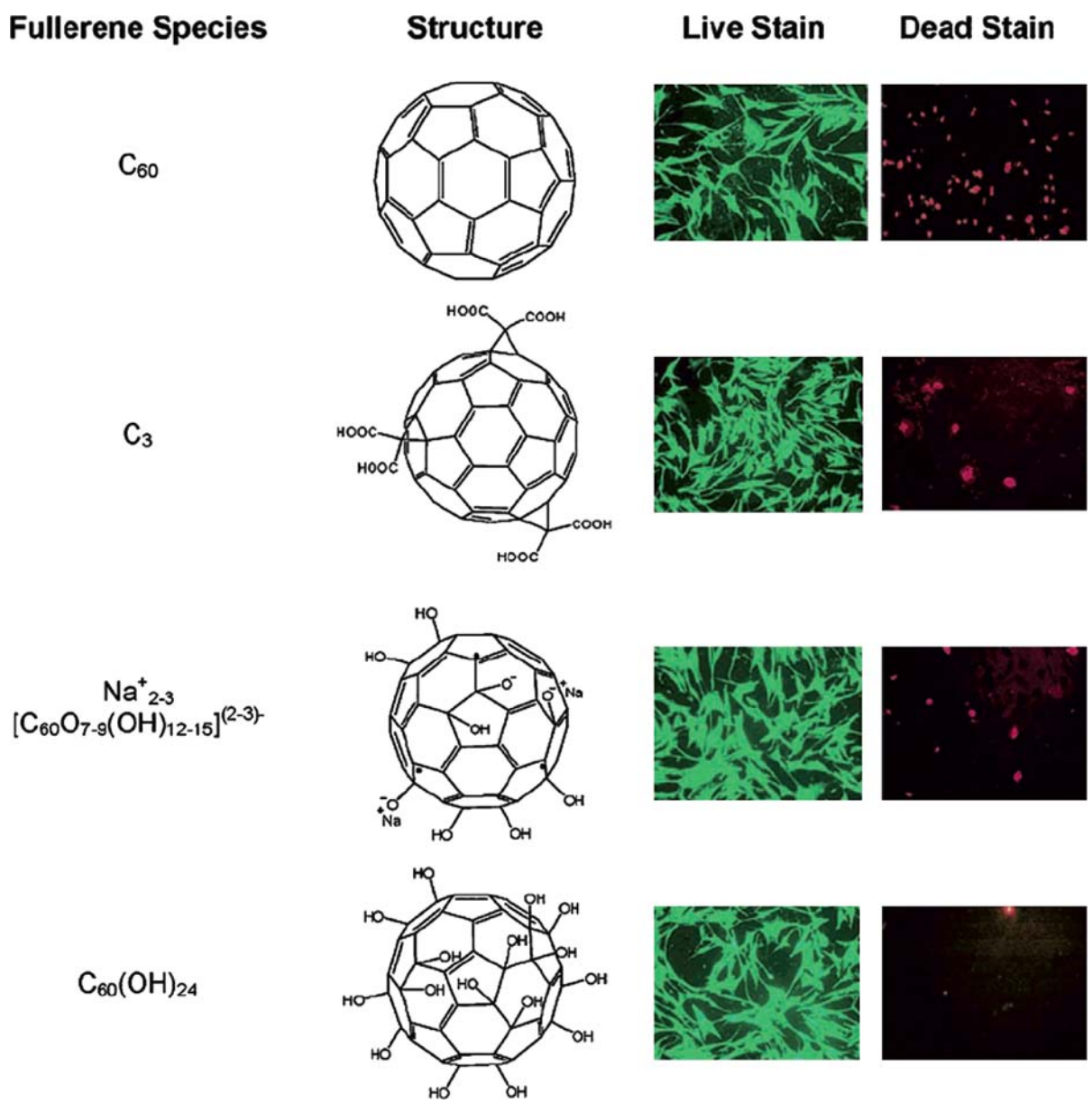

Fig. 36 Surface chemistry-dependent nanotoxicity properties. Surface chemistries associated with human dermal fibroblast live/dead cell viability assay results for C_{60} and its derivatives. Reprinted with permission from Sayes et al. (2004). Copyright: 2004 American Chemical Society

surface area per Z group (A_z), and refractive index as a function of generation clearly show maxima or minima at generations = 3–5. This parallels similar computer-assisted molecular-simulation predictions (Tomalia et al. 1990) as well as extensive photochemical probe experiments reported by Turro et al. (Gopidas et al. 1991; Turro et al. 1991; Ottaviani et al. 1996; Jockusch et al. 1999; Fréchet and Tomalia 2001).

Dendrimer-based intrinsic viscosities [η] increase in a classical fashion as a function of molar mass (generation), but decline beyond a critical generation due to a congestion-induced shape change. A shape change occurs from an extended compressible configuration in the early generations (i.e., $G = 0$–3) to more rigid globular shapes in the later generations (i.e., $G = 4$–10). In effect, at critical generations (i.e.,

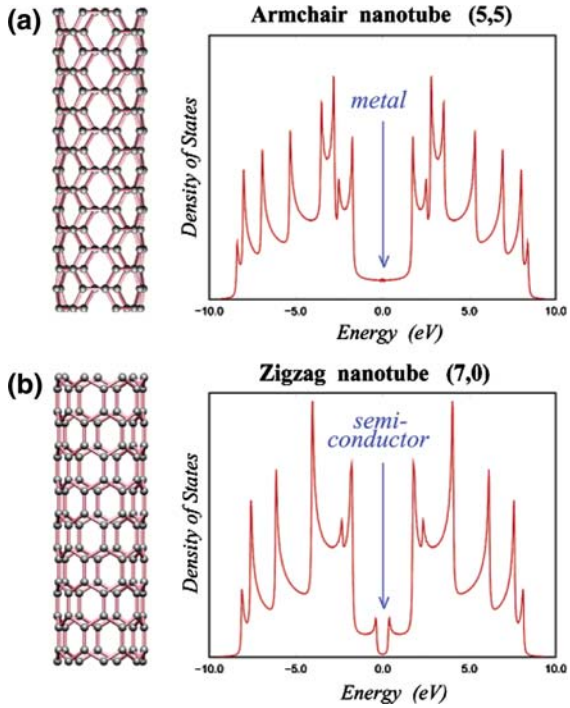

Fig. 37 Electronic properties of two different carbon nanotubes. **a** The armchair (5,5) nanotube exhibits a metallic behavior (finite value of charge carriers in the DOS at the Fermi energy, located at zero). **b** The zigzag (7,0) nanotube is a small-gap semiconductor (no charge carriers in the DOS at the Fermi energy). Sharp spikes in the DOS are van Hove singularities (**a**, **b**). Reprinted with permission from Charlier (2002). Copyright: 2002 American Chemical Society

$G = 3$–4), the dendrimer acts more like an Einstein spheroid. The intrinsic viscosity is a physical property expressed in dl/g, in essence the ratio of volume to a mass. As the generation number increases and transition to a spherical shape takes place, the volume of the spherical dendrimer roughly increases in cubic fashion while its mass increases exponentially; hence, the value of $[\eta]$ must decrease once a certain generation is reached. This prediction has now been confirmed experimentally (Tomalia et al. 1990; Fréchet 1994).

Size/surface congestion/architecture-dependent nanoperiodicity: *nanoencapsulation* (dendrimers [S-1] core–shell-type nanoelements)

Dendrimer surface congestion can be appraised mathematically as a function of generation according to the following simple relationship:

$$A_z = \frac{A_D}{N_Z} \alpha \frac{r^2}{N_c N_b^G},$$

where A_z is the surface area per terminal group Z, A_D the dendrimer surface area, and N_z the number of surface groups Z per generation. This relationship predicts that the surface area per Z group at higher generations G becomes increasingly smaller and experimentally approaches the cross-sectional area or van der Waals dimension of the surface group Z. Congestion at these generations (G) is referred to as "*de Gennes dense-packing*." Ideal dendritic growth without branch defects is possible only for those generations preceding this dense-packed state. This critical dendrimer property gives rise to self-limiting dendrimer dimensions, which are a function of the branch cell segment length (I), the core multiplicity N_c, the branch cell juncture multiplicity N_b, and the steric dimensions of the terminal group Z. Dendrimer radius r in the above expression is dependent on the branch cell segment lengths l, wherein large l values delay congestion. On the other hand, larger N_c, N_b values and larger Z dimensions dramatically enhance congestion. These congestion properties are unique for each dendrimer family, wherein N_c and N_b determine the generation levels within a family that will exhibit nanoencapsulation properties. Higher N_c and N_b values predict that lower generation levels will produce appropriate surface congestion properties to manifest encapsulation features (Fig. 39).

Shape/surface functionality/architecture-dependent nanoperiodicity: *designed bottom-up self-assembly* (dendron/dendrimer [S-1] core–shell-type nanoelements)

Percec et al. (Rudick and Percec 2008) have pioneered the introduction of mesogenic groups to prepare amphiphilic dendrons and dendrimers that produce a wide range of supramolecular self-assemblies (Percec et al. 1995). These amphiphilic dendritic building blocks are encoded with information that defines their 3D shape (e.g., flat-tapered or conical) and how they associate with each other. Dendron shapes and surface functionality play a key role in determining the course of these self-assemblies (Percec et al. 1998, 2003; Tomalia 2003). When

Table 6 Soft particle nanoelement periodic property patterns

	Soft particle nanoelement categories					
		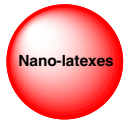	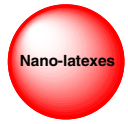	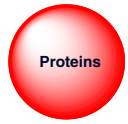	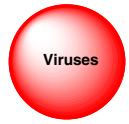	
	Soft particle nanoelement nanoperiodicity					
	Dendrimers/dendrons	Nanolatexes	Polymeric micelles	Proteins	Viruses	RNA/DNA
	[S-1]	[S-2]	[S-3]	[S-4]	[S-5]	[S-6]
Nanoelement (intrinsic physicochemical) periodic properties						
Encapsulation nanoreactors	Naylor et al. (1989), Tomalia et al. (1990), Balogh and Tomalia (1998), Hecht and Fréchet (2001), and Vriezema et al. (2005)			Vriezema et al. (2005)	Vriezema et al. (2005))	
Melting points/ glass transition temperatures	Tomalia and Dvornic (1996), Uppuluri (1998), and Dvornic and Tomalia (1999)					
Reactivity/ sterics	Tomalia et al. (1990), Singh (1998), and Swanson et al. (2007)	Larpent et al. (2004)		Singh (1998)		
Refractive indices	Tomalia et al. (1990)					
Self similar aggregation	Tomalia et al. (1985,1986) and Jackson et al. (1998)					
Valency/ directionality	Tomalia et al. (1990), Singh (1998), and Crespo et al. (2005)	Larpent et al. (2004)		Singh (1998) and Crespo et al. (2005)		Loweth et al. (1999) and Xu et al. (2006)
Viscosity	Tomalia et al. (1990) and Uppuluri et al. (1998)					
Nanoelement (functional/application) periodic properties						
Catalysis	Vriezema et al. (2005) and Andres et al. (2007)			Vriezema et al. (2005)	Vriezema et al. (2005))	
Electronic	Miller et al. (1997) and Tabakovic et al. (1997))					
Imaging	Wiener et al. (1994), Langereis et al. (2007), and Tomalia et al. (2007)					
Magnetic	Knecht and Crooks (2007)					
Nanotoxicity	Klajnert and Bryszewska (2007)					

Table 6 continued

	Soft particle nanoelement nanoperiodicity					
	Dendrimers/ dendrons [S-1]	Nanolatexes [S-2]	Polymeric micelles [S-3]	Proteins [S-4]	Viruses [S-5]	RNA/DNA [S-6]
Photonics	Mongin et al. (2007)					
Nanomedicine	Boas et al. (2006), Klajnert and Bryszewska (2007), and Tomalia et al. (2007)					

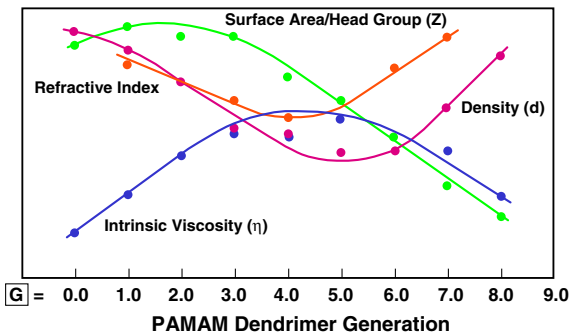

Fig. 38 Comparison of surface area/head group (Z), refractive index, density (d), and viscosity (η) as a function of generation $G = 1$–9 (Fréchet and Tomalia 2001). Copyright: Wiley-VCH Verlag GmbH & Co. KGaA

appended to a covalent linear backbone polymer, the self-assembling dendrons direct a folding process (i.e., intramolecular self-assembly). Alternatively, intermolecular self-assembly may occur due to non-covalent interaction between apex groups to generate a supramolecular backbone. These amphiphilic dendron-type self-organizations involve spontaneous supramolecular formation of periodic and quasiperiodic arrays to produce a wide variety of morphologies as shown in Fig. 40. Covalent and supramolecular polymers jacked with self-assembling dendrons may yield nanoscale cylinders (Hudson et al. 1997) or spheroids (Rudick and Percec 2008). The shape of the final assembled object is determined by the primary

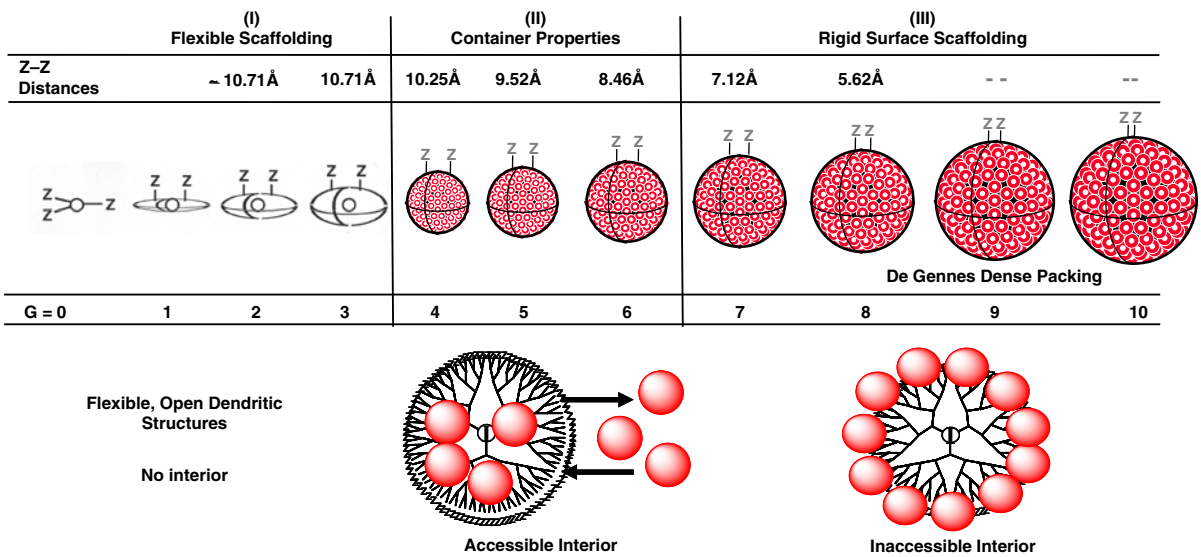

Fig. 39 Congestion-induced dendrimer shape changes (I, II, and III) with development of nanocontainer properties for a family of poly(amidoamine) (PAMAM) dendrimers: $N_c = 4$; $N_b = 2$, where Z–Z = distance between surface groups as a function of generation

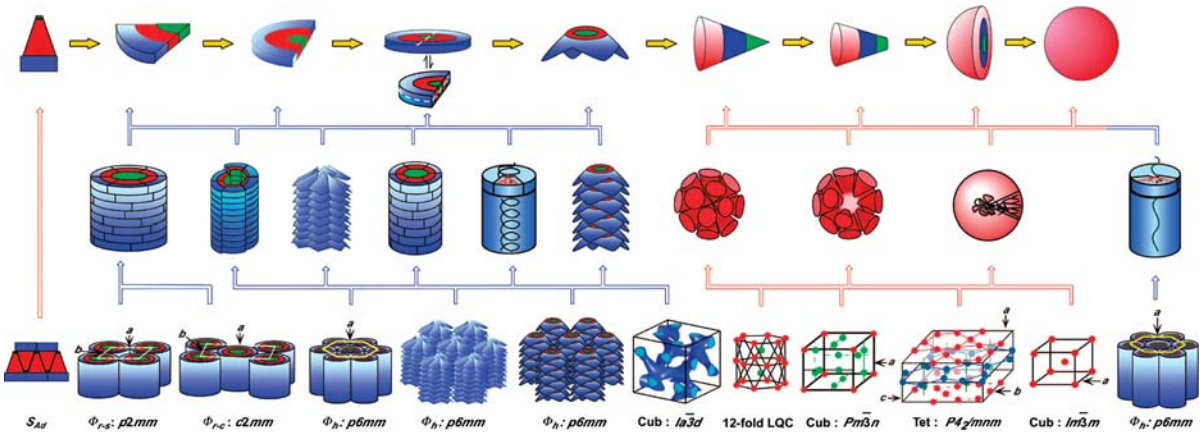

Fig. 40 Structural design of dendrons as a function of their size, shape, surface chemistry, flexibility, and composition to produce a wide variety of self-assembled nanocompounds. Reprinted with permission from Percec et al. (2007). Copyright: 2007 American Chemical Society

structure of the dendronized polymer, namely, the structure of the self-assembling dendron and the length of the polymer backbone to which it is appended. Based on these many accumulated nanoscale periodic assembly patterns, it is possible to predictably generate dendritic building blocks suitable for *designed bottom-up self-assembly* (Percec et al. 2008), (Percec et al. 1998; 2007, 2008a, b; Rudick and Percec 2008).

Related pioneering work by Zimmerman et al. (1996) demonstrated the self-assembly of suitable focal point-functionalized dendrons to produce very well-defined spheroidal-type dendrimer structures. These non-binding assembly processes are usually driven by selective hydrogen bonding of the focal point appended dendron to produce the more complex spheroidal dendrimers.

Surface chemistry/self-assembly/sequence architecture-dependent nanoperiodicity: *nanomedicine—(hemostasis)* (protein subunits; polypeptides [S-4]-type nanoelements)

Based on the early study of Rich et al. (Zhang et al. 1993), it has been found that an ionic, 16-residue $[Ala\text{-}Glu\text{-}Ala\text{-}Glu\text{-}Ala\text{-}Lys\text{-}Ala\text{-}Lys]_2$ self-complementary polypeptide nanoelement (1.3 × 5.0 nm), spontaneously self-assembles under physiological conditions to produce interwoven nanofilaments of (~ 10 to 20 nm). Such materials are referred to as "self-assembling peptide nanofiber scaffolds" (SAPNS) (Fig. 41; Ellis-Behnke et al. 2006b). These SAPNSs are obtained from specific polypeptide sequences that contain self-complementary positive/negative L-amino acids and form hydrated scaffolds in the presence of

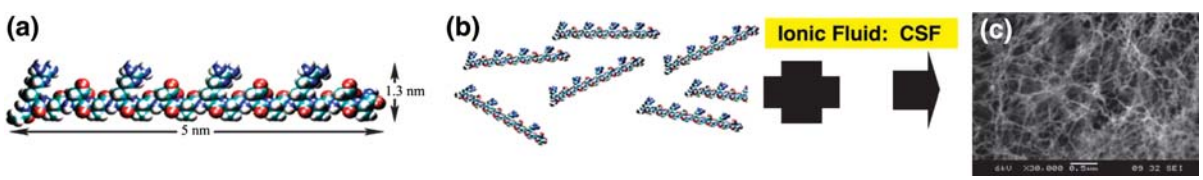

Fig. 41 Small self-complementary 16-residue polypeptide nanoelements that organize into "self-assembled peptide nanofiber scaffoldings" (SAPNS) and exhibit substantive adhesion to extracellular matrices (Ellis-Behnke et al. 2006a, b). Reproduced from Ellis-Behnke et al. (2006b). Copyright 2006, with permission from National Academy of Sciences, USA

physiological body fluids or serum. These nanoscale SAPDNs form highly substantive, adhesive interfaces with extracellular matrices surrounding a lesion. As such, recent study by Ellis-Behnke et al. (2006a) has shown that these materials are very effective as nanofiber adhesives/scaffolding for brain tissue repair and axon regeneration by providing unprecedented control over hemostasis (i.e., bleeding) (Fig. 42).

Size/surface chemistry-dependent nanoperiodicity: *nanotoxicology* (*in vitro*) (dendrimers [S-1] core–shell-type nanoelements)

In vitro cytotoxicology for dendrimers has been determined as a function of dendrimer surface groups using several widely recognized assays such as (a) LDH assay (i.e., cell membrane damage causes leakage of lactate dehydrogenase), (b) MTT assay (i.e., determines the extent of cell membrane damage based on MTT permeability into cell), and (c) hemolysis assay (determines cell membrane damage based on the release of hemoglobin) and AFM/SEM analysis (visualizes cell damage/viability) (Tomalia et al. 2007). Many of these assays as well as others were used to evolve the in vitro nanoperiodic toxicology patterns illustrated in Fig. 43. A well-known cytotoxicity pattern for both hard and soft nanoparticle elements is that the cationic surface functionality will cause severe size-, charge density-dependent cell membrane damage (Boas et al. 2006;

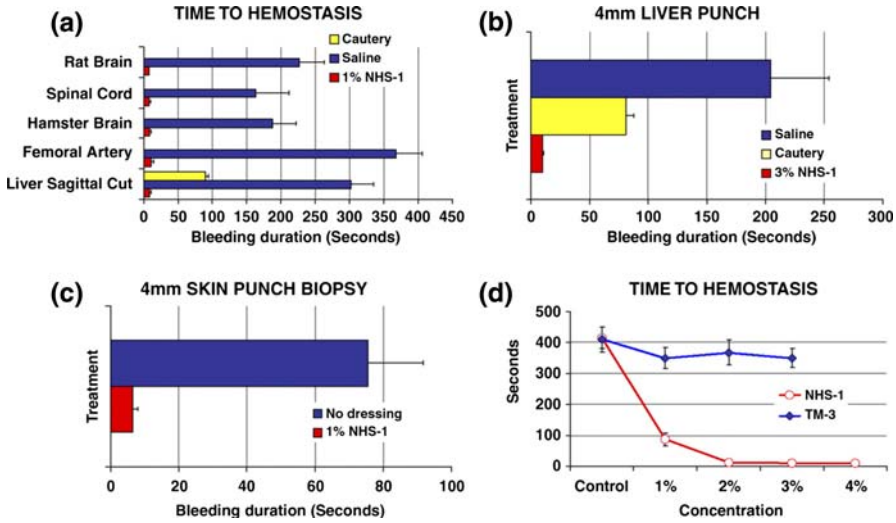

Fig. 42 Periodic functional properties of "self-assembled peptide nanofiber scaffoldings" (SAPNS): **a** time to hemostasis for various lesion sites; **b** bleeding duration for 4 mm liver punch; **c** bleeding duration for 4 mm skin punch; and **d** duration of hemostasis as a function of concentration (Ellis-Behnke et al. 2006a, b). Reprinted from Ellis-Behnke et al. (2006a). Copyright (2006), with permission from Elsevier

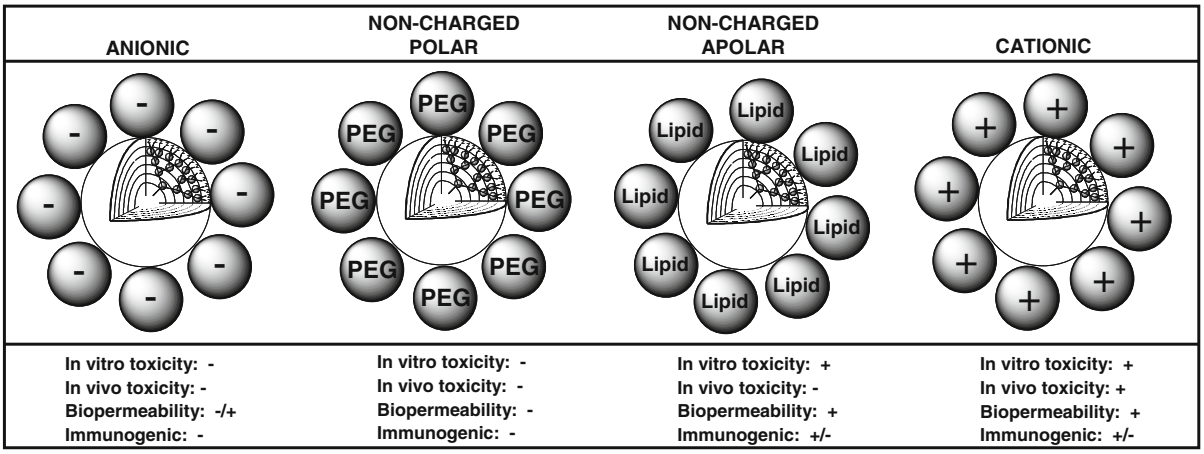

Fig. 43 Generalized patterns (±) illustrating in vitro nanotoxicity, biopermeability, and immunogenic properties as a function of dendrimer surface chemistry. Reprinted with permission from Tomalia et al. (2007b). Copyright: 2007 Biochemical Society, London

Klajnert and Bryszewska 2007). An in-depth nanotoxicity study on poly(amidoamine) (PAMAM) dendrimers has recently been reported by the Nanotechnology Characterization Laboratory (NCL) (http://ncl.cancer.gov) (2006) (Table 6).

Size, interior architecture-dependent nanoperiodicity: *nanocontainer properties* (fullerenes [H-5], nanotubes [H-6], dendrimers [S-1], proteins [S-4], and viruses [S-5]-type nanoelements)

Systematic nanoperiodic property patterns exist for both hard and soft nanoelements based on their inherent sizes and interior architectures. Both metal and organic guest molecules may be captured by many hard and soft particle nanoelement hosts. As shown in Fig. 44, the size and quantity of guest molecules increases from left to right. Only small numbers of metal atoms may be incarcerated in [H-4] fullerenes (Feng et al. 2008) with the possibility of larger numbers in [H-5] carbon nanotubes. In the case of larger soft particle nanoelement categories such as [S-1] dendrimers (Balogh and Tomalia 1998; Balogh et al. 2001; Hecht and Fréchet 2001), [S-4] proteins(Vriezema et al. 2005) (Mann and Meldrum 1991), and [S-5] viruses (Vriezema et al. 2005; Chen et al. 2006), it is possible to encapsulate many smaller hard nanoelement categories such as [H-1] metal nanoclusters, [H-2], metal chalcogenides, and [H-3] metal oxide-type categories. Large quantities of organic guest molecules may be encapsulated in either dendrimers (Naylor et al. 1989) or viruses. Figure 45 shows a TEM of gold nanoclusters within a BMV protein capsid cage to produce metal nanocluster:virus [H-1:S-5]-type core–shell nanocompounds. In fact, the pathogenic features of natural viruses are intrinsically based on the encapsulation of [S-6]-type DNA/RNA nanoelements within their interiors (Levine 1992).

Chen et al. (2006) have shown that gold nanoclusters may be used as templates for assembling viral-type protein cages (Fig. 45). They show that functionalized gold particles can initiate a virus-like particle (VLP) assembly by mimicking the electrostatic RNA/DNA behavior (i.e., nucleic acid component) of the native virus to produce [H-1:S-5] core–shell-type nanocompounds as shown in Fig. 45. It is important to note that by analogy, all common pathogenic virus particles containing RNA/DNA may actually be viewed as examples of the [S-6:S-5]-type core–shell nanocompounds (Levine 1992).

In conclusion, it may be stated that nanoencapsulation is clearly a periodic property shared by both hard and soft nanoelement categories.

Size/surface chemistry-dependent nanoperiodicity: *nanovalency/nanosterics* (dendrimers [S-1]-type nanoelements and [S-1:S-1] compounds)

Recent soft particle nanoelement [S-1] (Tomalia 2005) investigations have demonstrated that mathematically defined periodic size properties of spheroidal dendrimers determine chemical reactivity patterns involved in the assembly of precise dendrimer clusters [i.e., core–shell (tecto)dendrimers]. Mathematical relationships (i.e., the Mansfield–Tomalia–Rakesh equation) predict dendrimer cluster saturation levels (i.e., magic numbers for dendrimer shells) as a function of the size of the core dendrimer relative to the size of the shell dendrimers that are being used to construct the dendrimer cluster (Mansfield et al. 1996; Tomalia 2005). These periodic property patterns and magic shell relationships (Fig. 46) are very reminiscent of those observed for metal nanocrystals (Fig. 8). For example, in a core–shell gold nanocluster containing a single gold atom core, one observes 12 gold atoms in the first shell. This value is predicted in the Mansfield–Tomalia–Rakesh concept described in Fig. 46 when the ratio of core spheroid (r_1)/shell spheroid (r_2) = 1.

Size/surface functionality-dependent nanoperiodicity: *self-similar assembly (aggregation)* (metal nanocluster [H-1]-type nanoelements)

Giant clusters based on "magic number nuclearity" have been reported to form via self-assembly of core–shell Pd nanocrystals (i.e., nuclearity ~ 561 = closed atom shell (5), diameter 2.5 nm) (Thomas et al. 2001). Using transmission electron microscopy (TEM), discrete cluster diameters expected for Pd nanocrystals with nuclearities of 13, 55, 147, 309, 561, and 1,415 corresponding to clusters with closed shells of 1, 2, 3, 4, 5, and 7 were observed. Imaging at different tilt angles unequivocally confirmed the

Table 7 Nanoperiodic property patterns common to both hard and soft nanoelements

	Hard:hard/hard:soft/soft:soft nanocompound nanoperiodicity					
Hard particle nanoelements	Metal (M°) nanoclusters [H-1]	Metal chalcogenides nanocrystals [H-2]	Metal oxide nanocrystals [H-3]	Silica nanoparticles [H-4]	Fullerenes [H-5]	Carbon nanotubes [H-6]
Soft particle nanoelements	Dendrimers/ dendrons [S-1]	Nanolatexes [S-2]	Polymeric Micelles [S-3]	Proteins [S-4]	Viruses [S-5]	RNA/DNA [S-6]
Nanocompound (intrinsic physicochemical) periodic properties						
Encapsulation	[S-5:H-1]	Chen et al. (2006)				
	[S-5:H-3]	Vriezema et al. (2005)				
Melting points						
Reactivity/sterics	[S-6:H-1]	Xu et al. (2006)				
Refractive indices						
Self similar aggregation	[H-1:H-1]	Schmid et al. (2000) and Thomas et al. (2001)				
	[S-1:S-1]	Tomalia et al. (1985, 1986) and Jackson et al. (1998)				
Valency/ directionality	[S-1:H-1]	Huang and Tomalia (2005)				
	[S-1:H-3]	Martin et al. (2009)				
Viscosity						
Nanocompound (functional/application) periodic properties						
Catalysis	[S-1:H-1]	Wilson et al. (2006)				
	[S-4:H-1]	Ueno et al. (2004)				
	[H-1:H-1]	Chen et al. (2007)				
Electronic	[S-1:S-1]	Miller et al. (1997)				
Imaging	[H-1:H-1]	Su et al. (2007)				
	[H-4:H-2]	Koole et al. (2008)				
	[S-5:H-1]	Joo et al. (2008)				
	[H-3:H-4]	Bridot et al. (2007)				
Magnetic	[S-1:H-3]	Frankamp et al. (2005)				
Nanotoxicity	[S-1:H-5]	Kostarelos (2008)				
Photonics	[H-1:H-4]	Hirsch et al. (2003)				
	[H-2:H-2]	Zimmer et al. (2006)				
	[H-4:H-2]	Koole et al. (2008)				
	[S-4:H-1]	Bardhan et al. (2009)				
	[H-3:H-4]	Bridot et al. (2007)				
Nanomedicine	[S-1:H-3]	Martin et al. (2008)				
	[S-4:H-6]	McDevitt et al. (2007)				
	[S-3:S-6]	Nishiyama and Kataoka (2006)				

spherical nature of these giant hierarchical clusters. Giant clusters derived from Pd nanocrystals, nuclearity $\sim 1{,}415$ = closed atom shell (7), diameter = 3.2 nm, were observed in Fig. 10.

Metal nanocrystals with magic numbers of atoms, namely, 13, 55, 309, 561, and 1,415 corresponding to 1, 2, 3, 4, 5, and 7 closed shells have been prepared by chemical means (Vargaftik et al. 1991; Schmid et al. 1993, 2000; Rao 1994; Teranishi et al. 1997).

Analogous gold nanocrystals with nuclearities 13 and 55 have been reported by Schmid et al. (Schmid and Klein 1986; Schmid 1988; Fritsche et al. 1997). Generation of naked Au_{55} clusters under mild

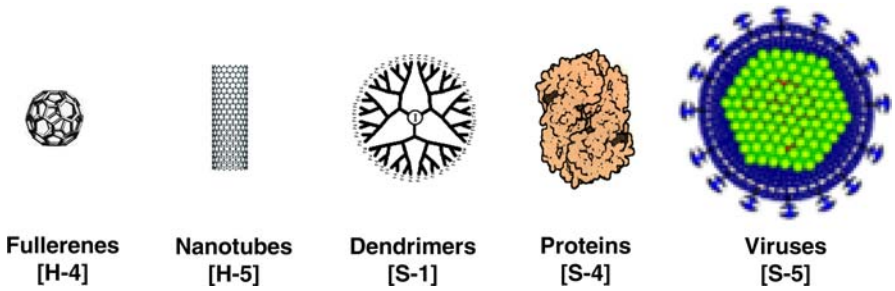

Fig. 44 Hard and soft particle nanoelements exhibiting nanoencapsulation properties that are dependent on guest size/composition as well as on interior features of nanoelement hosts. This is a property common to both hard and soft particle nanoelement hosts. Hosts are arranged as a function of size (left to right), and order generally approximates the size and amount of guest nanoencapsulation that is possible

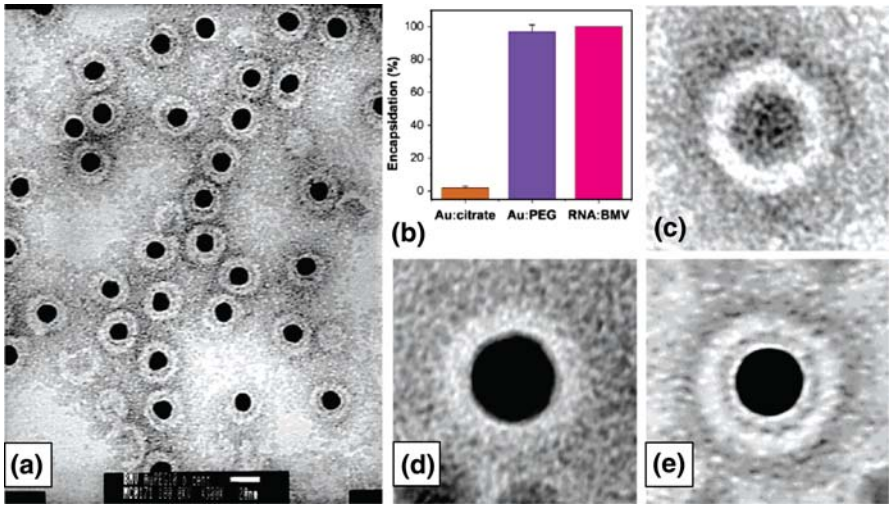

Fig. 45 **a** Transmission electron micrograph of negatively stained virus-like particles obtained from functionalized gold nanoparticles (black centers, 12 nm diameter) and BMV capsid protein. **b** Comparison of encapsulation yields for citrate: Au with the previous protocol8, Au:TEG, and native RNA. Averaged transmission electron micrograph of **c** empty BMV capsid, **d** citrate-coated VLP, and **e** TEG-coated VLP. The averages have been obtained by the superposition of 10 individual images, in each case. Reprinted with permission from Chen et al. (2006). Copyright: 2006 American Chemical Society

conditions was demonstrated by Schmid/Majoral et al. (Schmid et al. 2000; Fig. 47). Reaction of a $G = 4$ dendrimer (Z = 96 –SH surface groups) with $Au_{55}(PPh_3)_{12}Cl_6$ produced naked cubo-octahedra gold clusters that self-assembled into micron-sized crystals by metal–metal bonding via their edges in a regular manner to build superlattices which appear to be analogous to Pd super clusters reported by Rao et al. (Thomas et al. 2001).

Size/shape/architecture/composition-dependent nanoperiodicity: *photonics—(two-photon absorption)* (dendrimers [S-1] and metal nanoclusters [H-1]-type nanoelements)

Majoral et al. (Mongin et al. 2007) have pioneered the development of soft-particle nanoelements referred to as "organic quantum dots." These nanoparticles derived from [S-1]-type dendrimers

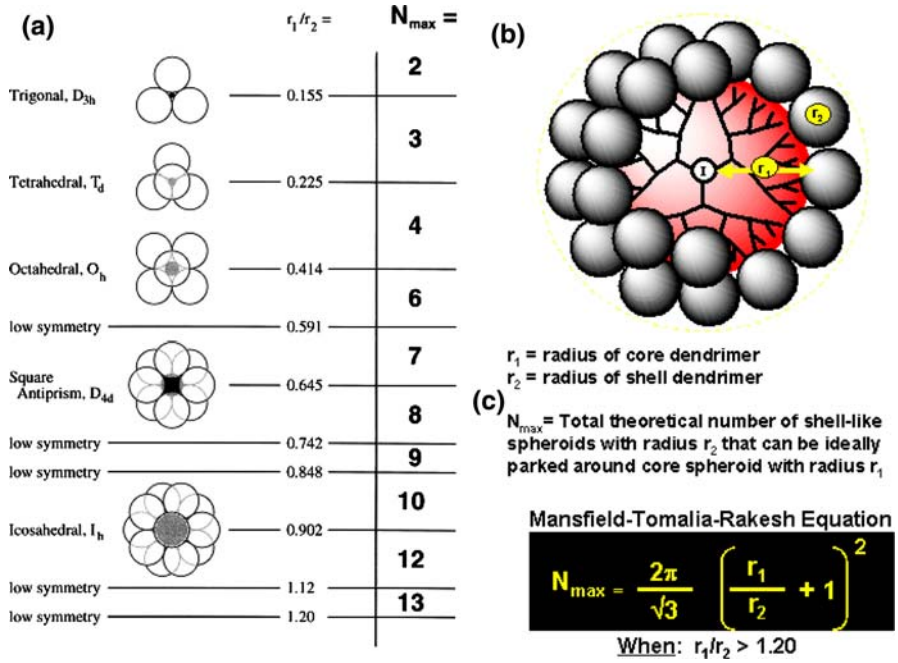

Fig. 46 **a** Symmetry properties of core–shell structures, where $r_1/r_2 < 1.20$. **b** Sterically induced stoichiometry based on the respective radii of core and shell dendrimers. **c** Mansfield–Tomalia–Rakesh equation for calculating the maximum shell filling when $r_1/r_2 > 1.20$. Reprinted with permission from Tomalia (2005) (Elsevier)

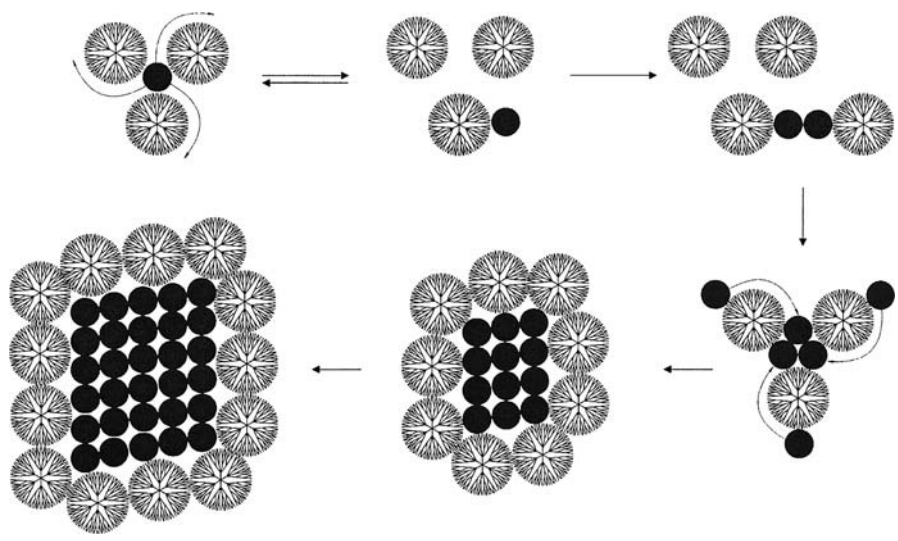

Fig. 47 Simplified illustration of the proposed (Au55) superstructure formation in the matrix of excess dendrimers. These peel off the PPh3 and Cl ligands from Au55(pph3)12Cl and thus allow cluster–cluster interactions, which subsequently leads to the observed microcrystals (Schmid et al. 2000). Copyright: Wiley-VCH Verlag GmbH & Co. KGaA

were found to exhibit two-photon absorption properties. This feature is based on conjugating high multiplicities of two-photon fluorophores on the surface of various dendrimer shapes. Two topologies were examined and referred to as "spheroidal-type organic nano dots" (SOND) or "dumb-bell-like organic nano dots" (DOND) (Fig. 48). Topology and size appear to influence the performance features by altering the proximity of surface fluorophores. As such, the more symmetrical SOND materials appear to exhibit better fluorescence properties. These lower toxicity organic QDs exhibit comparable brightness to hard particle QDs; they, however, have the advantage of not containing heavy metals and having high tunability for in vivo applications.

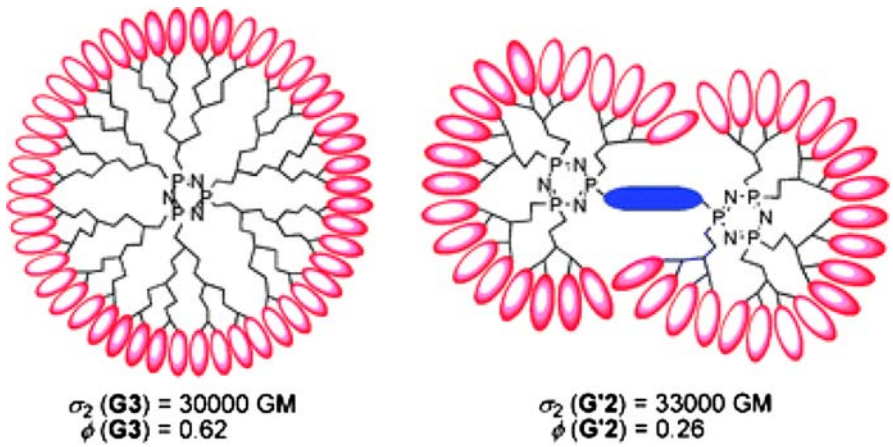

Fig. 48 Spheroidal-type nanodots (SONDs) and dumb-bell-like organic nanodots (DONDs) (Mongin et al. 2007). Reproduced by permission from The Royal Society of Chemistry (RSC) for the Centre National de la Recherche Scientifique (CNRS) and the RSC

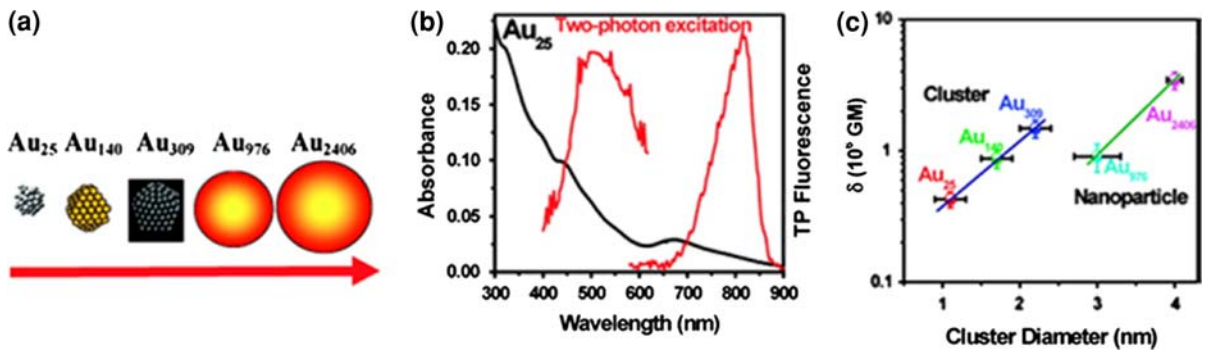

Fig. 49 **a** Nanoperiodic, two-photon fluorescence properties for various Au nanoclusters as a function of cluster sizes **b** absorbance of Au_{25} versus wavelength (nm). Note the two-photon absorption cross section (TPA) in **c** suggests a periodic transition between cluster Au_{309} and particle Au_{976}. Reprinted with permission from Ramakrishna et al. (2008). Copyright: 2009 American Chemical Society

Similarly, Goodson et al. (Ramakrishna et al. 2008) have reported two-photon absorption (TPA) features for [H-1]-type hard nanoparticle elements (i.e., small gold nanoclusters). The emission spectra of these gold nanoparticles were size dependent and tended to follow the surface plasmon absorption bands for gold clusters ranging from 25 (1.1 nm) to 2,406 (4 nm) (Fig. 49). The interesting trend of singularity in the TPA cross section suggests a periodic transition from cluster to nanoparticle behavior (Fig. 49c).

These (TPA) features observed for dendrimers [S-1] and metal nanoclusters [H-1]-type nanoparticles demonstrate a commonality of nanoperiodic properties that exist for both the hard and soft nanoelement categories.

Size/shape-dependent nanoperiodicity: *nanomedicine (MRI imaging; radiolabel imaging) nanotoxicity (renal clearance)* (dendrimers [S-1], metal chalcogenides [H-2], metal oxides [H-3], and carbon nanotubes [H-6]-type nanoelements

In vivo MRI imaging with dendrimer-based contrast agents was first demonstrated in the early 1990s by Lauterbur, Wiener, Brechbiel, and Tomalia (Wiener et al. 1994). These dendrimer-based MRI agents were found to exhibit enhanced relaxivity properties (R_1) as a function of generation as shown below (Fig. 50). This was attributed to enhanced gadolinium valency and larger sizes which contributed to more ideal rotational correlation coefficients. Based on the precise systematic continuum of dendrimer particle

sizes as a function of generation, Kobayashi and Brechbiel (2003; Kobayashi et al. 2003) were the first to define important nanoscale-dependent mammalian excretion routes (i.e., urinary vs. bile pathways). With these dendrimer-based systems, they found a very distinct preferred renal excretion mode below ~7 to 8 nm. Soft nanoparticle sizes above 8 nm tended to excrete via a bile pathway (Tomalia et al. 2007) (Fig. 50).

Similar nanosize-dependent renal excretion behavior (i.e., <10 nm diameter) has been reported only recently for hard nanoelements such as metal chalcogenides [H-2], (Zimmer et al. 2006), metal oxides [H-3], (Hultman et al. 2008), (Jain et al. 2008) and carbon nanotubes [H-6] (Kostarelos 2008).

It is interesting to note that rapid kidney clearance of radio-labeled carbon nanotubes does not appear to be sensitive to the longitudinal nanotube dimension. The CNT length used in this study is considerably larger than the dimensions of the glomerular capillary wall (i.e., minimum diameter of fenstra is 30 nm, thickness of the glomerular basement membrane in rats/humans is 200–400 nm, and width of the epithelial podocyte filtration slits is 40 nm) (Deen 2004). Therefore, the length of the CNT does not appear to be a critical parameter for renal clearance. A proposed mechanism suggests that the CNTs are ultra deformable in the blood circulation process and are able to reorient when they reach the glomerular filtration system and pass readily into the Bowman space and subsequently to the bladder.

Size/core–shell architecture-dependent nanoperiodicity: *photonics—(fluorescence-near IR)* (silica nanoparticle:metal nanoclusters [H-4:H-1] core–shell-type nanocompounds)

It has been shown by Halas et al. (Loo et al. 2004) that silica core–gold cluster shell nanocompounds exhibit systematic optical resonances as a function of their respective particle sizes as well as their core–shell thickness ratios as illustrated in Fig. 51. These investigators reported the development of an elegant nanoperiodic property pattern that relates the ratio of the

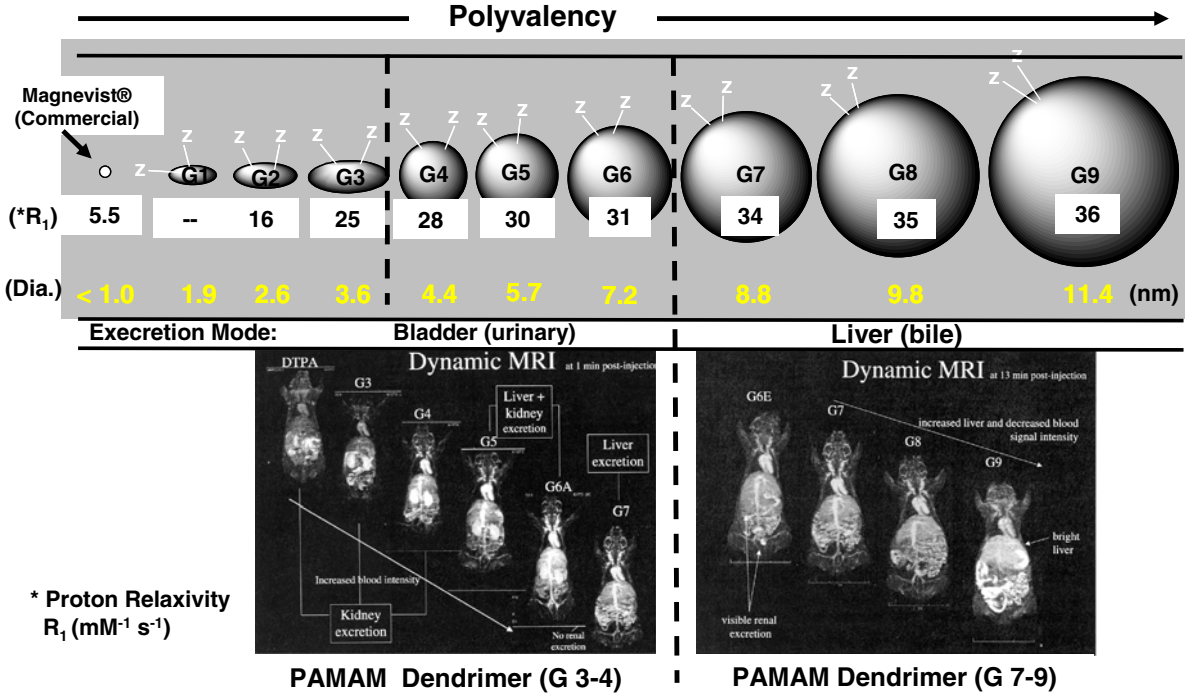

Fig. 50 Poly(amidoamine) (PAMAM) dendrimer generations 1–9 are scaled as spheroids. They are presented with their respective diameter sizes (nm) and proton relaxivity values, R_1 (mM^{-1} s^{-1}). Complete and rapid renal excretion is observed by MRI for generations smaller than $G = 6$. Liver (bile) pathways are observed for dendrimer generations larger than $G = 6$. MRI Images at bottom. Reprinted with permission from Kobayashi et al. (2003). Copyright (2003), with permission from BC Decker

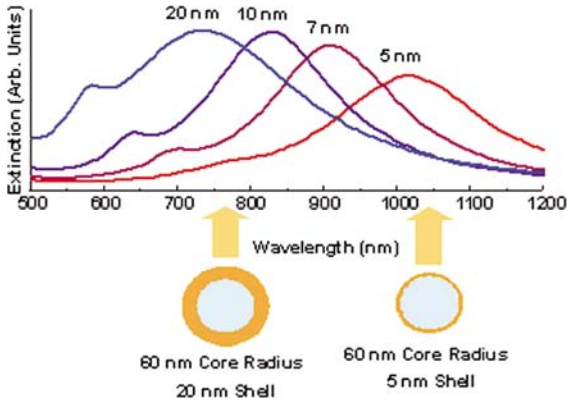

Fig. 51 Optical resonances of gold shell–silica core nanoshells as a function of their core/shell ratio. Respective spectra correspond to the nanoparticles depicted beneath (Loo et al. 2004). Published with permission from Loo et al. (2004). Copyright 2004: http://www.tcrt.org

silica core and metal shell (radii) to the observed resonance wavelength for the silica/metal-core–shell nanocompounds (Fig. 52; Table 8).

Size/surface chemistry/architecture-dependent nanoperiodicity: *nanovalency/sterics* (metal nanoclusters:dendron [H-1:S-1] and dendrimer–dendron:dendrimer–dendron [S-1:S-1]-type core–shell nanocompounds)

Surface reactions between polyvalent nanoparticle core substrates and nanoscale shell reagents have been shown to yield nanocompounds that upon analysis indicate that the actual core valency is reduced when allowed to react even with an excess of a nanoscale shell reagent. This phenomenon has been referred to as *sterically induced stoichiometry* (SIS) (Tomalia et al. 1990; Fréchet and Tomalia 2001; Tomalia 2005) or NSIS (Swanson et al. 2007). This nanoperiodic property pattern has now been documented for both hard [H-1] nanoelements (Gopidas et al. 2003a, b), Peng et al. (Aldana et al. 2001; Guo et al. 2003) and soft [S-1]-type nanoelements (Haddon et al. 2004; Huang and Tomalia 2005, 2006). Tomalia et al. have shown that monovalent, focal point-functionalized dendrons self assemble around metal nanoclusters or metal chalcogenide nanocrystals to produce core–shell nanocompounds that possess sterically saturated surfaces with unfulfilled surface valencies (Fig. 53). Related study noted a dendron-sized dependency as a function of core size (Love et al. 2004).

Similarly, the reaction of a poly(valent), amine-terminated, poly(amidoamine) (PAMAM) dendrimer ($G = 4$, $Z = 64$ surface groups) core with a nanoscale branch cell reagent (i.e., polyacrylate) yields a dendrimer–dendron [S-1:S-1] core–shell-type nanocompound, wherein only one half of its theoretical valency participates due to NSIS (Swanson et al. 2007).

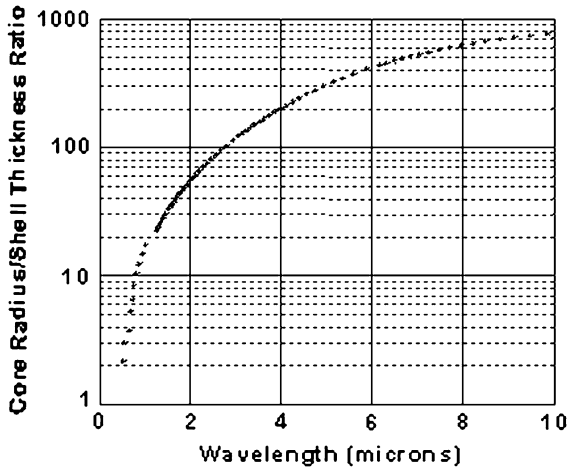

Fig. 52 Core/shell ratio as a function of resonance wavelength for gold/silica nanoshells (Loo et al. 2004). Published with permission from Loo et al. (2004). Copyright 2004: http://www.tcrt.org

Size/architecture/band gap-dependent nanoperiodicity: *photonics—(near infrared fluorescence)* (metal chalcogenide–metal chalcogenide [H-2:H-2] core–shell-type nanocompounds)

Lattice mismatching of semiconductor valence and conduction bands is a strategy used for optimizing certain core–shell nanocompound architectures. This approach allows one to systematically tune (near infrared) NIR fluorescence properties (Schmid 2004; Gao et al. 2008) (Fig. 54) and demonstrates a periodic relationship that exists between these mismatched (core–shell) nanoelement components. Simply controlling core (i.e., InAs), semiconductor shell (i.e., Ga, Cd, and Zn) compositions, and shell dimensions leads to lower toxicity, emission-enhanced QDs when compared to earlier cadmium chalcogenide-based systems (Xie et al. 2008) (Fig. 55).

Table 8 Hard:hard/hard:soft and soft:soft nanocompound nanoperiodic properties

	Hard:hard/hard:soft/soft:soft nanocompound nanoperiodicity					
Hard particle nanoelements	Metal (M°) nanoclusters [H-1]	Metal chalcogenides nanocrystals [H-2]	Metal oxide nanocrystals [H-3]	Silica nanoparticles [H-4]	Fullerenes [H-5]	Carbon nanotubes [H-6]
Soft particle nanoelements	Dendrimers/ dendrons [S-1]	Nanolatexes [S-2]	Polymeric micelles [S-3]	Proteins [S-4]	Viruses [S-5]	RNA/DNA [S-6]
Nanocompound (intrinsic physicochemical) periodic properties						
Encapsulation	[S-5:H-1]	Chen et al. (2006)				
	[S-5:H-3]	Douglas and Young (1998)				
Melting points						
Reactivity/sterics	[H-1:H-6]	Park et al. (2008)				
Refractive indices						
Self-similar aggregation	[S-1:H-1]	Schmid et al. (2000)				
Valency/ directionality	[S-1:H-1]	Huang and Tomalia (2005, 2006) and Gopidas et al. (2003a, b)				
	[S-1:H-2]	Huang and Tomalia (2005, 2006)				
	[S-6:H-1]	Loweth et al. (1999), Xu et al. (2006), Nykpanchuk et al. (2008), and Park et al. (2008)				
Atomic ordering	[S-1:H-1]	Petkov et al. (2008)				
Nanocompound (functional/application) periodic properties						
Catalysis	[S-1:H-1]	Wilson et al. (2006)				
	[S-4:H-1]	Ueno et al. (2004)				
	[H-1:H-1]	Schmid et al. (1993)				
Electronic	[S-1:S-1]	Miller et al. (1997)				
Imaging	[H-1:H-1]	Su et al. (2007)				
Magnetic	[S-1:H-3]	Frankamp et al. (2005)				
Nanotoxicity	[S-1:H-5]	(2007)				
Photonics	[H-1:H-4]	Loo et al. (2004)				
	[H-2:H-2]	Chen et al. (2008)				
	[S-1:H-1]	Srivastava et al. (2005)				
Nanomedicine	[S-1:H-3]	Martin et al. (2008)				
	[S-4:H-2]	Cai et al. (2006)				
	[S-4:H-6]	McDevitt et al. (2007)				

Size/composition-dependent nanoperiodicity: *magnetism* (dendrimer–metal oxide [S-1:H-3]-type nanocompounds)

Rotello et al. (Frankamp et al. 2002, 2005) prepared a series of magnetic-poly(amidoamine) (PAMAM) dendrimer: Fe_2O_3 type, 3D lattice nanocompounds by charge neutralization of cationic magnetic metal oxide [H-3]-type nanoelements with increasingly larger generations (i.e., $G = 0.5$–6.5) of [S-1], anionic PAMAM dendrimer-type nanoelements (Fig. 56). They were able to control inter-particle spacing of the magnetic nanoparticles as a function of dendrimer generation over a 2.4 nm range. This allowed them to demonstrate very effective modulation of collective magnetic behavior. Systematically lowering the dipolar coupling between the magnetic Fe_2O_3 particles using precisely sized [S-1] nanoelements, clearly demonstrated a systematic, periodic magnetic property pattern for these [S-1:H-3]-type nanocompounds as shown in Fig. 57.

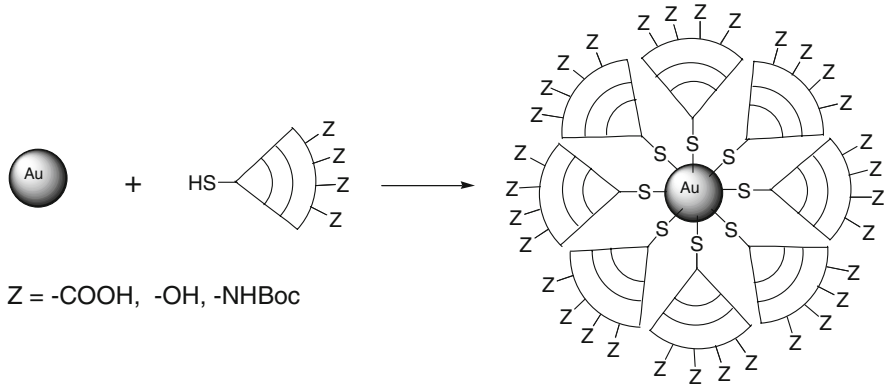

Fig. 53 Formation of dendronized gold nanoparticles. Reprinted from Huang and Tomalia (2005). Copyright (2005), with permission from Elsevier

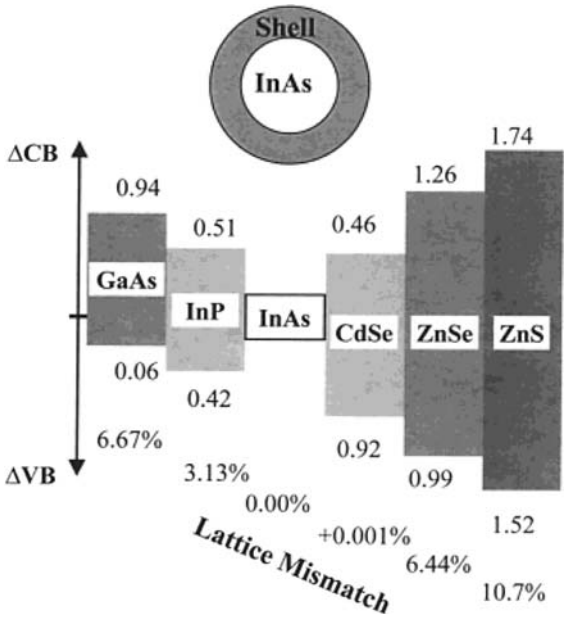

Fig. 54 Summary of the band offsets (in eV) and lattice mismatch (in %) between the core InAs and the III–V semiconductor shells (*left side*), and II–VI semiconductor shells (*right side*) grown in this study. CB Conduction band; VB valence band. Reprinted with permission from Cao and Banin (2000). Copyright: 2000 American Chemical Society

Particle size, (surface, defect, and face atom)-dependent nanoperiodicity: *catalysis* (metal nanocluster:dendrimer [H-1:S-1] core–shell-type nanocompounds)

An important class of dendrimer encapsulated metal nanocluster (DEN) assemblies pioneered by Tomalia et al. (Balogh and Tomalia 1998; Balogh et al. 1999) and Crooks et al. (Zhao et al. 1998) has received considerable attention as homogeneous catalysts for a wide variety of transformations. They are generally formed by nanoencapsulation of an appropriate metal salt followed by reduction with various reducing agents to produce the so-called [H-1(core):S-1(shell)] core–shell-type nanocompounds as illustrated in Fig. 58. Poly(amidoamine) (PAMAM) dendrimers have been used extensively as templates for producing these [H-1(core):S-1(shell)] core–shell-type nanocompounds (Petkov et al. 2008).

More recently, Crooks et al. (Wilson et al. 2006) have shown that the rate of hydrogenation of allyl alcohol in the presence of dendrimer-encapsulated Pd nanocluster (DEN) catalysts is electronic in nature for metal cluster sizes <1.5 nm (Fig. 59). For metal cluster diameters >1.5 nm, catalysis rates are dependent on nanoparticle geometric properties (i.e., number of surface atoms, defect atoms, and face atoms) illustrated in Fig. 59. Nanoperiodic patterns are based on turnover frequencies (TOF) as a function of nanoparticle diameter for these three types of active sites, and the total number of particles as shown in Fig. 59a, b.

Conclusions

Atom mimicry as proposed by Dalton's with wooden spheroids provided the first working premise and rationale for understanding the relationships and behavior of *well-defined* elemental atoms. It now appears that certain features of this atom mimicry and atom/molecular hypothesis may be successfully applied at the nanoscale level. These relationships were initially noted for soft nanomaterials such as dendrimers, wherein they were observed to behave as nanomodules much as elemental atoms. This unique

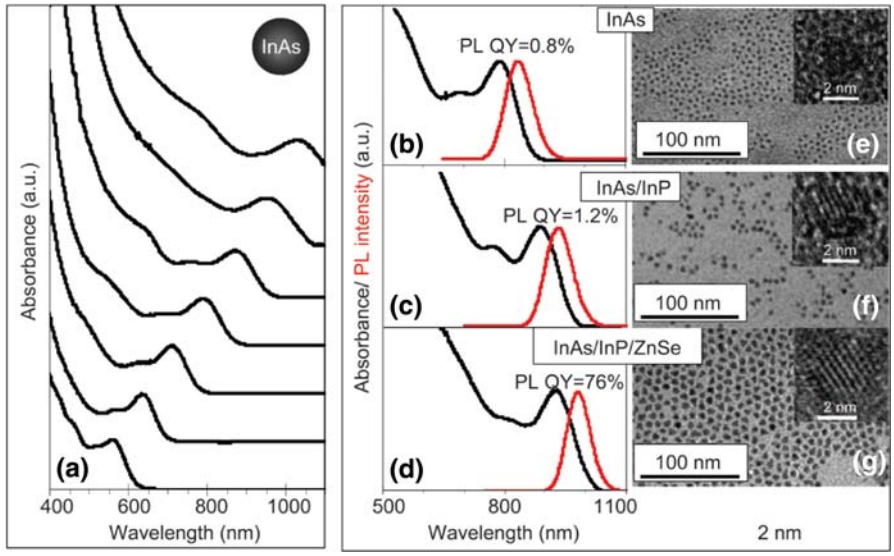

Fig. 55 Nanoperiodic absorption/emission properties for a series of mismatched lattice band gap, semiconducting, metal chalcogenide core–shell nanoparticles (Xie et al. 2008). Reproduced by permission from Springer. Reproduced with permission of the authors Xie et al. (2008)

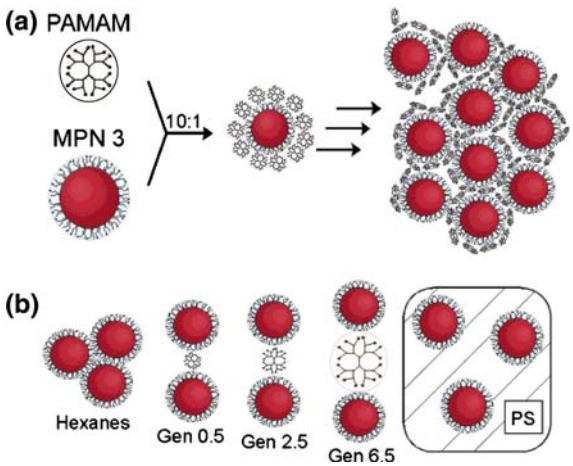

Fig. 56 **a** SAXS plots shown after background subtraction and normalization. **b** The systematic increase in inter-particle spacing, as the PAMAM generation increased (average spacing: d (Å) $2\eth/q$). Reprinted with permission from Frankamp et al. (2005). Copyright: 2005 American Chemical Society

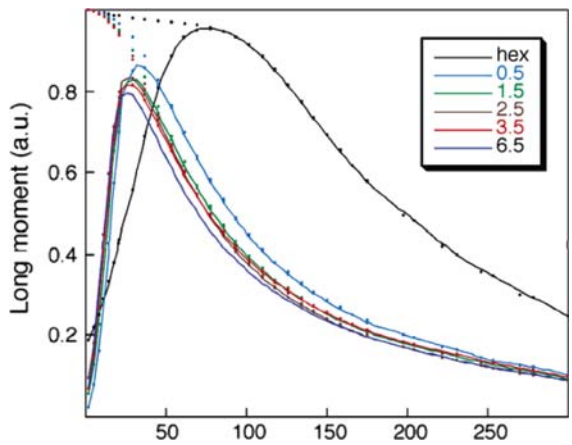

Fig. 57 Field-cooled (FC) and zero-field-cooled (ZFC) magnetization plots for each sample showing the steady decrease in T_B (magnetism), as the particles are spaced farther apart from one another. Reprinted with permission from Frankamp et al. (2005). Copyright: 2005 American Chemical Society

behavior was attributed to atom mimicry based on their analogous core–shell architectural features as well as their structure controlled *CNDPs*. These criteria were than applied to a wide range of well-defined *hard* and *soft nanoparticle* modules as illustrated below in Fig. 60.

Comparable behavior in a wide range of 0D/1D hard and soft nanomaterials encouraged us to refer to these new nanomodules as *nanoelement categories*. At present, six hard nanoelement categories and six soft nanoelement categories are proposed. The validity of this unifying concept and these proposed nanoelement categories is based on the experimental observation that these nanoelement categories manifest/exhibit many unique features normally associated with traditional elemental atoms. Most notable are their ability to form nanocompounds, as well as their manifestation of experimentally documented *nanoperiodic property patterns*. These periodic property patterns appear to be largely driven by the well-defined *CNDP's* that are associated with all the proposed nanoelement categories. These nanoelement categories and their compounds are expected

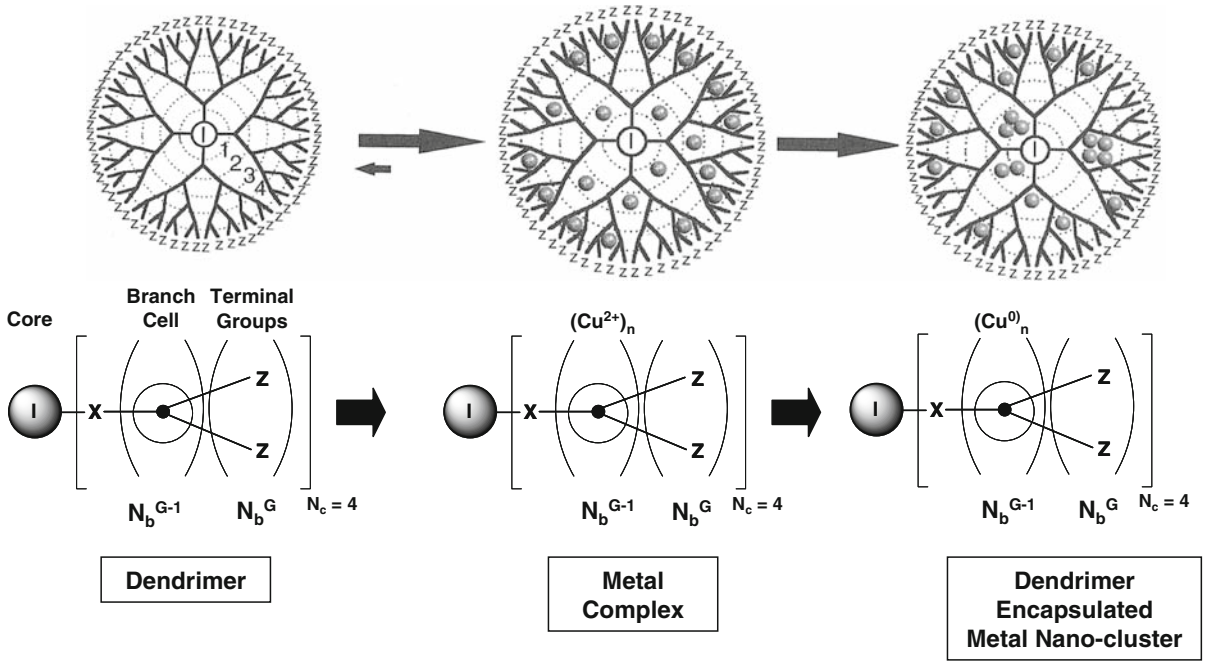

Fig. 58 Construction of a dendrimer-encapsulated metal nanocluster (DEN) involving **a** metal salt (Cu^{+2}) encapsulation and **b** reduction to (Cu^{0}) (Balogh and Tomalia 1998)

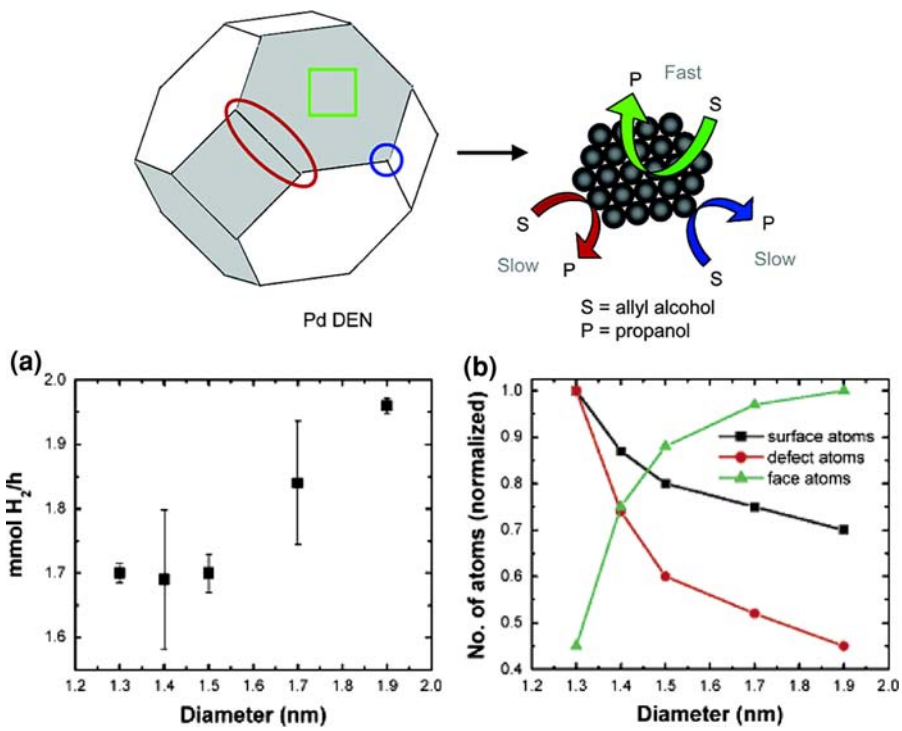

Fig. 59 **a** Plot of the rate of hydrogen consumption as a function of particle diameter. **b** Plot of the total, calculated numbers of surface, defect, and face atoms for each particle size. The data are normalized to the largest number of each type of atom. Reprinted with permission from Wilson et al. (2006). Copyright: 2006 American Chemical Society

to manifest totally different emerging properties and periodic patterns than those observed for traditional elemental atoms, according to Anderson (1972). The present experimental evidence clearly demonstrates that these documented properties and nanoperiodic patterns do follow Anderson's predictions.

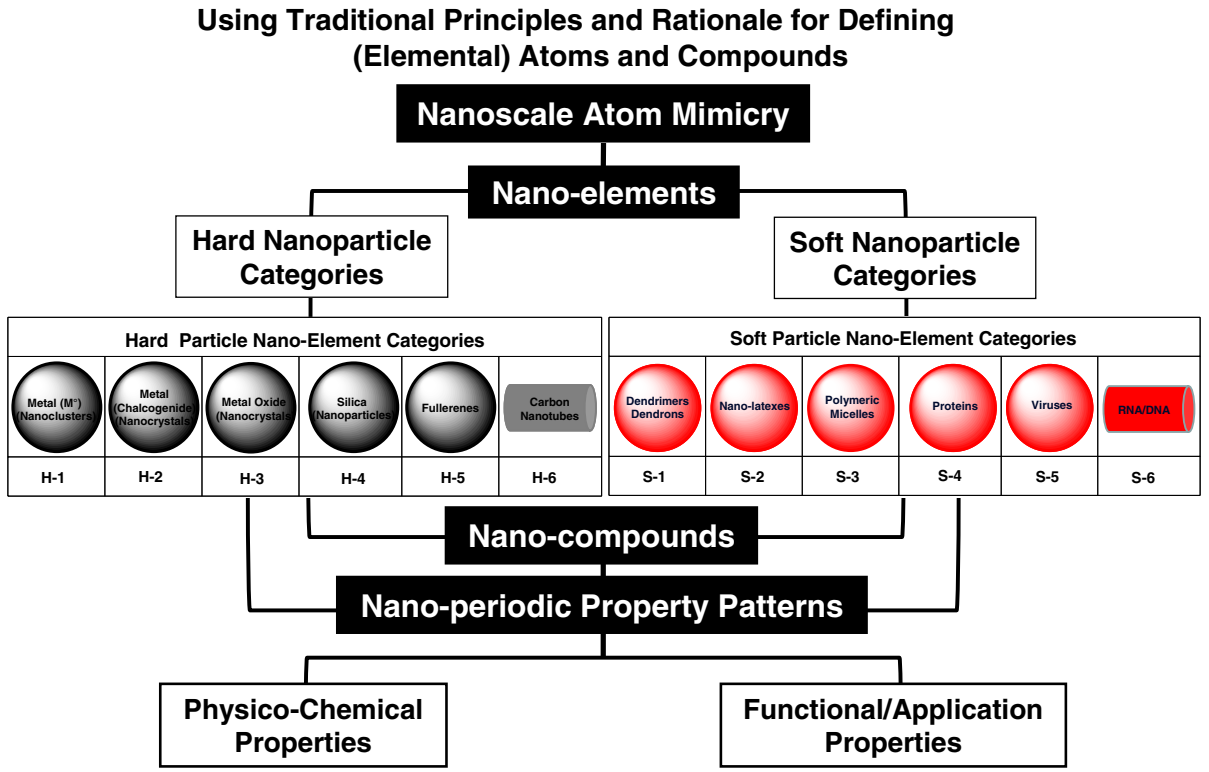

Fig. 60 Concept overview: using first principles and step logic that led to the "central dogma" for traditional chemistry, the criteria of nanoscale atom mimicry was applied to Category I-type, well-defined nanoparticles. This produced 12 proposed nanoelement categories which were classified into six hard particle and six soft particle nanoelement categories. Chemically bonding or assembling these hard and soft nanoelements leads to hard:hard, soft:hard, or soft:soft type nanocompound categories, many of which have been reported in the literature. Based on the discrete, quantized features associated with the proposed nanoelements and their compounds, an abundance of nanoperiodic property patterns related to their intrinsic physicochemical and functional/application properties have been observed and reported in the literature

We submit that experimentally documented nanoelement/compound and nanoperiodic property behavior provides a new system for defining the emerging discipline of *synthetic nanochemistry*. Furthermore, it is proposed that extension of historic first principles and step logic used for traditional chemistry to the nanoscale level has provided initial steps toward unifying and defining a *systematic framework for nanoscience*. Based on an abundance of literature examples documenting these proposed *nanoelement categories*, *nanocompounds*, and *nanoperiodic property patterns*, there is considerable optimism that in the context of this new concept appropriate first steps have been taken toward defining a *nanoperiodic system*.

The traditional self-assembly of protons/neutrons and electrons to produce atom-based elements provided a periodic system of modules/building blocks that could be largely defined by a single periodic table as demonstrated by Mendeleev. In contrast, the proposed nanoelement/compound categories and their intrinsic periodic property patterns are almost infinitely tunable and amenable to design. As such, this proposed concept must be thought of as a *nanoperiodic system* with many defining dimensions. Undoubtedly, this new complexity may require more than a single nanoperiodic table to capture and accommodate such a broad range of information and patterns. The daunting, but exciting task will be to document and consolidate these many emerging nanoperiodic property patterns into major trends and areas that will begin to crystallize into a grand perspective. Accomplishing this objective should allow dramatically more powerful means for predicting new nanoproperties and behavior as well as an effective system for anticipating new desirable nanomaterials yet to be discovered, while defining

important new unprecedented risk/benefit boundaries in the field of nanoscience.

"*The intended spirit of this perspective was not to advocate the disruption of any natural physicochemical laws, but to encourage new and different thinking that is steeped in historical first principles which hopefully may evolve into a comprehensive systematic framework for unifying nanoscience. Much more remains to be done*." *Donald A. Tomalia*

Acknowledgments I gratefully acknowledge the National Science Foundation for financial support of the CMU-NSF Workshop entitled: *Periodic Patterns, Relationships and Categories of Well-Defined Nanoscale Building Blocks*, NSF Award #0707510, the participants and especially the plenary speakers: Bradley D. Fahlman (Central Michigan University), William A. Goddard (Cal. Tech.), Theodore Goodson III (University of Michigan), Piotr Grodzinski (National Cancer Institute), Donald T. Haynie (Artificial Cell Technologies/Central Michigan), Scott McNeil (Nanotechnology Characterization Laboratory, NCL), Stephen O'Brien (Columbia University), Virgil Percec (University of Pennsylvania), Dmitrii F. Perepichka (McGill University), Mihail C. Roco (National Science Foundation), Robert Rodriquez (Cornell University), Dwight S. Seferos (Northwestern University), and Ulrich Wiesner (Cornell University) for many stimulating discussions both during and after the workshop. I extend special thanks to Prof. Jorn Christensen (University of Copenhagen, Denmark), Visiting Professorial Scholar at Central Michigan University (2008), and Prof. Nicholas Turro (Columbia University) for many in depth discussions and helpful suggestions in the development of the present concept. Finally, I wish to express sincere gratitude to Ms. Linda S. Nixon for her perseverance and skill in manuscript/graphics preparation.

References

Aldana J, Wang Y et al (2001) Photochemical instability of CdSe nanocrystals coated by hydrophilic thiols. J Am Chem Soc 123:8844–8850

Alivisatos AP (1996) Semiconductor clusters, nanocrystals, and quantum dots. Science 271:933–937

Anderson PW (1972) More is different. Science 177:393–396

Andres R, de Jesus E et al (2007) Catalysts based on palladium dendrimers. New J Chem 31:1161–1191

Azamian BR, Coleman KS et al. (2002) Directly observed covalent coupling of quantum dots to single-wall carbon nanotubes. Chem Commun 366–367

Balogh L, Tomalia DA (1998) Poly(Amidoamine) dendrimer-templated nanocomposites 1. Synthesis of zero valent copper nanoclusters. J Am Chem Soc 120:7355

Balogh L, Valluzzi R et al (1999) Formation of silver and gold dendrimer nanocomposites. J Nanopart Res 1:353–368

Balogh L, Swanson DR et al (2001) Dendrimer–silver complexes and nanocomposites as antimicrobial agents. Nano Lett 1(1):18–21

Banerjee S, Wong SS (2002) Synthesis and characterization of carbon nanotube-nanocrystal heterostructures. Nano Lett 2(3):195–200

Banerjee S, Hemraj-Benny T et al (2005) Routes towards separating metallic and semiconducting nanotubes. J Nanosci Nanotechnol 5:841–855

Bardhan R, Grady NK et al (2009) Fluorescence enhancement by au nanostructures: nanoshells and nanorods. ACS Nano. doi:10.1021/nn900001q

Bell TE (2007) Understanding risk assessment of nanotechnology. http://www.nano.gov/Understanding_Risk_Assessment.pdf

Betley TA, Hessler JA et al (2002) Tapping mode atomic force microscopy investigation of poly(amidoamine) core-shell tecto(dendrimers) using carbon nanoprobes. Langmuir 18: 3127–3133

Bielinska A, Eichman JD et al (2002) Imaging [Au^0-PAMAM] gold-dendrimer nanocomposites in cells. J Nanopart Res 4:395–403

Boas U, Christensen JB et al (2006) Dendrimers in medicine and biotechnology. The Royal Society of Chemistry, Cambridge, UK

Brack M (1993) The physics of simple metal clusters: self consistent jellium model and semiclassical approaches. Rev Mod Phys 65:677–732

Braun CS, Vetro JA et al (2005) Structure/function relationships of polyamidoamine/DNA dendrimers as gene delivery vehicles. J Pharm Sci 94(2):423–436

Bridot J-L, Faure A-C et al (2007) Hybrid gadolinium oxide nanoparticles: multimodal contrast agents for in vivo imaging. J Am Chem Soc 129(16):5076–5084

Burda C, Chen X et al (2005) Chemistry and properties of nanocrystals of different shapes. Chem Rev 105:1025–1102

Cai W, Shin D-W et al (2006) Peptide-labeled near-infrared quantum dots for imaging tumor vasculature in living subjects. Nano Lett 6(4):669–676

Cannizzo C, Mayer CR et al (2005) Covalent hybrid materials based on nanolatex particles and Dawson polyoxometalates. Adv Mater 17:2888–2892

Cao YW, Banin U (2000) Growth and properties of semiconductor core/shell nanocrystals with InAs cores. J Am Chem Soc 122:9692–9702

Carrero-Sanchez JC, Elias AL et al (2006) Biocompatibility and toxicological studies of carbon nanotubes doped with nitrogen. Nano Lett 6(8):1609–1616

Castro T, Reifenberger R et al (1990) Size-dependent melting temperature of individual nanometer-sized metallic clusters. Phys Rev B 42(13):8548–8556

Catalano VJ, Parodi N (1997) Reversible C binding to dendrimer-containing Ir(CO) CI(PPhR) complexes. Inorg Chem 36:561–567

Charlier J-C (2002) Defects in carbon nanotubes. Acc Chem Res 35(12):1063–1069

Chen C, Daniel M-C et al (2006) Nanoparticle-templated assembly of viral protein cages. Nano Lett 6(4):611–615

Chen C-H, Sarma LS et al (2007) Architecture of Pd–Au bimetallic nanoparticles in sodium bis(2-ethylhexyl)sulfosuccinate reverse micelles as investigated by X-ray absorption spectroscopy. ACS Nano 1(2):114–125

Chen Y, Vela J et al (2008) Giant multishell CdSe nanocrystal quantum dots with suppressed blinking. J Am Chem Soc 130: 5026–5027

Chidley C, Mosiewicz K et al (2008) A designed protein for the specific and covalent heteroconjugation of biomolecules. Bioconjug Chem 19:1753–1756

Cho B-K, Jain A et al (2007) Nanoparticle-induced packing transition in mesostructured Block dendron-silica hybrids. Chem Mater 19:3611–3614

Choi Y, Mecke A et al (2004) DNA-directed synthesis of generation 7 and 5 PAMAM dendrimer nanoclusters. Nano Lett 4(3):391–397

Choi Y, Thomas T et al (2005) Synthesis and functional evaluation of DNA-assembled polyamidoamine dendrimer clusters for cancer cell-specific targeting. Chem Biol 12: 35–43

Cozzoli PD, Pellegrino T et al (2006) Synthesis, properties and perspectives of hybrid nanocrystal structures. Chem Soc Rev 35:1195–1208

Crespo L, Sanclimens G et al (2005) Peptide and amide bond-containing dendrimers. Chem Rev 105:1663–1681

Damha MJ, Oglivie KK (1988) Synthesis and spectroscopic analysis of branched RNA fragments: messenger RNA splicing intermediates. J Org Chem 53:3710–3722

Damha MJ, Zabarylo SV (1989) Automated solid-phase synthesis of branched oligonucleotides. Tetrahedron Lett 30: 6295–6298

Damha MJ, Giannaris PA et al (1990) An improved procedure for derivatization of controlled-pore glass beads for solid-phase oligonucleotide synthesis. Nucleic Acid Res 18: 3813–3821

Deen WM (2004) What determines glomerular capillary permeability? J Clin Invest 114:1412–1414

DeMattei CR, Huang B et al (2004) Designed dendrimers syntheses by self-assembly of single-site, ssDNA functionalized dendrons. Nano Lett 4(5):771–777

Dendrimer-based MRI Contrast Agents NCL200612A (2006) Nanotechnology Characterization Laboratory, pp 1–58

Desai A, Shi X et al (2008) CE of poly(amidoamine) succinamic acid dendrimers using a poly(vinyl alcohol)-coated capillary. Electrophoresis 29:510–515

Deschenaux R, Donnio B et al (2007) Liquid-crystalline fullerodendrimers. New J Chem 31:1064–1073

DeVries GA, Brunnbauer M et al (2007) Divalent metal nanoparticles. Science 315:358–361

DeVries GA, Talley FR et al (2008) Thermodynamic study of the reactivity of the two topological point defects present in mixed self-assembled monolayers on gold nanoparticles. Adv Mater 9999:1–5

Douglas T, Young M (1998) Host–guest encapsulation of materials by assembled virus protein cages. Nature 393:152–155

Duxin N, Liu F et al (2005) Cadmium sulphide quantum dots in morphologically tunable triblock copolymer aggregates. J Am Chem Soc 127(28):10063–10069

Dvornic PR, Tomalia DA (1999) Poly(amidoamine) dendrimers. In: Mark JE (ed) Polymer data handbook. Oxford University Press, New York, pp 266–270

Ellis-Behnke RG, Liang Y-X et al (2006a) Nano hemostat solution: immediate hemostasis at the nanoscale. Nanomedicine 2:207–215

Ellis-Behnke RG, Liang Y-X et al (2006b) Nano neuro knitting: peptide nanofiber scaffold for brain repair and axon regeneration with functional return of vision. Proc Natl Acad USA 103(13):5054–5059

El-Sayed M, Rhodes CA et al (2003) Transport mechanism(s) of poly(amidoamine) dendrimers across Caco-2-cell monolayers. Int J Pharm 265:151–157

Feng M, Zhao J et al (2008) Atomlike, hollow-core-bound molecular orbitals of C_{60}. Science 320:359–362

Frankamp BL, Boal AK et al (2002) Controlled interparticle spacing through self-assembly of Au nanoparticles and poly(amidoamine) dendrimers. J Am Chem Soc 124: 15146–15147

Frankamp BL, Boal AK et al (2005) Direct control of the magnetic interaction between iron oxide nanoparticles through dendrimer-mediated self-assembly. J Am Chem Soc 127:9731–9735

Fréchet JMJ (1994) Functional polymers and dendrimers: reactivity, molecular architectures, and interfacial energy. Science 263:1710–1715

Fréchet JMJ, Tomalia DA (2001) Dendrimers and other dendritic polymers. Wiley, Chichester

Fritsche H-G, Muller H et al (1997) Formation of superclusters from metallic clusters. Zeitschrift Fur Physikalische Chemie—Int J Res Phys Chem Chem Phys 199:87–98

Functionalized fullerenes NCL200701A (2007) Nanotechnology Characterization Laboratory, pp 1–46. http://ncl.cancer.gov/NCL200701A_073007.pdf

Gao X, Chen J et al (2008) Quantum dots bearing lectin-functionalized nanoparticles as a platform for in vivo brain imaging. Bioconjug Chem 19:2189–2195

Gentleman DJ, Chan WCW (2009) A systematic nomenclature for codifying engineered nanostructures. Small 5:426–431. doi:10.1002/smll.c00800490

Gomez-Romero P, Sanchez C (eds) (2004) Functional hybrid materials. Wiley-VCH, Weinheim

Gopidas KR, Leheny AR et al (1991) Photophysical investigation of similarities between Starburst dendrimer and anionic micelles. J Am Chem Soc 113:7335–7342

Gopidas KR, Whitesell JK et al (2003a) Metal-core-organic shell dendrimers as unimolecular micelles. J Am Chem Soc 125:14168–14180

Gopidas KR, Whitesell JK et al (2003b) Nanoparticle-cored dendrimers: synthesis and characterization. J Am Chem Soc 125:6491–6502

Gu H, Yang Z et al (2005) Heterodimers of nanoparticles: formation at a liquid–liquid interface and particle-specific surface modification by functional molecules. J Am Chem Soc 127:34–35

Guo W, Li J et al (2003) Luminescent CdSe/CdS core/shell nanocrystals in dendron boxes: superior chemical, photochemical and thermal stability. J Am Chem Soc 125: 3901–3909

Haddon RC, Sippel J et al (2004) Purification and separation of carbon nanotubes. Mater Res Bull 29:252–259

Haremza JM, Hahn MA et al (2002) Attachment of single CdSe nanocrystals to individual single-walled carbon nanotubes. Nano Lett 2(11):1253–1258

Hawker CJ, Wooley KL et al (1994) Dendritic fullerenes—a new approach to polymer modification of C-60. J Chem Soc-Chem Commun (8):925–926

Hecht S, Fréchet JMJ (2001) Dendritic encapsulation of function: applying nature's site isolation principle from biomimetics to materials science. Angew Chem Int Ed 40(1):74–91

Heilbronner E, Dunitz JD (1993) Reflections on symmetry. VCH Publishers, Inc, New York

Hersam MC (2008) Progress towards monodisperse single-walled carbon nanotubes. Nat Nanotechnol 3:387–394

Hirsch LR, Stafford RJ et al (2003) Nanoshell-mediated near-infrared thermal therapy of tumors under magnetic resonance guidance. Proc Natl Acad Sci 100(23):13549–13554

Hostetler MJ, Wingate JE et al (1998) Alkanethiolate gold cluster molecules with core diameters from 1.5 to 5.2 nm: core and monolayer properties as a function of core size. Langmuir 14:17–30

Huang B, Tomalia DA (2005) Dendronization of gold and CdSe/CdS (core-shell) quantum dots with Tomalia type, thiol core, functionalized poly(amidoamine) (PAMAM) dendrons. J Lumin 111:215–223

Huang B, Tomalia DA (2006) Poly(ether) dendrons possessing phosphine focal points for stabilization and reduced quenching of luminescent quantum dots. Inorg Acta 359:1961–1966

Hudson SD, Jung H-T et al (1997) Direct visualization of individual cylindrical and spherical supramolecular dendrimers. Science 278:449–452

Hultman KL, Raffo AJ et al (2008) Magnetic resonance imaging of major histocompatibility class II expression in the renal medulla using immunotargeted superparamagnetic iron oxide nanoparticles. ACS Nano 2(3):477–484

Islam MT, Majoros IJ et al (2005a) HPLC analysis of PAMAM dendrimer based multifunctional devices. J Chromatogr B 822:21–26

Islam MT, Shi X et al (2005b) HPLC separation of different generations of poly(amidoamine) dendrimers modified with various terminal groups. Anal Chem 77:2063–2070

Jackson JL, Chanzy HD et al (1998) Visualization of dendrimer molecules by transmission electron (TEM): staining methods and cryo-TEM of vitrified solutions. Macromolecules 31:6259–6265

Jain TK, Reddy MK et al (2008) Biodistribution, clearance, and biocompatibility of iron oxide, magnetic nanoparticles in rats. Mol Pharm 5(2):316–327

Jensen AW, Maru BS et al (2005) Preparation of fullerene-shell dendrimer-core nanoconjugates. Nano Lett 5(6): 1171–1173

Jiang W, Kim BYS et al (2008) Nanoparticle-mediated cellular response is size-dependent. Nat Nanotechnol 3:145–150

Jockusch J, Ramirez J et al (1999) Comparison of nitrogen core and ethylenediamine core Starburst dendrimers through photochemical and spectroscopic probes. Macromolecules 32:4419–4423

Joo K, Lei Y et al (2008) Site-specific labelling of enveloped viruses with quantum dots for single virus tracking. ACS Nano 2(8):1553–1562

Juttukonda V, Paddock RL et al (2006) Facile synthesis of tin oxide nanoparticles stabilized by dendritic polymers. J Am Chem Soc 128:420–421

Kanungo M, Lu H et al (2009) Suppression of metallic conductivity of single-walled carbon nanotubes by cycloaddition reactions. Science 323:234–237

Kelly KL, Coronado E et al (2003) The optical properties of metal nanoparticles: the influence of size, shape and dielectric environment. J Phys Chem B 107:668–677

Kiely CJ, Fink J et al (2000) Ordered colloidal nanoalloy. Adv Mater 12(9):640–643

Klabunde KJ (2001) Nanoscale materials in chemistry. Wiley, New York

Klajnert B, Bryszewska M (2007) Dendrimers in medicine. Nova Science Publishers, Inc, New York

Knecht MR, Crooks RM (2007) Magnetic properties of dendrimer-encapsulated iron nanoparticles containing an average of 55 and 147 atoms. New J Chem 31:1349–1353

Kobayashi H, Brechbiel MW (2003) Dendrimer-based macromolecular MRI contrast agents: characteristics and application. Mol Imag 2(1):1–10

Kobayashi H, Kawamoto S et al (2003) Comparison of dendrimer-based macromolecular contrast agents for dynamic micro-magnetic resonance lymphangiography. Magn Reson Med 50:758–766

Koole R, van Schooneveld MM et al (2008) Paramagnetic lipid-coated silica nanoparticles with a fluorescent quantum dot core: a new contrast agent platform for multimodality imaging. Bioconjug Chem 19:2471–2479

Kostarelos K (2008) The long and short of carbon nanotube toxicity. Nat Biotechnol 7:774–775

Kostiainen MA, Szilvay GR et al (2007) Precisely defined protein–polymer conjugates: construction of synthetic DNA binding domains on proteins by using multivalent dendrons. ACS Nano 1(2):103–113

Kruger C, Agarwal S et al (2008) Stoichiometric functionalization of gold nanoparticles in solution through a free radical polymerization approach. J Am Chem Soc 130: 2710–2711

Krupke R, Hennrich F (2005) Separation techniques or carbon nanotubes. Adv Eng Mater 7:111–116

Kwon K-W, Shim M (2005) Fe_2O_3/II-VI sulfide nanocrystal heterojunctions. J Am Chem Soc 127:10269–10275

Lacerda L, Soundararajan A et al (2008) Dynamic imaging of functionalized multi-walled carbon nanotube systemic circulation and urinary excretion. Adv Mater 20:225–230

Landers JJ, Cao Z et al (2002) Prevention of influenza pneumonitis by sialic acid conjugated dendritic polymers. J Infect Dis 186:1222–1230

Langereis S, Dirksen A et al (2007) Dendrimers and magnetic resonance imaging. New J Chem 31:1152–1160

Larpent C, Genies C et al (2004) Giant dendrimer-like particles from nanolatexes. Chem Commun 1816–1817

Levine AJ (1992) Viruses. Scientific American Library, New York

Lewinski N, Colvin V et al (2008) Cytotoxicity of nanoparticles. Small 4(1):26–49

Li J, Piehler LT et al (2000) Visualization and characterization of poly(amidoamine) dendrimers by atomic force microscopy. Langmuir 16:5613–5616

Loo C, Lin A et al (2004) Nanoshell-Enabled Photonics-Based Imaging and Therapy of Cancer. Technol Cancer Res Treat 3:33–40

Love CS, Chechik V et al (2004) Dendron-stabilized gold nanoparticles: generation dependence of core size and thermal stability. J Mater Chem 14:919–923

Loweth CJ, Caldwell WB et al (1999) DNA-based assembly of gold nanocrystals. Angew Chem Int Ed 38(12):1808–1812

Mamedova NN, Kotov NA et al (2001) Albumin-CdTe nanoparticle bioconjugates: preparation, structure, and interunit energy transfer with antenna effect. Nano Letters 1(6):1–286

Mann S, Meldrum FC (1991) Controlled synthesis of inorganic materials using supramolecular assemblies. Adv Mater 3(6): 316–318

Mansfield ML, Rakesh L et al (1996) The random parking of spheres on spheres. J Chem Phys 105(8):3245–3249

Martin AL, Bernas LM et al (2008) Enhanced cell uptake of superparamagnetic iron oxide nanoparticles functionalized with dendritic guanidines. Bioconjug Chem 19:2375–2384

Martin AL, Li B et al (2009) Surface functionalization of nanomaterials with dendritic groups: toward enhanced binding to biological targets. J Am Chem Soc 131(2):734–741

McDevitt MR, Chattopadhyay D et al (2007) Tumor targeting with antibody-functionalized, radiolabeled carbon nanotubes. The Journal of Nuclear Medicine 48(7):1180–1189

Medintz IL, Pons T et al (2008) Intracellular delivery of quantum dot–protein mediated by cell penetrating peptides. Bioconjug Chem 19:1785–1795

Miller LL, Duan RG et al (1997) Electrically conducting dendrimers. J Am Chem Soc 119(5):1005–1010

Mirkin CA (2005) The beginning of a small revolution. Small 1(1):14–16

Mongin O, Pla-Quintana A et al (2007) Organic nanodots for multiphotonics: synthesis and photophysical studies. New J Chem 31:1354–1367

Mucic RC, Storhoff JJ et al (1998) DNA-directed synthesis of binary nanoparticle network materials. J Am Chem Soc 120:1275–12674

Myc A, Patri A et al (2007) Dendrimer-based BH3 conjugate that targets human carcinoma cells. Biomacromolecules 8:2986–2989

Naylor AM, Goddard WA III et al (1989) Starburst dendrimers 5. Molecular shape control. J Am Chem Soc 111:2339–2341

Newkome GR, Moorfield CN et al (1996) Dendritic molecules. Weinheim, VCH

Nilsen TW, Grayzel J et al (1997) Dendritic nucleic acid structures. J Theor Biol 187:273–284

Nishiyama N, Kataoka K (2006) Current state, achievements, and future prospects of polymeric micelles as nanocarriers for drug and gene delivery. Pharmacol Ther 112:630–648

Nykpanchuk D, Maye MM et al (2008) DNA-guided crystallization of colloidal nanoparticles. Nature 451:549–552

Ottaviani MF, Turro NJ et al (1996) Characterization of Starburst dendrimers by EPR. 3. Aggregational processes of a positively charged nitroxide surfactant. J Phys Chem 100: 13675–13686

Ottaviani MF, Sacchi B et al (1999) An EPR study of the interactions between Starburst dendrimers and polynucleotides. Macromolecules 32:2275–2282

Ozin GA, Arsenault AC (2005) Nanochemistry: a chemical approach to nanomaterials. Royal Society of Chemistry, Cambridge, p 70

Park SY, Lytton-Jean AKR et al (2008) DNA-programmable nanoparticle crystallization. Nature 451:553–556

Patil ML, Zhang M et al (2009) Internally cationic polyamidoamine PAMAM-OH dendrimers for siRNA delivery: effect of the degree of quaternization and cancer targeting. Biomacromolecules 10:258–266

Patri AK, Myc A et al (2004) Synthesis and in vitro testing of J591 antibody-dendrimer conjugates for targeted prostate cancer therapy. Bioconjugate Chem 15:1174–1181

Percec V, Chu P et al (1995) Rational design of the first nonspherical dendrimer which displays calamitic nematic and smectic thermotropic liquid crystalline phases. J Am Chem Soc 117:11441–11454

Percec V, Ahn C-H et al (1998) Controlling polymer shape through the self-assembly of dendritic side-groups. Nature 391:161–164

Percec V, Glodde M et al (2003) Transformation of a spherical supramolecular dendrimer into a pyramidal columnar supramolecular dendrimer mediated by the fluorophobic effect. Angew Chem Int Ed 42:4338–4342

Percec V, Won BC et al (2007) Expanding the structural diversity of self-assembling dendrons and supramolecular dendrimers via complex building blocks. J Am Chem Soc 129:11265–11278

Percec V, Rudick JG et al (2008a) Supramolecular structural diversity among first-generation hybrid dendrimers and twin dendrons. Chem Eur J 14:3355–3362

Percec V, Won BC et al (2008b) Expanding the structural diversity of self-assembling dendrons and supramolecular dendrimers via complex building blocks. J Am Chem Soc 129:11265–11278

Perepichka DF, Rosei F (2007) Metal nanoparticles: From "artificial atoms" to "artificial molecules". Angew Chem Int Ed 46:6006–6008

Petkov V, Bedford N et al (2008) Periodicity and atomic ordering in nanosized particles of crystals. J Phys Chem C 112:8907–8911

Pullman B (1998) The atom in the history of human thought. Oxford University Press, New York

Qu X, Komatsu T et al (2008) Structure, photophysical property, and cytotoxicity of human serum albumin complexed with tris(dicarboxymethylene) [60] fullerene. Bioconjug Chem 19:1556–1560

Ramakrishna G, Varnavski O et al (2008) Quantum-sized gold clusters as efficient two-photon absorbers. J Am Chem Soc 130(15):5032–5033

Rao CNR (1994) Chemical approaches to the synthesis of inorganic materials. Wiley Eastern, New Delhi

Rao C, Tam JP (1994) Synthesis of peptide dendrimer. J Am Chem Soc 116:6975–6976

Ravindran S, Chaudhary S et al (2003) Covalent coupling of quantum dots to multiwalled carbon nanotubes for electronic device applications. Nano Lett 3(4):447–453

Redl FX, Cho K-S et al (2003) Three-dimensional binary superlattices of magnetic nanocrystals and semiconductor quantum dot. Nature 423:968–971

Reuter JD, Myc A et al (1999) Inhibition of viral adhesion and infection by sialic-acid-conjugated dendritic polymers. Bioconjug Chem 10:271–278

Rio Y, Accorsi G et al (2003) A fullerene core to probe dendritic shielding effects. Tetrahedron 59:3833–3844

Roberts JC, Adams YE et al (1990) Using Starburst dendrimers as linker molecules to radiolabel antibodies. Bioconjug Chem 2:305–308

Roco MC (2008) Possibilities for global governance of converging technologies. J Nanopart Res 10:11–29

Rudick JG, Percec V (2008) Induced helical backbone conformations of self-organizable dendronized polymers. Acc Chem Res. doi:10.1021/ar800066w

Sander JV, Murray MJ (1978) Ordered arrangements of spheres of two different sizes in opal. Nature 275: 201–203
Sayes CM, Fortner JD et al (2004) The differential cytotoxicity of water-soluble fullerenes. Nano Lett 4(10):1881–1887
Sayes CM, Liang F et al (2006) Functionalization density dependence of single-walled carbon nanotubes cytotoxicity in vitro. Toxicol Lett 161:135–142
Scerri ER (2007) The periodic table. Oxford University Press, New York
Schmid G (1988) Metal clusters and cluster metals. Polyhedron 7:2321–2329
Schmid G (1990) Clusters and colloids: bridges between molecular and condensed material. Endeavour 14(4): 172
Schmid G (ed) (2004) Nanoparticles. Wiley-VCH, Weinheim
Schmid G, Klein N (1986) Novel modifications of gold, rhodium, ruthenium–M_{13} clusters as building blocks for superclusters. Angew Chem Int Ed Engl 25:922–923
Schmid G, Harms M et al (1993) Ligand -stabilized giant palladium clusters:promising candidates in heterogeneous catalysis. J Am Chem Soc 115:2046–2048
Schmid G, Meyer-Zaika W et al (2000) Naked Au_{55} clusters: dramatic effect of a thiol-terminated dendrimer. Chem Eur J 6(9):1693–1697
Seeman NC (1998) DNA nanotechnology: novel DNA constructions. Annu Rev Biophys Biomol Struct 27:225–248
Seeman NC (2007) Nanotechnology and the double helix. Sci Am Rep Spec Ed Nanotechnol 17(3):30–39
Seeman NC, Lukeman PS (2005) Nucleic acid nanostructures: bottom-up control of geometry on the nanoscale. Rep Prog Phys 68:237–270
Shevchenko E, Talapin DV et al (2006a) Structural diversity in binary nanoparticle superlattices. Nature 439:55–59
Shevchenko E, Talapin DV et al (2006b) Structural characterization of self-assembled multifunctional binary nanoparticle superlattices. J Am Chem Soc 128:3620–3637
Shevchenko E, Kortright JB et al (2007) Quasi-ternary nanoparticle superlattices through nanoparticle design. Adv Mater 19:4183–4188
Shi X, Ganser TR et al (2006) Characterization of crystalline dendrimer-stabilized gold nanoparticles. Nanotechnology 17:1072–1078
Shi X, Wang S et al (2007) Dendrimer-entrapped gold nanoparticles as a platform for cancer-cell targeting and imaging. Small 3(7):1245–1252
Shi W, Zeng H et al (2006) A general approach to binary and ternary hybrid nanocrystals. Nano Lett 6(4):875–881
Singh P (1998) Terminal groups in Starburst dendrimers: activation and reactions with proteins. Bioconjug Chem 9:54–63
Singh P (2001) Dendrimer-based biological reagents: preparation and applications in diagnostics. In: Fréchet JMJ, Tomalia DA (eds) Dendrimers and dendritic polymers. Wiley, Chichester, pp 463–484
Springholz G, Holy V et al (1998) Self-organized growth of three-dimensional quantum-dot crystals with fcc-like stacking and a tunable lattice constant. Science 282: 734–737
Srivastava S, Frankamp BL et al (2005) Controlled plasmon resonance of gold nanoparticles self-assembled with PAMAM dendrimers. Chem Mater 17:487–490
Strable E, Johnson JE et al (2004) Natural nanochemical building blocks: icosahedral virus particles organized by attached oligonucleotides. Nano Lett 4(8):1385–1389
Su C-H, Sheu H-S et al (2007) Nanoshell magnetic resonance imaging contrast agents. J Am Chem Soc 129(7):2139–2146
Swanson DR, Huang B et al (2007) Unique steric and geometry induced stoichiometries observed in the divergent synthesis of poly(ester-acrylate) (PEA) dendrimers. New J Chem 31:1368–1378
Tabakovic I, Miller LL et al (1997) Dendrimers peripherally modified with anion radicals that form Pi-dimers and Pi-stacks. Chem Mater 9:736–745
Teranishi T, Hori H et al (1997) ESR study on palladium nanoparticles. J Phys Chem B101:5774–5776
Thomas PJ, Kulkarni GU et al (2001) Magic nuclearity giant clusters of metal nanocrystals formed by mesoscale self-assembly. J Phys Chem B 105:2515–2517
Thomas TP, Patri AK et al (2004) In vitro targeting of synthesized antibody-conjugated dendrimer nanoparticles. Biomacromolecules 5:2269–2274
Tomalia DA (1993) Starburst/cascade dendrimers: fundamental building blocks for a new nanoscopic chemistry set. Aldrichimica Acta 26(4):91–101
Tomalia DA (1994) Starburst/cascade dendrimers: fundamental building blocks for a new nanoscopic chemistry set. Adv Mater 6:529–539
Tomalia DA (2003) Fluorine makes a difference. Nat Mater 2:711–712
Tomalia DA (2004) Birth of a new macromolecular architecture: dendrimers as quantized building blocks for nanoscale synthetic organic chemistry. Aldrichimica Acta 37(2): 39–57
Tomalia DA (2005) Birth of a new macromolecular architecture: dendrimers as quantized building blocks for nanoscale synthetic polymer chemistry. Prog Polym Sci 30: 294–324
Tomalia DA (2008) Periodic patterns, relationships and categories of well-defined nanoscale building blocks. National Science Foundation Final Workshop Report, pp 1–156. http://www.nsf.gov/crssprgm/nano/GC_Charact08_Tomalia_nsf9_29_08.pdf
Tomalia DA, Durst HD (1993) Topics in current chemistry, vol. 165. In: Weber EW (ed) Supramolecular chemistry I—Directed synthesis and molecular recognition. Springer Verlag, Berlin, pp 193–313
Tomalia DA, Dvornic PR (1996) Dendritic polymers, divergent synthesis (Starburst polyamidoamine dendrimers). In: Salamone JC (ed) Polymeric materials encyclopedia. CRC Press, Boca Raton, FL, 3(D–E), pp 1814–1840
Tomalia DA, Fréchet JMJ (2002) Discovery of dendrimers and dendritic polymers: a brief historical perspective. J Polym Sci 40(16):2719–2728
Tomalia DA, Baker H et al (1985) A new class of polymers: Starburst dendritic macromolecules. Polym J (Tokyo) 17: 117–132
Tomalia DA, Baker H et al (1986) Dendritic macromolecules: synthesis of Starburst dendrimers. Macromolecules 19:2466–2468
Tomalia DA, Naylor AM et al (1990) Starburst dendrimers: molecular level control of size, shape, surface chemistry,

topology and flexibility from atoms to macroscopic matter. Angew Chem Int Ed Engl 29(2):138–175

Tomalia DA, Uppuluri S et al (2000) Dendrimers as reactive modules for the synthesis of new structure controlled, higher complexity—megamers. Pure Appl Chem 72:2343–2358

Tomalia DA, Brothers II HM et al (2002) Partial shell-filled core-shell tecto(dendrimers): a strategy to surface differentiated nano-clefts and cusps. Proc Natl Acad Sci USA 99(8):5081–5087

Tomalia DA, Mardel K et al (2003) Dendrimers—An enabling synthetic science to controlled organic nanostructures. In: Goddard WAIII, Brenner DW, Lyshevski SE, Iafrate GJ (eds) Handbook of nanoscience, engineering and technology. CRC Press, Boca Raton, FL, pp 1–34

Tomalia DA, Henderson SA et al (2007a) Dendrimers—An enabling synthetic science to controlled organic nanostructures. In: Goddard WAIII, Brenner DW, Lyshevski SE, Iafrate GJ (eds) Handbook of nanoscience, engineering and technology. CRC Press, Boca Raton, FL, pp 24.1–24.47

Tomalia DA, Reyna LA et al (2007b) Dendrimers as multipurpose nanodevices for oncology drug delivery and diagnostic imaging. Biochem Soc Trans 35(1):61–67

Turro NJ, Barton JK et al (1991) Molecular recognition and chemistry in restricted reaction spaces. Acc Chem Res 24 (11):332–340

Ueno T, Suzuki M et al (2004) Size-selective olefin hydrogenation by a Pd nanocluster provided in an apo-ferritin cage. Angew Chem Int Ed 43:2527–2530

Uppuluri S (1998) Rheological properties of dendrimers. PhD Thesis, Michigan Technological University

Uppuluri S, Keinath SE et al (1998) Rheology of dendrimers. I. Newtonian flow behavior of medium and highly concentrated solutions of polyamidoamine (PAMAM) dendrimers in ethylenediamine (EDA) solvent. Macromolecules 31:4498–4510

Uppuluri S, Swanson DR et al (1999) Tecto(dendrimer) core-shell molecules: macromolecular tectonics for the systematic synthesis of larger controlled structure molecules. Polym Mater Sci & Eng (ACS) 80:55–56

Uppuluri S, Piehler LT et al (2000) Core-shell tecto(dendrimers): I. Synthesis and characterization of saturated shell models. Adv Mater 12(11):796–800

Vargaftik MN, Moiseev II et al (1991) Giant palladium clusters: synthesis and characterization. Faraday Discuss 92:13–29

von Maltzahn G, Ren Y et al (2008) In vivo tumor cell targeting with "click" nanoparticles. Bioconjug Chem 19: 1570–1578

Vriezema DM, Aragones MC et al (2005) Self-assembled nanoreactors. Chem Rev 105:1445–1489

Wales DJ (1996) Structure, dynamics, and thermodynamics of clusters: tales from topographic potential surfaces. Science 271:925–929

Wang J, Rivas G et al (1998) Adsorption and detection of DNA dendrimers at caron electrodes. Electroanalysis 10(8): 553–556

Wang YA, Li JJ et al (2002) Stabilization of inorganic nanocrystals by organic dendrons. J Am Chem Soc 124:2293–2298

Wang X, Inapagolla R et al (2007) Synthesis, characterization, and in vitro activity of dendrimer-streptokinase conjugates. Bioconjug Chem 18:791–799

Weller H (1993) Colloid semiconductor Q-particles: chemistry in the transition region between solid state and molecules. Angew Chem Int Ed Engl 32:41–53

Wiener EC, Brechbiel MW et al (1994) Dendrimer-based metal chelates: a new class of magnetic resonance imaging contrast agents. Magn Reson Med 31(1):1–8

Wilcoxon JP, Abrams BL (2006) Synthesis, structure and properties of metal nanoclusters. Chem Soc Rev 35:1162–1194

Wilcoxon JP, Martin JE et al (2000) Size distribution of gold nanoclusters studied by liquid chromatography. Langmuir 16(25):9912–9920

Wilson OM, Knecht MR et al (2006) Effect of Pd nanoparticle size on the catalytic hydrogenation of allyl alcohol. J Am Chem Soc 128:4510–4511

Wooley KL, Hawker CJ et al (1993) Fullerene-bound dendrimers: soluble, isolated carbon clusters. J Am Chem Soc 115:9836–9837

Xie R, Chen K et al (2008) In As/InP/ZnSe core/shell/shell quantum dots as near-infrared emitters: bright, narrow-band, non-cadmium containing, and biocompatible. Nano Res 1:457–464

Xu X, Rosi NL et al (2006) Asymmetric functionalization of gold nanoparticles with oligonucleotides. J Am Chem Soc 128:9286–9287

Yavuz CT, Mayo JT et al (2006) Low-field magnetic separation of monodisperse Fe_3O_4 nanocrystals. Science 314: 964–967

Yu WW, Qu L et al (2003) Experimental determination of the extinction coefficient of CdTe, CdSe, and CdS nanocrystals. Chem Mater 15:2854–2860

Zhang S, Holmes T et al (1993) Spontaneous assembly of a self-complimentary oligopeptide to form a stable macroscopic membrane. Proc Natl Acad USA 90:3334–3338

Zhang C, O'Brien S et al (2002) Comparison and stability of CdSe nanocrystals covered with amphiphilic poly(amidoamine) dendrimers. J Phys Chem B 106:10316–10321

Zhang K, Fang H et al (2008) Shape effects of nanoparticles conjugated with cell-penetrating peptides (HIV Tat PTD) on CHO cell uptake. Bioconjug Chem 19:1880–1887

Zhao M, Sun L et al (1998) Preparation of Cu nanoclusters within dendrimer templates. J Am Chem Soc 120:4877–4878

Zimmer JP, Kim S-W et al (2006) Size series of small indium arsenide-zinc selenide core-shell nanocrystals and their application to in vivo imaging. J Am Chem Soc 128(8): 2526–2527

Zimmerman SC, Zeng F et al (1996) Self-assembling dendrimers. Science 271:1095–1098

Zumdahl SS, Zumdahl SA (2007) Chemistry. Houghton Mifflin Company, Boston